Thesis for the degree of Doctor of Philosophy

Fast Particle Driven Instabilities in Tokamak Plasmas

Robert Nyqvist

CHALMERS

Department of Earth and Space Sciences
Chalmers University of Technology
Göteborg, Sweden 2013

Fast Particle Driven Instabilities in Tokamak Plasmas
ROBERT NYQVIST

ISBN 978-91-7385-881-6

Doktorsavhandlingar vid Chalmers Tekniska Högskola
Ny serie nr 3562
ISSN 0346-718X

Department of Earth and Space Sciences
Plasma Physics and Fusion Energy
Chalmers University of Technology
SE-412 96 Göteborg, Sweden
Telephone + 46 (0) 31 – 772 10 00

Printed by
Reproservice
Chalmers Tekniska Högskola
Göteborg, Sweden 2013

Fast Particle Driven Instabilities in Tokamak Plasmas

Robert Nyqvist
Department of Earth and Space Sciences
Chalmers University of Technology
SE-412 96 Göteborg, Sweden

Abstract

The burning plasmas of the next generation tokamak fusion experiment ITER will contain significant populations of highly energetic ions. Both fusion generated alpha particles and fast ions accelerated by auxiliary heating schemes are capable of exciting instabilities in the Alfvén frequency range, which may in turn cause redistribution of energetic particles and lead to deleterious events such as e.g. monster sawtooth crashes. On present day machines, many aspects of fast ion collective effects are observed and well understood, including e.g. excitation of toroidal Alfvén eigenmodes (TAEs) and frequency sweeping Alfvén cascades. However, a currently hot topic is the role of kinetic and nonlinear Alfvénic instabilities, including explanations for rapid frequency sweeping and unambiguous identification of energetic particle modes.

This thesis presents theoretical research carried out on the linear and nonlinear dynamics of fast particle driven instabilities, with a major focus on such events in tokamaks. In the linear regime, we investigate particle behavior in the presence of a given electromagnetic perturbation. In particular, we formulate a condition on the prescribed wave amplitude to cause stochastic particle motion and we calculate the rate coefficients for the associated diffusive random walks. We also derive analytic expressions for the damping rate of even and odd TAEs, which arises as a result of non-ideal coupling to radially propagating waves. The damping is found to be weak for the odd mode, which raises concern for the confinement of energetic particles on ITER, where antiballooning instabilities are likely to be resonantly driven by passing, fusion born alpha particles.

Nonlinearly, we develop a simple one-dimensional model to investigate the impact of significant frequency shifts on the dynamics of frequency sweeping, weakly driven modes. We include a number of previously neglected long range effects that are all capable of significantly altering the temporal frequency sweeping patterns. In the case when the fast particle collision operator con-

tains both a drag-like slowing-down term, due to binary, small-angle Coulomb collisions, and velocity space diffusion, the model predicts transiently hooked and steady state frequency sweeping patterns. The latter scenario turns out to be analytically tractable.

Keywords: Fusion plasma physics, wave-particle interaction, toroidal Alfvén eigenmodes, kinetic Alfvén wave, radiative damping, bump-on-tail, holes and clumps, hooked and snaking frequency sweeping.

Publications

[A] R. M. Nyqvist, M. Lisak and J. Zalesny, *On wave-particle interaction in axisymmetric toroidal systems*, Phys. Scr. **84**, 015503 (2011).

[B] R. M. Nyqvist, M. K. Lilley and B. N. Breizman, *Adiabatic description of long range frequency sweeping*, Nucl. Fusion **52**, 094020 (2012).

[C] R. M. Nyqvist and B. N. Breizman, *Modeling of long range frequency sweeping for energetic particle modes*, Phys. Plasmas **20**, 042106 (2013).

[D] R. M. Nyqvist and S. E. Sharapov, *Asymmetric radiative damping of low shear toroidal Alfvén eigenmodes*, Phys. Plasmas **19**, 082517 (2012).

Other contributions (not included)

[1] R. Nyqvist, D. Anderson and M. Lisak, *Spreading of Collimated Particle Beams Within a Generalized Fokker-Planck Diffusion Equation*, Nucl. Science and Engn. **163** (1), 85 (2009).

[2] R. Nyqvist, M. Lisak, D. Anderson and J. Zalesny, *On Wave-Particle Interaction in Axisymmetric Toroidal Systems*, RUSA Meeting of the Swedish Fusion Research Unit, Uppsala, Sweden, May 5 – 6, 2009.

[3] R. Nyqvist, B. N. Breizman, M. Lisak and S. E. Sharapov, *Fast Ion Driven Alfvén Eigenmodes within the $q = 1$ Radius*, Proceedings of the 36th EPS Conference on Plasma Physics, Sofia, Bulgary, June 29 – July 3, 2009.

[4] R. Nyqvist, B. N. Breizman, M. Lisak and S. E. Sharapov, *Alfvénic Eigenmodes within the $q = 1$ Radius in Sawtoothing Plasmas*, Proceedings of the 11th IAEA Technical Meeting on Energetic Particles in Magnetic Confinement Systems, Kyiv, Ukraine, September 21 – 23, 2009.

[5] R. Nyqvist, S. E. Sharapov and M. Lisak, *Radiative Damping of Low Shear Toroidal Alfvén Eigenmodes*, Proceedings of the 37th EPS Conference on Plasma Physics, Dublin, Ireland, June 21 – 25, 2010.

[6] R. Nyqvist, S. E. Sharapov and M. Lisak, *Alfvén Waves in Tokamaks*, Oral presentation at the RUSA Meeting of the Swedish Fusion Research Unit, Stockholm, Sweden, November 10 – 11, 2010.

[7] R. Nyqvist, M. K. Lilley, M. Lisak and B. N. Breizman, *Collisional Nonlinear Energetic Particle Modes*, RUSA Meeting of the Swedish Fusion Research Unit, Stockholm, Sweden, November 10 – 11, 2010.

[8] M. K. Lilley, R. Nyqvist, M. Lisak and G. Galant, *Collective Fast Ion Effects in Tokamaks*, RUSA Meeting of the Swedish Fusion Research Unit, Stockholm, Sweden, November 10 – 11, 2010.

[9] R. Nyqvist, B. N. Breizman, M. K. Lilley and S. E. Sharapov, *Modeling of Long-Range Sweeping Phenomena*, Joint US-EU TTF Workshop, San Diego, California, April 6 – 9, 2011.

[10] M. K. Lilley, R. M. Nyqvist, B. N. Breizman and S. E. Sharapov, *Drag Induced Energetic Particle Modes*, International Sherwood Fusion Theory Conference, Austin, Texas, May 2 – 4, 2011.

[11] S. E. Sharapov, I. Voitsekhovitch, D. N. Borba, T. Gassner, V. G. Kiptily, F. Nabais, R. Nyqvist, S. D. Pinches and JET-EFDA Contributors, *Scenario for Alpha Driven Alfvén Modes in Deuterium-Tritium JET Plasmas*, Proceedings of the 38th EPS Conference on Plasma Physics, Strasbourg, France, June 27 – July 1, 2011.

[12] R. M. Nyqvist, M. K. Lilley and B. N. Breizman, *Adiabatic Description of Long Range Frequency Sweeping*, Oral presentation at the 5th IAEA Technical Meeting on the Theory of Plasma Instabilities, Austin, Texas, USA, September 5 – 7, 2011.

[13] R. M. Nyqvist, M. K. Lilley and B. N. Breizman, *Adiabatic Description of Long Range Frequency Sweeping*, Proceedings of the 5th IAEA Technical Meeting on Energetic Particles in Magnetic Confinement Systems, Austin, Texas, USA, September 7 – 10, 2011.

[14] R. Nyqvist, B. N. Breizman and M. K. Lilley, *Non-Monotonic Frequency Sweeping of Fast Particle Driven Instabilities*, Proceedings of the 39th EPS Conference on Plasma Physics, Stockholm, Sweden, July 2 – 6, 2012.

[15] H. L. Berk, G. Wang, B. N. Breizman, N. Gorelenkov, K. Ghantous, M. Lilley, R. Nyqvist and M. Van Zeeland, *Energetic Particle Long Range Frequency Sweeping and Quasilinear Relaxation*, Proceedings of the 24th IAEA Fusion Energy Conference, San Diego, California, USA, October 8 – 13, 2012.

[16] S. E. Sharapov *et al.* (incl. R. Nyqvist), *Energetic Particle Instabilities in Fusion Plasmas*, Proceedings of the 24th IAEA Fusion Energy Conference, San Diego, California, USA, October 8 – 13, 2012.

[17] R. M. Nyqvist, M. Lisak and F. Håkansson, *Fast Particle Driven Instabilities in Burning Fusion Experiments*, Oral presentation at the RUSA Meeting of the Swedish Fusion Research Unit, Göteborg, Sweden, September 17 – 18, 2012.

[18] R. M. Nyqvist and B. N. Breizman, *Modeling of Long Range Frequency Sweeping Events*, Oral presentation at the 6th IAEA Technical Meeting on the Theory of Plasma Instabilities, Vienna, Austria, May 27 – 29, 2013.

[19] R. M. Nyqvist and B. N. Breizman, *Modeling of Long Range Frequency Sweeping Events*, Oral presentation at the Meeting on Impurity Transport, Göteborg, Sweden, June 24 – 28, 2013.

[20] F. E. Håkansson, R. M. Nyqvist and M. K. Lilley, *Directivity of Frequency Sweeping Kinetic Instabilities*, Proceedings of the 40th EPS Conference on Plasma Physics, Espoo, Finland, July 1 – 5, 2013.

Acknowledgments

A number of people have been central in the making of this thesis and during the work presented herein. I am grateful to my supervisors, the late Prof. Mietek Lisak and Prof. Dan Anderson at Chalmers University of Technology, Dr. Sergei Sharapov at Culham Science Centre for Fusion Energy and Prof. Boris Breizman at the Institute for Fusion Studies in Austin, Texas, for their help and guidance, and for giving me the opportunity to work with something so fascinating (and demanding). A special thank you goes out to Dr. Matthew Lilley at Imperial College, for general guidance but also for providing graphs and results for this thesis.

Next, my collegues and co-workers at Chalmers University of Technology all deserve a thank you.

Finally, family, friends and my loving Jack. Thank you.

Contents

1 Introduction **1**

2 Dynamics of Fast Particles in Toroidal Systems **7**
2.1 The Motion of Single Particles 8
2.1.1 Variational Formulations of Classical Mechanics 9
2.1.2 Exact Motion in Static, Uniform Fields 14
2.1.3 Guiding Center Motion in Slowly Varying Fields 17
2.2 Particle Orbits in Tokamaks 20
2.2.1 Toroidal Coordinates 21
2.2.2 Magnetic Field Structure 22
2.2.3 Large Aspect Ratio Approximation 28
2.2.4 Tokamak Guiding Center Trajectories 30
2.3 Statistical Description of Energetic Particles 40

3 Plasma Waves and their Interaction with Particles **45**
3.1 Kinetic Theory of Linear Plasma Waves 46
3.2 Landau Damping 51
3.3 Kinetic Instabilities in Tokamak Plasmas 56
3.4 Nonlinear Wave-Particle Interaction within a One-Dimensional Bump-On-Tail Model 57

4 Toroidal Alfvén Eigenmodes **65**
4.1 The Magnetohydrodynamic Model 66
4.1.1 Equilibrium Analysis 68
4.1.2 Linear Stability 69
4.2 Alfvén Waves in a Uniform Plasma 70
4.3 Alfvén Waves in Toroidal Plasmas 71
4.3.1 Cylindrical Limit 73
4.3.2 Toroidal Alfvén Eigenmodes 75
4.3.3 Alfvén Cascades 83
4.3.4 Kinetic TAEs and Radiative Damping 83
4.4 Interaction between TAEs and Fast Ions 85

4.4.1 Energetic Particle Drive 85
4.4.2 Nonlinear Mode Evolution 87

5 Brief Summary of the Included Articles **93**
5.1 Paper A 93
5.2 Papers B and C 95
5.3 Paper D 97

6 Summary and Conclusion **99**

Bibliography **103**

Papers A–D **111**

1

Introduction

The world population is growing, and so is our need for energy in order to develop and retain a high average standard of living. By 2035, the total energy consumption is predicted to have increased by 50 % from today's usage [1], and virtually all projections conclude that by the year 2100, the world energy demand will have at least doubled. Limited supplies of today's major energy sources – fossil fuels – and the increasing awareness of associated environmental issues place severe restrictions on tomorrow's energy production. In these dark hours, controlled thermonuclear fusion emerges as one of the most promising candidates for an environmentally friendly, in practice inexhaustible, large-scale energy source.

Thermonuclear fusion is the energy source that powers our Sun. On a subatomic level, it is the process whereby two atomic nuclei merge to form a third nucleus. To do so, however, the binding energy of the end state must by higher than the total binding energy of the reactants. The discrepancy, given by Einstein's law

$$E = \Delta m c^2 \ , \tag{1.1}$$

where Δm is the difference in total rest mass between the reactants and products, is released in the form of kinetic energy carried away by the reaction products. Due to the large factor c^2 in equation (1.1), the energy yield per unit mass of fusion is huge, roughly 10^7 times higher than that of burning fossil fuels and 100 times higher than the kinetic energy per unit mass released from splitting Uranium atoms in fission power plants.

In order to bring positively charged nuclei close enough to fuse, a significant repulsion due to the electrostatic Coulomb force must somehow be overcome. In the solar core this is accomplished through the action of gravity, which balances the net outward pressure from the energy released in the thermonuclear reactions. Here on Earth, conditions for nuclear fusion have to be created by

other means, and the Coulomb repulsion puts extreme demands on the technology. For instance, the temperatures required to accomplish economically feasible thermonuclear fusion on Earth range from 10^7 K to a few 10^8 K. The latter is substantially higher than the temperature in the center of the Sun. At such temperatures, the fuel is a completely ionized gas and constitutes what is known as a plasma.

From a practical point of view, the most promising reactions considered for a fusion reactor are

$$\mathrm{D} + \mathrm{D} \longrightarrow \mathrm{He}^3 + n + 3.27 \text{ MeV} \tag{1.2a}$$

$$\mathrm{D} + \mathrm{D} \longrightarrow \mathrm{T} + \mathrm{H} + 4.05 \text{ MeV} \tag{1.2b}$$

$$\mathrm{D} + \mathrm{T} \longrightarrow \mathrm{He}^4 + n + 17.58 \text{ MeV} \tag{1.2c}$$

In these reaction formulae, deuterium (D) and tritium (T) are heavy hydrogen isotopes, carrying one and two neutrons, respectively, and the helium isotope He^4 will be referred to as an alpha particle throughout this thesis. Deuterium occurs naturally in sea water, which contains 0.015 % D, whereas the radioactive isotope T is most easily obtained through neutron bombardment of lithium. Of the three reactions listed in (1.2), the so called D–T reaction (1.2c) has the advantage of having the highest reaction probability at the lowest temperature. It also has, by far, the highest energy output: In each D–T reaction, 17.58 MeV is released in the form of kinetic energy shared between the neutron and the alpha particle, with the lighter neutron carrying away on average 80 % of that. The D–T reaction will most likely dominate in early fusion reactors, although most experiments are currently running D–D reactions (with a significantly lower, but measurable, flux of neutrons generated in reaction (1.2c)), and certainly all the reactions in (1.2), as well as others, will occur inside a burning fusion reactor.

Two main paths have so far been explored in order to establish nuclear fusion as a reliable power source: Inertial and magnetic confinement. The former relies in an intricate way on the inertia of the reactants. A small, spherical target capsule that contains a D–T mixture is irradiated uniformly by a short, high power pulse (laser or particle beam). As the capsule outer layer evaporates explosively due to the heating generated by the radiation, the remainder of the target implodes with great force into a central hot spot where the fusion reactions occur. Magnetic confinement schemes, on the other hand, utilizes that at fusion temperatures the fuel is in the plasma state. It thus consists of coexisting ions and electrons, i.e. charged particles, which can be confined by magnetic fields. So far, magnetic fusion has been the more successful route, with the often used fusion performance measure $n_i T_i \tau_E$ [2], the so called *fusion triple product*, historically doubling approximately every second year for a special class of toroidal magnetic confinement devices known

as tokamaks [3]. In the triple product, n_i is the density of ions, T_i is their temperature, and τ_E is the relaxation time of the plasma energy due to heat conduction – the so called energy confinement time.

In tokamaks [4], the plasma particles are confined by a magnetic field whose field lines trace out nested, toroidal surfaces. The main field component points along the toroidal direction. It is generated by a set of external coils that carry large currents poloidally around the torus. A smaller poloidal field component is generated inside the device by running a toroidal current through the plasma itself. The plasma current is partly ohmic, induced through transformer action, and partly due to non-inductive current drive such as neutral beam injection (NBI) and radio frequency (RF) heating. The largest tokamak currently in operation is the Joint European Torus (JET), located in Culham, UK, which in 1997 set the world record fusion power output of 16.1 MW during one second of D–T operation. JET has also succeeded in producing a steady state power output of 5 MW for 5 seconds.

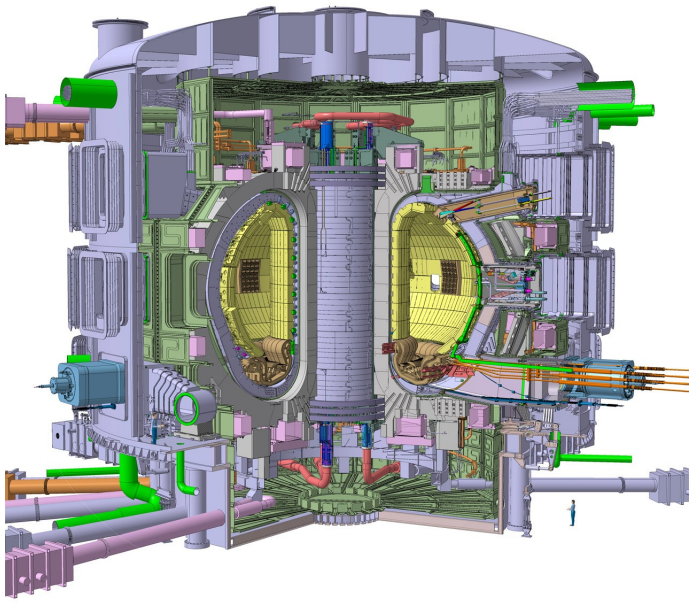

Figure 1.1: View of ITER, obtained from [5].

The next generation tokamak experiment ITER is being constructed at present time in the south of France. ITER, see Figure 1.1, will be a long-pulsed tokamak with a plasma volume of 837 m^3 and superconducting coils to generate a large and long-lasting toroidal field. The main physics objectives for the ITER project are [6]:

- To momentarily produce ten times more energy from thermonuclear fusion reactions than is supplied by auxiliary heating ($Q = 10$).

- To demonstrate steady-state operation with $Q \geq 5$.
- To maintain a fusion pulse for up to eight minutes.

The reasons for the immense size of ITER, almost twice the linear size of JET, as well as the powerful, superconducting coils, are that the fusion triple product scales with both plasma radius and magnetic field strength, making operation of large plasma volumes at high magnetic field strength key issues in reaching the outlined goals.

Burning D–T plasmas on ITER will rely heavily on the self-heating provided by fusion generated alpha particles. Alpha particles carry off 20 % of the 17.58 MeV produced in each D–T reaction, so they are highly energetic ions with large velocities that on average greatly exceed the thermal velocity of the bulk ions. In addition to alpha particles, auxiliary heating systems such as NBI and RF heating also produce and maintain significant energetic ion populations, even in today's devices (where, in fact, alpha particles are rare, and the externally heated ions constitute by far the largest energetic particle populations). Common to all these types of fast ions is that they tend to concentrate in the plasma core, with particle speeds intermediate between the thermal electron and ion speeds, $v_i < v_f < v_e$, and that their large kinetic energy content is slowly (as compared to their rapid motion) transferred to the bulk plasma as the fast particles decelerate due to small angle Coulomb collisions, mainly with thermal electrons. As a result, fast particles are not in thermodynamical equilibrium, and so their velocities do not conform to Maxwellian distributions.

The presence of energetic ions in the tokamak center has major impact on achieving and maintaining high plasma temperatures and long energy confinement times. In particular, the free energy available in their non-Maxwellian velocity distribution can destabilize wave like perturbations from the plasma equilibrium, if the mode phase velocity resonates with the motion of the energetic particles. When the fast ion pressure is high enough, or the modes are weakly damped, instability occurs [7]. Once destabilized, such modes interact heavily with the resonant fast particles, which may result in rapid radial transport, and even expulsion, of fast particles [8]. In a sense, these instabilities are therefore unwanted features that can lead to significant degradation of the plasma confinement. However, their presence also unveils new diagnostic opportunities, providing means of probing the otherwise inaccessible plasma core by measuring the wave fields at the plasma edge.

The work presented in this thesis is devoted to the study of energetic particle driven instabilities in tokamaks. Particular emphasis is placed on a special class of magnetohydrodynamic perturbations known as shear Alfvén waves. Such modes oscillate in a relatively low frequency range, and they propagate along the tokamak magnetic field at the characteristic *Alfvén speed*, denoted

by v_A. The importance of Alfvénic modes stems from the magnitude of the Alfvén speed, which is often comparable to the incipient velocities of fast ions in tokamak experiments. In particular, if $v_A \leq v_f$ holds, as is, e.g., expected for alpha particles on ITER, the fast ions will almost inevitable destabilize and interact with Alfvénic waves as they slow down due to collisions with the bulk plasma.

The remainder of this thesis is organized as follows: In Chapter 2, we discuss the dynamics of fast ions in tokamaks. We consider the motion of single, charged particles in a given magnetic field, including the toroidal geometry and magnetic field topology of tokamak experiments, and we briefly touch upon some statistical properties of the fast particles. Chapter 3 is devoted to linear and nonlinear aspects of wave-particle interaction in the case of fast particle driven instabilities. We discuss the importance of so called resonant particles, which move in synch with the wave, and we develop simple one-dimensional models for the descriptions of Landau damping and nonlinear wave-particle interaction. Chapter 4 concerns the dynamics of Alfvén waves in tokamaks. We discuss magnetohydradynamic features such as the Alfvén continuum and the associated continuum damping, toroidal Alfvén eigenmodes and Alfvén cascades, and we briefly mention how nonideal effects lead to mode conversion into so called kinetic Alfén waves, resulting in e.g. radiative damping of TAEs. We also discuss the possibility of a one-dimensional, nonlinear description of evolving TAEs. Finally, Chapters 5 and 6 contains, respectively, short summaries of the work presented in the four amended papers and some concluding thoughts on future research directions.

2

Dynamics of Fast Particles in Toroidal Systems

Most tokamak experiments comprise a population of ions with kinetic energies that by far exceed the thermal energy of the bulk ions. Such *fast ions* are created in fusion reactions (as, e.g., the highly energetic alpha particles produced in D–T reactions), but also by means of auxiliary heating systems such as NBI and RF heating. The large majority of these particles is concentrated in the tokamak center, with velocities intermediate between the thermal ion and electon speeds, $v_i < v_f < v_e$, and they contribute significantly to the heating of the plasma as they slow down and thermalize due to collisions with thermal bulk particles. However, the fast ions are also prone to resonate with and destabilize thermonuclear wave instabilities, in which case their heating efficiency and confinement may be significantly lowered.

In contrast to neutral gases, whose constituent particles move on straight paths until colliding head on, tokamak fusion plasmas are governed by the laws of electrodynamics. Loosely speaking, each plasma particle continuously interacts with many others through the action of long-range Coulomb forces mediated by electromagnetic fields (or, from an equivalent quantum mechanical point of view, via emission and absorption of light quanta, so called photons). Various mathematical models exist that describe, with varying degree of complexity and accuracy, the intricate aggregate of such interactions in a plasma. For fast ions, whose velocities do not conform to Maxwellian distributions, the relevant framework is so called *kinetic theory*. Such models describe the energetic population statistically in terms of a density function of phase space coordinates and time. The distribution of fast ions evolves according to the combined laws of statistical physics and electromagnetics. It is determined primarily by two dominant mechanisms: Fast ion sources such as fusion

reactions, NBI, RF heating etc., and small-angle Coulomb collisions, which mainly act to slow the ions down as a result of the average drag force from the thermal electrons. However, during RF heating, particle acceleration in the electromagnetic RF wave field must also be taken into account, and whenever thermonuclear wave instabilities are present the ensuing wave-particle interaction may well dominate the evolution of the fast particle distribution.

Much insight can also be gained through a careful study of charged particle trajectories in a given electromagnetic field, so called *single particle motion* theory. In fact, single particle trajectories form the basis for kinetic theory: Jeans' theorem states that any function constructed from constants of single particle motion is a solution to the Vlasov equation, which describes the evolution of the fast ion distribution when collisions are neglected. Moreover, single particle trajectories are often employed in perturbative descriptions of wave-particle interaction: As a first approximation, the single particle orbits can be used as lowest order results around which expansions in one or several small parameters are performed.

In this chapter, we consider the dynamics of fast ions in tokamak experiments by neglecting all kinds of wave-particle interactions. Such models are highly sophisticated, and are therefore postponed until later chapters in this thesis. We start off in Section 2.1 with a general discussion of single particle motion in a given electromagnetic field. Then, in Section 2.2, we apply the general formalism to describe particle orbits in the special geometry and equilibrium fields of a tokamak. Finally, Section 2.3 contains a statistical description of fast particles in terms of a phase space distribution that evolves according to the famous Boltzmann equation.

2.1 The Motion of Single Particles

The motion of a charged particle in the presence of a given electromagnetic field is, in fact, very complex. Its components include a gyration around the magnetic field lines (so called *Larmor* gyration), parallel motion along the field lines, which may include acceleration if the electric field has a parallel component, and drifts across the magnetic field. In order to fully appreciate the effects of forces and field inhomogeneities on the particle trajectories, a careful perturbative analysis has to be carried out. This section gives the results, and presents some important aspects, of such an analysis, without going too much into the details. First, in Section 2.1.1, we give an introduction to the variational formulations of Lagrangian and Hamiltonian mechanics, needed for the subsequent discussion in which particle trajectories in the presence of electromagnetic fields are treated with increasing degree of complexity: We start off in Section 2.1.2 with a discussion of static and uniform fields. Finally,

in Section 2.1.3, we generalize somewhat and discuss the case of slowly varying fields via a guiding center approach.

2.1.1 Variational Formulations of Classical Mechanics

In Lagrangian mechanics [9], the particle motion is governed by the Lagrangian $\mathcal{L}(\mathbf{q}, \dot{\mathbf{q}}, t)$, a function of some set of generalized coordinates $\mathbf{q}$, and their (total) time derivatives $\dot{\mathbf{q}}$, that may depend explicitly on time. The equations of motion are given by the so called *Euler-Lagrange* equations

$$\frac{d}{dt}\frac{\partial \mathcal{L}}{\partial \dot{\mathbf{q}}} = \frac{\partial \mathcal{L}}{\partial \mathbf{q}} \ , \tag{2.1}$$

which follow from demanding that the trajectory between two positions $\mathbf{q}(t_1)$ and $\mathbf{q}(t_2)$ at distinct times t_1 and t_2 minimizes the integral

$$\int_{t_1}^{t_2} \mathcal{L}(\mathbf{q}, \dot{\mathbf{q}}, t)\, dt \ . \tag{2.2}$$

As an example, consider the motion of a charged particle in an electromagnetic field

$$\mathbf{E} = -\nabla\phi - \frac{\partial \mathbf{A}}{\partial t} \ , \quad \mathbf{B} = \nabla \times \mathbf{A} \ . \tag{2.3}$$

Here, $\phi(\mathbf{q}, t)$ is the electrostatic potential and $\mathbf{A}(\mathbf{q}, t)$ is the magnetic vector potential. They are both functions of space and time, but not of the velocity $\dot{\mathbf{q}}$. In Cartesian coordinates the Lagrangian is given by

$$\mathcal{L}(\mathbf{x}, \dot{\mathbf{x}}, t) = \frac{M}{2}\dot{\mathbf{x}} \cdot \dot{\mathbf{x}} + e\left[\mathbf{A}(\mathbf{x}, t) \cdot \dot{\mathbf{x}} - \phi(\mathbf{x}, t)\right] \ , \tag{2.4}$$

where M and e are the particle mass and charge, respectively. The corresponding Euler-Lagrange equations are given by

$$M\ddot{\mathbf{x}} + e\frac{d\mathbf{A}}{dt} = e\dot{\mathbf{x}} \times (\nabla \times \mathbf{A}) + e\dot{\mathbf{x}} \cdot \nabla\mathbf{A} - e\nabla\phi \ . \tag{2.5}$$

Keeping in mind that

$$\frac{d}{dt} = \frac{\partial}{\partial t} + \dot{\mathbf{x}} \cdot \nabla \ , \tag{2.6}$$

application of (2.3) yields

$$M\ddot{\mathbf{x}} = e\big[\mathbf{E} + \dot{\mathbf{x}} \times \mathbf{B}\big] \ , \tag{2.7}$$

which is immediately recognized as the usual Newtonian equations of motion with a Lorentz force right hand side.

The Lagrangian formalism has the advantage of being coordinate independent. That is, the Euler-Lagrange equations (2.1) hold for any set of generalized coordinates $\mathbf{q}$. In practice, this means that given a coordinate transformation

$$\mathbf{q} = \mathbf{f}\left(\mathbf{Q}, t\right) \tag{2.8}$$

from $\mathbf{q}$ to a new set $\mathbf{Q}$, the transformed Lagrangian is found via direct substitution of (2.8) and

$$\dot{\mathbf{q}} = \frac{\partial \mathbf{f}}{\partial t} + \sum_i \dot{Q}^i \frac{\partial \mathbf{f}}{\partial Q^i} \tag{2.9}$$

into $\mathcal{L}\left(\mathbf{q}, \dot{\mathbf{q}}, t\right)$. The equations of motion will then be given by equation (2.1), with $\mathbf{q}$ replaced by $\mathbf{Q}$. As an example, the transformation

$$x = r\cos\varphi \ , \quad y = r\sin\varphi \ , \quad z = z \tag{2.10}$$

from Cartesian to cylindrical coordinates produces

$$\dot{\mathbf{x}} \cdot \dot{\mathbf{x}} = \dot{x}^2 + \dot{y}^2 + \dot{z}^2 = \dot{r}^2 + r^2\dot{\varphi}^2 + \dot{z}^2 \ . \tag{2.11}$$

The transformed form of, e.g., the charged particle Lagrangian (2.4) can then be found by transforming the factors $\mathbf{A}\left(\mathbf{x}, t\right) \cdot \dot{\mathbf{x}}$ and $\phi\left(\mathbf{x}, t\right)$ similarly.

Another merit of the Lagrangian formalism is that it allows for easy identification of conserved quantities. Consider a Lagrangian $\mathcal{L}\left(\mathbf{q}, \dot{\mathbf{q}}, t\right)$ that is independent of one or several of the generalized coordinates $\mathbf{q}$. Such a coordinate q^i is called cyclic, and its *conjugate canonical momentum*, given by

$$p_i = \frac{\partial \mathcal{L}}{\partial \dot{q}^i} \ , \tag{2.12}$$

is conserved in accordance with the Euler-Lagrange equations (2.1). Moreover, if $\mathcal{L}$ has no explicit time dependence, then the total energy

$$E = \dot{\mathbf{q}} \cdot \frac{\partial \mathcal{L}}{\partial \dot{\mathbf{q}}} - \mathcal{L} \tag{2.13}$$

is preserved during the motion, since

$$\frac{dE}{dt} = -\frac{\partial \mathcal{L}}{\partial t} \ . \tag{2.14}$$

As a particular example, consider again the charged particle Lagrangian (2.4). When there is no electric field, $\nabla\phi = 0$, there are no accelerating forces, so the particle kinetic energy

$$W = \frac{M}{2}\, \dot{\mathbf{q}} \cdot \dot{\mathbf{q}} \tag{2.15}$$

is a constant of motion.

An alternative, but equivalent, description is given in terms of the Hamiltonian function $\mathcal{H}$ [9], obtained from the Lagrangian via a Legendre transformation of the form

$$\mathcal{H}(\mathbf{q},\mathbf{p},t) = \mathbf{p}\cdot\dot{\mathbf{q}}(\mathbf{q},\mathbf{p},t) - \mathcal{L}(\mathbf{q},\mathbf{p},t) \ . \tag{2.16}$$

The Hamiltonian is equal in value to the total energy E, but it is a function of the phase-space coordinates $\mathbf{q}$ and $\mathbf{p}$ rather than $\mathbf{q}$ and its time derivative. The Hamiltonian framework can be employed whenever the relations (2.12) may be inverted to give $\dot{\mathbf{q}}$ as a function of $\mathbf{q}$, $\mathbf{p}$ and t. It is obvious that cyclic coordinates also do not figure in $\mathcal{H}$, in which case the Hamilton equations of motion,

$$\dot{\mathbf{q}} = \frac{\partial\mathcal{H}}{\partial\mathbf{p}} \ , \quad \dot{\mathbf{p}} = -\frac{\partial\mathcal{H}}{\partial\mathbf{q}} \ , \tag{2.17}$$

immediately give $\dot{p}_i = 0$ for their conjugate momenta. In this sense, the total energy E can be thought of as a "momentum" conjugate to to the time variable t, satisfying

$$\dot{E} = -\frac{\partial\mathcal{L}}{\partial t} = \frac{\partial\mathcal{H}}{\partial t} \ , \tag{2.18}$$

i.e. a conserved quantity if the time variable is cyclic.

As an example, we review once more the motion of a charged particle in an electromagnetic field. The canonical momenta are given by differentiating (2.4) with respect to $\dot{\mathbf{x}}$,

$$\mathbf{p} = M\dot{\mathbf{x}} + e\mathbf{A}(\mathbf{x},t) \ , \tag{2.19}$$

which gives

$$\dot{\mathbf{x}} = \frac{\mathbf{p} - e\mathbf{A}(\mathbf{x},t)}{M} \ . \tag{2.20}$$

and, subsequently,

$$\mathcal{H}(\mathbf{p},\mathbf{x},t) = \frac{1}{2M}\left[\mathbf{p} - e\mathbf{A}(\mathbf{x},t)\right]^2 + e\phi(\mathbf{x},t) \ . \tag{2.21}$$

The relevant Hamilton equations of motion, $\dot{\mathbf{x}} = \partial\mathcal{H}/\partial\mathbf{p}$ and $\dot{\mathbf{p}} = -\partial\mathcal{H}/\partial\mathbf{x}$, then give, respectively, equation (2.20) and

$$\dot{\mathbf{p}} = \frac{e}{M}\left[(\mathbf{p} - e\mathbf{A})\cdot\nabla\mathbf{A} + (\mathbf{p} - e\mathbf{A})\times(\nabla\times\mathbf{A})\right] - e\nabla\phi \tag{2.22}$$

Finally, substitution of the expressions (2.3) and (2.19) gives, once more, the charged particle equations of motion (2.7).

The beauty of the Hamiltonian description becomes apparent when $\mathcal{H}$ lacks a complete set of cyclic coordinates, but is still known to describe integrable

particle orbits. It is then advantageous to seek a canonical transformation to a new set of canonical coordinates and momenta $(\boldsymbol{\Theta}, \mathbf{J})$, such that all the new coordinates $\boldsymbol{\Theta}$ are cyclic in the transformed Hamiltonian. We shall not give the details of such a transformation here, but simply state the form of the momenta $\mathbf{J}$: They are to be chosen as the phase space areas [10]

$$J_i = \oint_{\gamma_i} \mathbf{p} \cdot d\mathbf{q} \ , \tag{2.23}$$

where the integration paths are defined by the particle trajectories, denoted here γ_i. When new momenta are introduced in this way, the transformed Hamiltonian is a function merely of $\mathbf{J}$, $\mathcal{H} = \mathcal{H}(\mathbf{J})$, so that $\boldsymbol{\Theta}$ are cyclic and $\mathbf{J}$ are constant. Such a set of canonical phase space coordinates are called *action-angle* variables. Integration of Hamilton's equations

$$\dot{\boldsymbol{\Theta}} = \frac{\partial \mathcal{H}}{\partial \mathbf{J}} \equiv \boldsymbol{\Omega}(\mathbf{J}) \tag{2.24}$$

for the angle variables then gives

$$\boldsymbol{\Theta} = \boldsymbol{\Omega}(\mathbf{J})\, t + \boldsymbol{\Theta}(t=0) \ , \tag{2.25}$$

where $\boldsymbol{\Omega}$ are the orbital frequencies.

Integrals of the form (2.23) in fact remain constant even when the particle motion is only nearly periodic. Such particle orbits arise, e.g., when the Hamiltonian has a slow explicit time dependence, or if a periodic trajectory is slightly offset during each revolution due to another, slower motion, e.g. an overall drift. This sort of invariance relies on the concept of *adiabaticy*, meaning that the change in the Hamilitonian during one period is small enough to ensure sufficient differentiability, and the conserved quantities are called *adiabatic invariants*. Formally, such systems are represented by a Hamiltonian on the form $\mathcal{H}(p, q, \mathbf{Z}; t)$, where p and q are phase space coordinates that describe the almost periodic motion, and $\mathbf{Z}$ represents dynamical variables (both coordinates and momenta) that evolve slowly as compared to the variations in p and q, as does the energy itself,

$$\left[\frac{\partial \mathcal{H}}{\partial \mathbf{Z}}, \frac{\partial \mathcal{H}}{\partial t}\right] \sim \delta \left[\frac{dp}{dt}, \frac{dq}{dt}\right] \ , \quad \delta \ll 1 \ . \tag{2.26}$$

The adiabatic invariant is given by the phase space area

$$J(E, \mathbf{Z}; t) = \oint p(q, E, \mathbf{Z}; t)\ dq \ , \tag{2.27}$$

and it is preserved to all orders in δ [11]. The function p is defined implicitly in terms of the instantaneous value for the energy,

$$E = \mathcal{H}(p, q, \mathbf{Z}; t) \ , \tag{2.28}$$

and the integral is to be taken over one period of the *frozen* system, i.e. holding E, $\mathbf{Z}$ and t fixed.

A third useful framework is the variational theory of the so called *phase space Lagrangian*. The phase space Lagrangian equals the configuration space Lagrangian in value, but is a function of the canonical phase space coordinates $\mathbf{q}$ and $\mathbf{p}$ and their time derivatives rather than $\mathbf{q}$ and $\dot{\mathbf{q}}$. It is defined via the expression

$$\mathcal{L}\left(\mathbf{q},\mathbf{p},\dot{\mathbf{q}},\dot{\mathbf{p}},t\right)=\mathbf{p}\cdot\dot{\mathbf{q}}-\mathcal{H}\left(\mathbf{q},\mathbf{p},t\right)\ , \tag{2.29}$$

and gives two sets of Euler-Lagrange equations when minimized under independent variations of both $\mathbf{q}$ and $\mathbf{p}$,

$$\frac{d}{dt}\left(\frac{\partial\mathcal{L}}{\partial\dot{\mathbf{q}}}\right)=\frac{\partial\mathcal{L}}{\partial\mathbf{q}}\ ,\quad \frac{d}{dt}\left(\frac{\partial\mathcal{L}}{\partial\dot{\mathbf{p}}}\right)=\frac{\partial\mathcal{L}}{\partial\mathbf{p}} \tag{2.30}$$

Due to the special form of the phase space Lagrangian (2.29), these equations immediately reproduce the Hamilton equations (2.17).

As with the configuration space Lagrangian $\mathcal{L}\left(\mathbf{q},\dot{\mathbf{q}},t\right)$, the phase space Lagrangian framework admits transformations to any set of phase space coordinates, including non-canonical pairs of coordinates and momenta. As an example, consider for the last time the motion of a charged particle in an electromagnetic field. The phase space Lagrangian is, in Cartesian coordinates,

$$\mathcal{L}\left(\mathbf{x},\mathbf{p},\dot{\mathbf{x}},\dot{\mathbf{p}},t\right)=\mathbf{p}\cdot\dot{\mathbf{x}}-\mathcal{H}\left(\mathbf{x},\mathbf{p},t\right)\ , \tag{2.31}$$

with $\mathcal{H}$ given by (2.21). If we transform to another, non-canonical momentum $\mathbf{v}$, defined via

$$\mathbf{p}=M\mathbf{v}+e\mathbf{A}\ , \tag{2.32}$$

the phase space Lagrangian in (2.31) becomes

$$\mathcal{L}\left(\mathbf{x},\mathbf{v},\dot{\mathbf{x}},\dot{\mathbf{v}},t\right)=\left[M\mathbf{v}+e\mathbf{A}\left(\mathbf{x},t\right)\right]\cdot\dot{\mathbf{x}}-\left[\frac{M}{2}\mathbf{v}\cdot\mathbf{v}+e\phi\left(\mathbf{x},t\right)\right]\ . \tag{2.33}$$

For this transformed phase space Lagrangian, the Euler-Lagrange equations are

$$\frac{d}{dt}\left(\frac{\partial\mathcal{L}}{\partial\dot{\mathbf{x}}}\right)=\frac{\partial\mathcal{L}}{\partial\mathbf{x}}\ ,\quad \frac{d}{dt}\left(\frac{\partial\mathcal{L}}{\partial\dot{\mathbf{v}}}\right)=\frac{\partial\mathcal{L}}{\partial\mathbf{v}}\ . \tag{2.34}$$

Since $\partial\mathcal{L}/\partial\dot{\mathbf{v}}=0$, the latter equation immediately gives $\dot{\mathbf{x}}=\mathbf{v}$. The first equation gives

$$\frac{d}{dt}\left[M\mathbf{v}+e\mathbf{A}\right]=\nabla\left[e\mathbf{A}\cdot\dot{\mathbf{x}}-e\phi\right]\ , \tag{2.35}$$

which, with the identification $\dot{\mathbf{x}}=\mathbf{v}$, may be written as the Newtonian equations of motion for a charged particle, i.e. equations (2.7).

2.1.2 Exact Motion in Static, Uniform Fields

Uniform **E**- and **B**-fields constitute a special case for which the charged particle motion is exactly integrable. When there is only a **B**-field, the Lorentz force $e\dot{\mathbf{x}} \times \mathbf{B}$ in (2.7) is perpendicular to both the particle velocity and **B**, and therefore does no work. The resulting motion, usually referred to as the *Larmor gyration*, or simply the *gyromotion*, is a rotation in the plane perpendicular to **B**, at constant radius r_L. The gyration frequency is

$$\omega_c = \frac{|e|B}{M} \ , \tag{2.36}$$

where $B = |\mathbf{B}|$ is the magnitude of the magnetic field strength **B**. The motion parallel to **B** is unaffected by the presence of the field, and therefore consists of a constant drift at the initial parallel velocity. Hence, the overall trajectory is a helix. Usually, one thinks of the motion as decomposed into a rapid gyration around the so called *guiding center* position, which meanwhile drifts at constant speed along the field lines. When a uniform electric field **E** is present as well, two additional guiding center velocity components are introduced: Any component of **E** along **B** will result in an acceleration/deceleration of the guiding center rather than the constant parallel drift. Further, non-zero components of **E** in the plane perpendicular to **B** induces a drift of the guiding center, with constant velocity

$$\mathbf{v}_E = \frac{\mathbf{E} \times \mathbf{B}}{B^2} \ , \tag{2.37}$$

usually called the $\mathbf{E} \times \mathbf{B}$-drift.

We proceed by means of the Lagrangian formulation outlined in the previous section. Without loss of generality, we consider a uniform magnetic field aligned with the z-axis, $\mathbf{B} = B\hat{z}$, where B is constant. In Cartesian coordinates, the relevant charged particle Lagrangian was given in (2.4), and it can be shown that the choice

$$\mathbf{A} = -\frac{B}{2}\big[y\hat{x} - x\hat{y}\big] \ , \quad \phi = -\big[E_x x + E_y y + E_z z\big] \tag{2.38}$$

reproduces the considered **E**- and **B**-fields via equations (2.3) when E_x, E_y and E_z are constants. The motion is most readily assessed by performing a Galilean transformation to an inertial frame moving with the drift velocity (2.37), i.e. the frame in which there are no electric field components perpendicular to **B**. Under such a transformation, the Lagrangian retains the form (2.4), with $\mathbf{x}$, $\dot{\mathbf{x}}$, $\mathbf{A}$ and ϕ replaced with their transformed versions. If we let (x, y, z) denote Cartesian coordinates in the transformed frame too, the form of the vector potential remains as given in (2.38), while the electrostatic potential transforms into

$$\phi = -E_z z \ . \tag{2.39}$$

The Galilean transformation is actually non-trivial. One has to integrate by parts and remove some total derivatives from the transformed Lagrangian, and the $E_x x$- and $E_y y$- terms in ϕ are canceled out by identical, but oppositely signed terms, stemming from the transformation of $\dot{\mathbf{x}} \cdot \mathbf{A}$.

We now perform a second transformation to the set of cylindrical coordinates (r, θ, z) defined in (2.10). The kinetic part of the resulting Lagrangian was given in (2.11). Similarly, the potentials $\mathbf{A}$ and ϕ transform into

$$\mathbf{A} = \frac{rB}{2}\,\hat{\theta}\ , \quad \phi = -E_z z\ . \tag{2.40}$$

In total, then, the transformed Lagrangian reads

$$\mathcal{L} = \frac{M}{2}\left[\dot{r}^2 + r^2\dot{\theta}^2 + \dot{z}^2\right] + \frac{eBr^2\dot{\theta}}{2} + eE_z z\ . \tag{2.41}$$

The canonical momenta are given by

$$p_r = M\dot{r}\ , \quad p_\theta = Mr^2\left[\dot{\theta} \pm \frac{\omega_c}{2}\right]\ , \quad p_z = M\dot{z}\ , \tag{2.42}$$

where the $\pm$ refers to ions/electrons, respectively, and the corresponding Euler-Lagrange equations become

$$M\ddot{r} = Mr\dot{\theta}\left[\dot{\theta} \pm \omega_c\right]\ , \quad \dot{p}_\theta = 0\ , \quad M\ddot{z} = eE_z\ . \tag{2.43}$$

The θ- and z-equations can be immediately integrated to give

$$p_\theta = \text{Const.} \tag{2.44}$$

and the parallel motion

$$z = \frac{eE_z}{2}t^2 + \dot{z}\,(t=0)\,t + z\,(t=0)\ , \tag{2.45}$$

which represents an acceleration/deceleration in the parallel electric field E_z. The r-equation is more cumbersome. In general, it involves two non-trivial integrations. However, a convenient class of solutions are those with $\ddot{r} = 0$. For such orbits, the r-equation immediately gives, for $r \neq 0$,

$$\dot{\theta} = \mp\omega_c\ . \tag{2.46}$$

Then, the conserved canonical momentum becomes $p_\theta = \mp Mr^2\omega_c/2$, so that

$$\dot{r} = 0\ . \tag{2.47}$$

Equations (2.46) and (2.47) represents a circular orbit at constant radius, denoted r_L, in the plane perpendicular to $\mathbf{B}$, whose direction depends on the

charge of the particle. In fact, the direction is such that the motion is always diamagnetic, i.e. the particle gyrates as to oppose the magnetic field $\mathbf{B}$. In terms of the constant angular velocity $v_L = r_L\omega_c$ and the *magnetic moment*

$$\mu = \frac{Mv_L^2}{2B} \ , \tag{2.48}$$

the conserved canonical momentum reads

$$p_\theta = -\frac{M}{e}\mu \ . \tag{2.49}$$

Hence, μ is also a constant of motion. The corresponding action variable is given by integrating p_θ along the orbit of one gyration, which effectively changes the overall sign for the ions, but not the electrons,

$$J_\theta = \frac{M}{|e|}\mu \ . \tag{2.50}$$

We note briefly that not all particles satisfy $\ddot{r} = 0$, and therefore do not qualify for the present analysis. However, such particles simply execute similar orbits, with their gyration centers offset from the origin, thus making the current description (in terms of cylindrical coordinates) a particularly inconvenient one. In fact, particles that gyrate off the origin are more easily described, as in most introductory textbooks, by solving the uncoupled harmonic oscillator equations for x and y that result from the coupled equations of motion (2.7) when sticking to Cartesian coordinates [12].

If we now transform back to the original frame, in which the electric field components perpendicular to $\mathbf{B}$ do not vanish, the particle acquires the additional velocity $\mathbf{v}_E$, given in equation (2.37). Thus, in the original frame, the overall motion consists of a gyration, perpendicular to $\mathbf{B}$, at constant frequency ω_c and radius r_L, around the particle guiding center, which meanwhile accelerates/decelerates along $\mathbf{B}$ according to (2.45) and drifts across $\mathbf{B}$ at the $\mathbf{E} \times \mathbf{B}$-velocity (2.37). We note that for thermal particles in tokamaks, r_L is usually very small, typically in the millimeter range for ions and about 2 % of that for electrons.[1] Fast ions, however, can have much larger r_L, up to the decimeter range. On the contrary, ω_c is one of the highest frequencies encountered in fusion plasma physics.

[1]These are just rules of thumb, however. For thermal particles, v_L scales with species temperature, which in general is not the same for ions and electrons.

2.1.3 Guiding Center Motion in Slowly Varying Fields

When $\mathbf{E}$ and $\mathbf{B}$ vary slowly in space and time (as compared to the characteristic length r_L and time ω_c^{-1} of the Larmor gyration), the particle motion is still integrable. However, in this case the particle orbits can only be found perturbatively by means of a series expansion in the small parameter

$$\delta \equiv \max\left[\frac{r_L}{L}\,,\frac{1}{\omega_c T}\right]\,, \tag{2.51}$$

where L and T are characteristic length and time scales associated with the spatial and temporal variations in $\mathbf{E}$ and $\mathbf{B}$. To lowest order, the particles still gyrate at radius $r_L = v_L/\omega_c$ around their guiding centers. However, ω_c and v_L are no longer constant. The cyclotron frequency changes due to the variation in B, and there is an energy exchange between the kinetic energy $\mu B = M v_L^2/2$ of the Larmor gyration and the kinetic energy aligned parallel to the magnetic field, $M v_\parallel^2/2$. Moreover, the guiding center now drifts across the magnetic field lines not only due to the occurrence of electric fields, but also as a result of the inhomogeneity and curvature of the magnetic field.

In introductory textbooks, a set of particle velocity components, valid though first order in the expansion parameters, are usually found via direct integration of the equations of motion (2.7), once expanded appropriately. We will however utilize the more complicated, but also more rewarding, phase space Lagrangian approach presented at the end of section 2.1.1. The analysis follows the review [13], but uses the assumptions and approximations of [14]. The method yields expressions for the particle guiding center velocity that are higher order in δ than those of the usual textbook approach. However, we will evaluate these expressions explicitly merely through first order, upon which the resulting equations concur with the usual textbook analysis (nicely reviewed in [15]).

The Lagrangian approach utilizes that the magnetic moment μ as given in (2.48), previously exactly conserved, remains adiabatically invariant when the fields vary slowly, and that the drifts across the magnetic field are small. Strictly speaking, μ is preserved only to lowest order in the expansion parameter δ, i.e. it has a time derivative $\dot{\mu} = \mathcal{O}(\delta)$. Higher order adiabatic invariants have been calculated, see e.g. [14], but the present form suffices well to obtain the guiding center motion to first order in δ. The guiding center phase space Lagrangian $\mathcal{L}_{gc}$ is a function of the following non-canonical phase space coordinates: The guiding center position $\mathbf{x}_{gc}$, around which the Larmor gyration occurs; the guiding center velocity along the magnetic field, $v_\parallel = \mathbf{b}\cdot\dot{\mathbf{x}}_{gc}$; the canonical momentum $p_\alpha = M\mu/e$ for the gyromotion; and the gyroangle α. It is given by [14]

$$\mathcal{L}_{gc}\left(\mathbf{x}_{gc}, v_\parallel, p_\alpha, \alpha; t\right) = \Big[e\mathbf{A}\left(\mathbf{x}_{gc};t\right) + M v_\parallel \mathbf{b}\left(\mathbf{x}_{gc};t\right)\Big]\cdot\dot{\mathbf{x}}_{gc} + p_\alpha\dot{\alpha} - \mathcal{H}_{gc}\,, \tag{2.52}$$

where the guiding center Hamiltonian (the total energy of the guiding center) is

$$\mathcal{H}_{gc}\left(\mathbf{x}_{gc}, v_{\parallel}, p_{\alpha}, \alpha; t\right) = \frac{M}{2} v_{\parallel}^{2} \mp p_{\alpha}\omega_{c}\left(\mathbf{x}_{gc}; t\right) + e\phi\left(\mathbf{x}_{gc}; t\right) \ , \tag{2.53}$$

and the upper/lower signs apply for ions/electrons, respectively. Note that we have written explicitly the dependencies of the non-coordinate quantities $\mathbf{A}$, $\mathbf{b}$, ω_c and ϕ, which are to be evaluated at the guiding center position $\mathbf{x}_{gc}$, at time t, rather than the actual particle position. Note also that the term $\mp p_{\alpha}\omega_c$ is often written as μB. It is worth mentioning that the guiding center Lagrangian (2.52) is constructed from the assumption that the $\mathbf{E}\times\mathbf{B}$-drift (2.37) is first order in δ. On the contrary, in [13], $\mathbf{v}_E$ is allowed to be $\mathcal{O}(1)$. The corresponding, more general analysis is only marginally more difficult, but we refrain from presenting it here since we simply do not need to consider such fast $\mathbf{E}\times\mathbf{B}$-drifts in tokamaks.

The Euler-Lagrange equations for p_{α}, α and $v_{\parallel}$ trivially give $\dot{\alpha} = \mp\omega_c$, $\dot{p}_{\alpha} = 0$ and $v_{\parallel} = \mathbf{b}\cdot\mathbf{x}_{gc}$. However, the equations for $\mathbf{x}_{gc}$ are far more difficult to analyze. After some algebra, one obtains

$$\begin{aligned} M\dot{v}_{\parallel}\mathbf{b} = &\left\{\frac{\partial}{\partial t}\left[e\mathbf{A} + Mv_{\parallel}\mathbf{b}\right] - \nabla\left[\phi \mp p_{\alpha}\omega_c\right]\right\} \\ &+ \dot{\mathbf{x}}_{gc}\times\left\{\nabla\times\left[e\mathbf{A} + Mv_{\parallel}\mathbf{b}\right]\right\} \ . \end{aligned} \tag{2.54}$$

Equation (2.54) is sometimes compactified by defining

$$e\mathbf{A}^{*} \equiv e\mathbf{A} + Mv_{\parallel}\mathbf{b} \ , \quad \phi^{*} \equiv \phi \mp p_{\alpha}\omega_c \ , \tag{2.55}$$

with

$$\mathbf{E}^{*} = -\frac{\partial\mathbf{A}^{*}}{\partial t} - \nabla\phi^{*} = \mathbf{E} - \frac{M}{e}v_{\parallel}\frac{\partial\mathbf{b}}{\partial t} \mp p_{\alpha}\nabla\omega_c \ , \tag{2.56}$$

and

$$\mathbf{B}^{*} = \nabla\times\mathbf{A}^{*} = \mathbf{B} + \frac{M}{e}v_{\parallel}\nabla\times\mathbf{b} \ . \tag{2.57}$$

It then becomes

$$M\dot{v}_{\parallel}\mathbf{b} = e\left[\mathbf{E}^{*} + \dot{\mathbf{x}}_{gc}\times\mathbf{B}^{*}\right] \ . \tag{2.58}$$

Equation (2.58) has a deceivably simple form. It is most easily analyzed via application of the operations $\mathbf{B}^{*}\cdot$ and $\mathbf{b}\times$, which yields expressions for $\dot{v}_{\parallel}$ and $\dot{\mathbf{x}}_{gc}$. If the resulting equations are evaluated explicitly to first order in δ, one finds

$$M\dot{v}_{\parallel} = eE_{\parallel} - \mu\mathbf{b}\cdot\nabla B \tag{2.59}$$

and

$$\dot{\mathbf{x}}_{gc} = v_{\parallel}\mathbf{b} + \mathbf{v}_D \ , \tag{2.60}$$

where the drift velocity now consists of three pieces,

$$\mathbf{v}_D = \mathbf{v}_E + \mathbf{v}_{\nabla B} + \mathbf{v}_\kappa \ . \tag{2.61}$$

Apart from the previously discussed $\mathbf{E} \times \mathbf{B}$-drift given in (2.37), these drifts are known as the ∇B- and the curvature drift. They are given by

$$\mathbf{v}_{\nabla B} = \pm \frac{v_L^2}{2\omega_c} \frac{\mathbf{b} \times \nabla B}{B} \ , \quad \mathbf{v}_\kappa = \pm \frac{v_\parallel^2}{\omega_c} \mathbf{b} \times \vec{\kappa} \ . \tag{2.62}$$

In the equation for $\mathbf{v}_\kappa$,

$$\vec{\kappa} \equiv (\mathbf{b} \cdot \nabla)\, \mathbf{b} = -\mathbf{b} \times (\nabla \times \mathbf{b}) \tag{2.63}$$

is the curvature of the magnetic field evaluated at the guiding center position. It may also be written as

$$\vec{\kappa} = -\frac{\mathbf{R}_c}{R_c^2} \ , \tag{2.64}$$

where R_c is the radius of curvature of the magnetic field and $\mathbf{R}_c$ is the vector pointing radially outwards from the center of curvature to the guiding center.

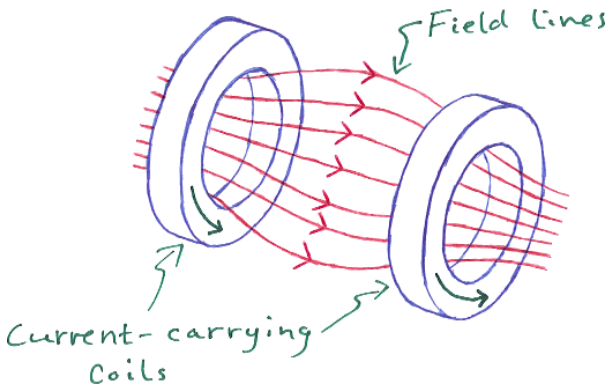

Figure 2.1: A magnetic mirror. A pair of current-carrying coils generate an inhomogeneous magnetic field with two maxima. Particles with small enough $v_\parallel$ are trapped between the two maxima of B, whereas particles with $E > \mu B_{\max}$ escape through the coils.

A particularly neat application of guiding center theory can be found in the analysis of the so called *magnetic mirror*, on display in Figure 2.1. Such devices operate in steady state by means of merely a non-uniform magnetic field $\mathbf{B}$, generated by two circular, current-carrying coils. The system is rotationally symmetric around the axis connecting the center of the two coils, and the magnetic field strength exhibits a minimum midway between the coils and maxima at the coil positions. Since the guiding center Hamiltonian (2.53)

does not depend explicitly on time, the guiding center energy (actually the *kinetic* energy in the absence of electric fields)

$$E = \frac{M}{2} v_{\parallel}^2 + \mu B \tag{2.65}$$

is a constant of motion. Solving for $v_{\parallel}$, we find

$$v_{\parallel} = \pm \sqrt{\frac{2}{M} \left(E - \mu B \right)} \, , \tag{2.66}$$

which changes only due to the variation in B when μ is an adiabatic invariant. Therefore, as a particle moves in the magnetic mirror towards a maximum of B, its parallel velocity decreases. If the ratio $v_{\parallel}/v_{\perp}$ at, say, the midpoint is sufficiently low,

$$\left. \frac{v_{\parallel}}{v_{\perp}} \right|_{\text{midpoint}} \leq \sqrt{\frac{B_{\max} - B_{\min}}{B_{\min}}} \, , \tag{2.67}$$

the parallel velocity vanishes within the machine and the motion reverses. As a result, mirror machines can be used to confine charged particles. A major drawback with this scheme, however, is that particles that do not satisfy (2.67) are immediately lost, and eventually small-angle Coulomb collisions will have scattered a large majority of the originally confined particle population onto such unconfined orbits.

2.2 Particle Orbits in Tokamaks

Tokamaks are toroidal devices designed to confine high temperature plasmas through the action of magnetic fields, loosely speaking much like a number of mirror machines (see Section 2.1.3) placed in line in a circular fashion, so that the last mirror closes on the first. A detailed design drawing for the planned tokamak ITER was shown in Figure 1.1 in Section 1. Another example, a cross sectional drawing of the JET experiment, is on display in Figure 2.2.

Tokamak plasma particles move predominantly along the magnetic field, and the actual geometry of the device prevents them from leaving the vessel by making the field lines continuously encircle the central, toroidal axis. The peculiar doughnut shape derives from the mathematical theorem that the only geometrical surfaces (such as the outer boundary of a magnetic confinement device) that can be covered by a non-vanishing vector field (such as a confining magnetic field) are those of torii. In fact, the entire tokamak volume is completely filled with nested such *magnetic flux surfaces*,[2] each carrying a

[2]Plasma turbulence may of course destroy some, or all, of the flux surfaces. We are considering, here and throughout this thesis, the ideal case with no turbulence and well defined flux surfaces.

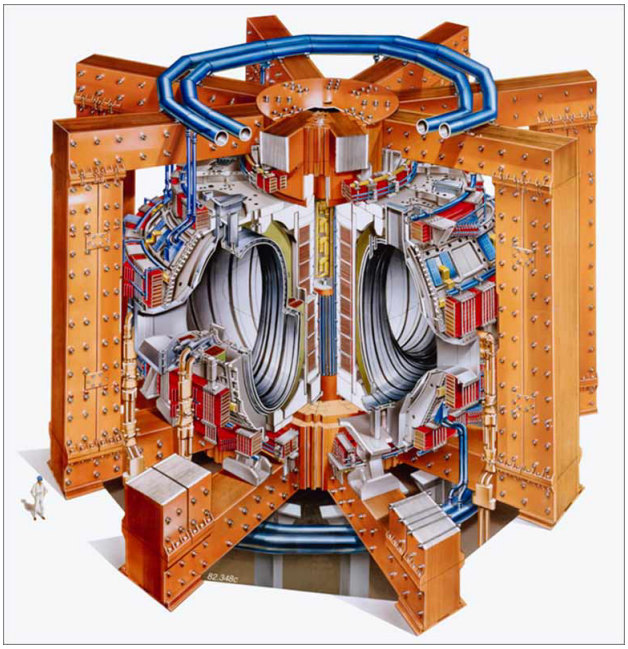

Figure 2.2: Design plan for the Joint European Torus (JET), the largest currently operational tokamak experiment in the world.

set of magnetic field lines that wind around the torus toroidally (the long way around) and poloidally (the short way around). The plasma particles do not follow the field lines exactly, however. As previously discussed, the particles gyrate around their guiding center positions at the cyclotron frequency ω_c. Moreover, the guiding centers themselves are allowed to slowly drift across the magnetic field lines as a result of inhomogeneities in and curvature of the magnetic field, so the guiding center orbits also deviate somewhat from the magnetic flux surfaces.

2.2.1 Toroidal Coordinates

In Figure 2.3 is shown the cross section of a circular tokamak, including two sets of coordinates. The toroidal coordinates (r, θ, ζ) relate to the usual cylindrical coordinates (R, φ, z) as

$$\begin{cases} R = R_0 + r\cos\theta \\ \varphi = -\zeta \\ z = r\sin\theta \end{cases} \quad \Longleftrightarrow \quad \begin{cases} r = \sqrt{z^2 + (R - R_0)^2} \\ \theta = \arctan\frac{z}{R - R_0} \\ \zeta = -\varphi \end{cases} \tag{2.68}$$

Here, R_0 is the value of the cylindrical radius R at the geometrical center of the circular cross section. The cylindrical coordinates relate to ordinary

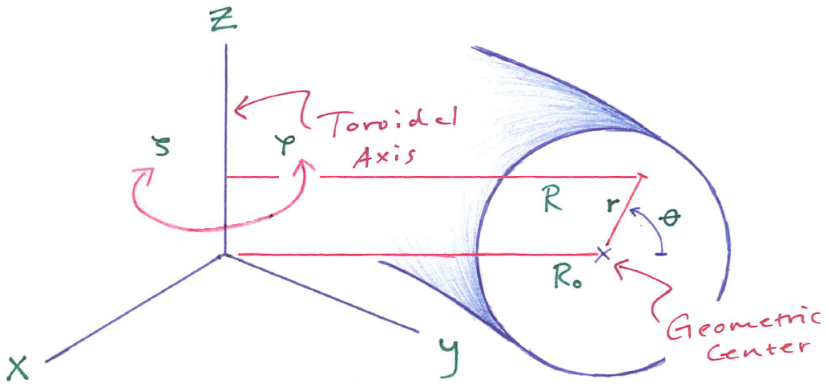

Figure 2.3: Cross section of a circular tokamak. The set (R, φ, z) are the usual cylindrical coordinates, and (r, θ, ζ) are so called toroidal coordinates, given by equation (2.68). The distance R_0 from the *toroidal axis* to the geometric center of the cross section is called the *major* radius. On the contrary, the *minor* radius r denotes radial distances within the cross section, from the geometric center out to the edge of the device.

Cartesians in the usual way,

$$\begin{cases} x = R\cos\varphi \\ y = R\sin\varphi \\ z = z \end{cases} \quad \Longleftrightarrow \quad \begin{cases} R = \sqrt{x^2 + y^2} \\ \varphi = \arctan\frac{y}{x} \\ z = z \end{cases} \tag{2.69}$$

Although modern tokamak cross sections in general are D-shaped, we will nevertheless use this idealized, circular approximation throughout the main part of this thesis. Of course the coordinates in (2.68) and (2.69) may well be used to describe any type of cross section. However, their use is most fruitful when the cross section is indeed circular and, moreover, the nested magnetic flux surfaces inside the torus align as concentric tubes centered at R_0. A natural generalization towards the more accurate D-shape is to include parameters that describe ellipticity, triangularity and offset of each magnetic flux surface from the geometrical center of the cross section. The latter effect will be discussed in more detail in Chapter 4, where such an offset will be needed in order to properly account for toroidal effects.

2.2.2 Magnetic Field Structure

The equilibrium magnetic field in a tokamak is a combination of two field components, $\mathbf{B}_T$ and $\mathbf{B}_P$. The larger part $\mathbf{B}_T$ points in the toroidal direction, along ζ. It is generated entirely by currents running in a set of exterior coils that encircle the torus poloidally, along θ. While a finite number, say n, of such

toroidal field coils naturally produces a magnetic field structure with an n-fold rotational symmetry around the toroidal axis, we will throughout this thesis make the simplifying assumption that tokamaks are completely axisymmetric, i.e. that all equilibrium quantities satisfy

$$\frac{\partial}{\partial \zeta}(\dots) = 0 \ . \tag{2.70}$$

The smaller component $\mathbf{B}_P$ points in the poloidal θ-direction. It is due to a net toroidal current in the plasma, generated inductively by transformer action and/or by non-inductive current drive schemes such as NBI and RF heating. The total magnetic field therefore has a helical structure, with field lines that encircle the torus toroidally and poloidally as they trace out nested magnetic flux surfaces across which there is no magnetic flux. The field lines may eventually close upon themselves (after many, many revolutions, or sometimes after just a few), or they may not (in which case a single field line densely covers the surface).

It is clear on a conceptual level what is the effect of the poloidal field $\mathbf{B}_P$ and why it is needed: A toroidal component $\mathbf{B}_T$ alone would indeed exhibit field lines that close upon themselves after a toroidal revolution. However, in the absence of plasma currents and electric fields, one can integrate Ampére's law,

$$\nabla \times \mathbf{B} = \mu_0 \mathbf{J} + \mu_0 \epsilon_0 \frac{\partial \mathbf{E}}{\partial t} \ , \tag{2.71}$$

written here in its post-Maxwell, generalized version that includes the displacement current, along a path that encircles the toroidal axis at constant radius R. Employing Stoke's theorem, one finds

$$B_T = \frac{\mu_0 I_C}{2\pi R} \ , \tag{2.72}$$

where I_C is the total current in all the exterior coils. As discussed in Section 2.1.3, the inverse R-scaling introduces particle drifts. Specifically, the ∇B- and curvature drifts will jointly result in a vertical separation of ions and electrons that sets up an associated electric field. The resulting $\mathbf{E} \times \mathbf{B}$-drift rapidly transport particles of both species radially outwards. A convenient way to counteract this drift-induced transport is to introduce the small component $\mathbf{B}_P$. With the resulting helical magnetic field, the unwanted drifts average out as the particles follow the field lines around the torus, not only toroidally but also poloidally.

There is a generic class of curvilinear, toroidal coordinates, so called *magnetic flux coordinates* or *straight field line coordinates*, which are often employed for the description of toroidal plasmas. Such a set (r_f, θ_f, ζ_f) is designed as to satisfy the following two requirements: 1) The radial flux coordinate r_f

is to remain constant on each magnetic flux surface; 2) the magnetic field lines are to form straight lines (on the flux surfaces) in the poloidal and toroidal flux angles θ_f and ζ_f. Mathematically, the requirement on r_f can be formulated as

$$\nabla r_f \cdot \mathbf{B} = 0 \ , \tag{2.73}$$

so that any monotonic function of r_f alone serves well to label magnetic flux surfaces (and is accordingly called a *flux label*). The relation (2.73) also means that the contravariant component B^{r_f} vanishes identically throughout the device. Thus, the total magnetic field

$$\mathbf{B} = \mathbf{B}_P + \mathbf{B}_T \tag{2.74}$$

may be expanded in terms of covariant flux coordinate basis vectors as

$$\mathbf{B}_P = B^{\theta_f} \frac{\nabla \zeta_f \times \nabla r_f}{J_f} \ , \quad \mathbf{B}_T = B^{\zeta_f} \frac{\nabla r_f \times \nabla \theta_f}{J_f} \ , \tag{2.75}$$

where

$$J_f = \nabla r_f \cdot \nabla \theta_f \times \nabla \zeta_f \tag{2.76}$$

is the flux coordinate Jacobian. The second requirement, that the magnetic field lines are to form straight lines on the magnetic flux surfaces, can be expressed through an equation of the form

$$\zeta_f = q\left(r_f\right) \theta_f + \text{Const.} \ , \tag{2.77}$$

where q is a flux label commonly referred to as the *safety factor*. Upon comparing equation (2.77) with the equation for a magnetic field line,

$$\frac{d\zeta_f}{d\theta_f} = \frac{\mathbf{B} \cdot \nabla \zeta_f}{\mathbf{B} \cdot \nabla \theta_f} = \frac{B^{\zeta_f}}{B^{\theta_f}} = q \ , \tag{2.78}$$

it is obvious that the total magnetic field can be written as

$$\mathbf{B} = \frac{B^{\theta_f}}{J_f} \nabla \left(\zeta_f - q \theta_f\right) \times \nabla r_f \ . \tag{2.79}$$

It is important to understand that r_f does not measure the radial distance from the geometric center of the vessel, as does the usual toroidal radius r. Rather, r_f denotes distances from the innermost, degenerate flux surface, the so called *magnetic axis*, located at the cylindrical radius $R = R_A$. We also note that the usual toroidal coordinate system given in (2.68) is not flux-type. To begin with, general plasma equilibria do not have circular flux surfaces centered at R_0, so usually r is not a flux label. Moreover, even when the flux surfaces are

circular and concentric, the usual toroidal angle θ is not a flux angle, simply because it does not yield straight field lines.

Flux coordinates are extra useful for the description of axisymmetric toroidal systems, in which case identifying ζ_f with the usual toroidal coordinate ζ simplifies the analysis considerably. The co- and contravariant basis vectors in the toroidal direction then relate to the unit vector $\hat{\zeta}$ as

$$\nabla\zeta = \frac{1}{R^2}\frac{\nabla\zeta \times \nabla r_f}{J_f} = \frac{\hat{\zeta}}{R} \ . \tag{2.80}$$

Moreover, axisymmetry renders

$$\nabla \cdot \mathbf{B} = J_f \frac{\partial}{\partial \theta_f}\left(\frac{B^{\theta_f}}{J_f}\right) = 0 \ , \tag{2.81}$$

which shows that B^{θ_f}/J_f is a flux label in axisymmetric systems. We can then define another flux label,

$$\Psi_P\left(r_f\right) \equiv \int_0^{r_f} \frac{B^{\theta_f}}{J_f}\, dr'_f \ , \tag{2.82}$$

such that the magnetic field becomes

$$\mathbf{B} = \nabla\left(\zeta - q\theta_f\right) \times \nabla\Psi_P \ . \tag{2.83}$$

In fact, Ψ_P constitutes a slight renormalization of the *poloidal magnetic flux*,

$$F_P\left(r_f\right) \equiv \frac{1}{2\pi}\oint_{V\left(r_f\right)} \mathbf{B}\cdot\nabla\theta_f\, d^3\mathbf{x} = 2\pi\Psi_P\left(r_f\right) \ , \tag{2.84}$$

through a ribbon-like surface that extends toroidally around the tokamak from its magnetic axis to the flux surface $\partial V\left(r_f\right)$, enclosing the volume $V\left(r_f\right)$. If we also introduce the *toroidal magnetic flux* through any cross sectional disk whose rim lies on $\partial V\left(r_f\right)$, defined similarly to F_P as

$$F_T\left(r_f\right) \equiv \frac{1}{2\pi}\oint_{V\left(r_f\right)} \mathbf{B}\cdot\nabla\zeta_f\, d^3\mathbf{x} \ , \tag{2.85}$$

the safety factor may be written as the ratio

$$q\left(r_f\right) = \frac{dF_T/dr_f}{dF_P/dr_f} = \frac{dF_T}{dF_P} \ . \tag{2.86}$$

Equation (2.86) is the usual definition of the safety factor. As such, it is always a flux label, regardless of the choice of coordinates, the purpose of which is to measure the average pitch of the magnetic field lines on a flux surface (the average number of toroidal circuits per poloidal circuit). In flux coordinates, however, the field lines are straight, so q measures not the average but local field line pitch. If q is irrational, the surface is densely covered by just one field line that never closes on itself. On the contrary, on surfaces where q is rational the field lines eventually close after, say, n poloidal and m toroidal circuits, and the rational value of q equals the ratio m/n.

The introduction of F_T also enables simple representations for the magnetic field strength and vector potential in terms of the poloidal and toroidal magnetic fluxes. If we first define the renormalized toroidal flux $\Psi_T \equiv F_T/2\pi$, the safety factor reads

$$q = \frac{d\Psi_T/dr}{d\Psi_P/dr} = \frac{d\Psi_T}{d\Psi_P} \ , \tag{2.87}$$

and the magnetic field strength becomes

$$\mathbf{B} = \nabla\Psi_T \times \nabla\theta_f + \nabla\zeta \times \nabla\Psi_P \ . \tag{2.88}$$

Now, in a gauge where the covariant component A_{r_f} vanishes,[3] i.e. where

$$\mathbf{A} = A_{\theta_f}\nabla\theta_f + A_\zeta\nabla\zeta \ , \tag{2.89}$$

the magnetic field strength relates to the covariant components of $\mathbf{A}$ via

$$\mathbf{B} = \nabla \times \mathbf{A} = \nabla A_{\theta_f} \times \theta_f + \nabla A_\zeta \times \nabla\zeta \ . \tag{2.90}$$

Comparing with (2.88), it is easily seen that $A_{\theta_f} = \Psi_T$ and $A_\zeta = -\Psi_P$.

[3]Such a gauge can always be chosen, in fact regardless of the choice of coordinates. For instance, with unspecified toroidal coordinates (r, θ, ζ), in which the magnetic vector potential has the generic form

$$\mathbf{A} = A_r\nabla r + A_\theta\nabla\theta + A_\zeta\nabla\zeta \ ,$$

one may define

$$\eta\,(r,\theta,\zeta) \equiv \int^r A_r\,(r',\theta,\zeta)\,dr' \ , \quad A'_\theta = A_\theta - \frac{\partial\eta}{\partial\theta} \ , \quad A'_\zeta = A_\zeta - \frac{\partial\eta}{\partial\zeta} \ ,$$

which transforms $\mathbf{A}$ to

$$\mathbf{A} = A'_\theta\nabla\theta + A'_\zeta\nabla\zeta + \nabla\eta \ .$$

The third term on the right hand side may of course be removed via a gauge transformation, which puts $\mathbf{A}$ in the desired form.

To proceed further with the flux coordinate formalism, we need to consider the governing equations for toroidal plasma configurations in static equilibrium. The simplest and most important class of toroidal equilibria are characterized by a force balance equation of the form

$$\mathbf{J} \times \mathbf{B} = \nabla P \ , \tag{2.91}$$

where the plasma current density is given by Ampére's law for static fields,

$$\mu_0 \mathbf{J} = \nabla \times \mathbf{B} \ , \tag{2.92}$$

and P is the total plasma pressure. The set of equations for $\mathbf{B}$, $\mathbf{J}$ and P is closed by means of the Maxwell equation

$$\nabla \cdot \mathbf{B} = 0 \ . \tag{2.93}$$

Equation (2.91) immediately tells us that P is a flux label,

$$\nabla P \cdot \mathbf{B} = 0 \quad \Longrightarrow \ P = P\left(r_f\right) \ . \tag{2.94}$$

Hence, the magnetic surfaces are also surfaces of constant plasma pressure. Moreover, (2.91) reveals that there is no net flux of plasma particles across the magnetic flux surfaces,

$$\nabla P \cdot \mathbf{J} = \frac{dP}{dr_f} J^{r_f} = 0 \quad \Longrightarrow \ J^{r_f} = 0 \ , \tag{2.95}$$

a property sometimes referred to as *ambipolarity*. Thus, the plasma current lines are confined to lie in the magnetic flux surfaces (although they are not parallel to the magnetic field lines). When the magnetic field is axisymmetric, Ampére's law provides additional information on the magnetic field itself: Evaluation of the contravariant r_f-component of equation (2.92) gives

$$J^{r_f} = \frac{J_f}{\mu_0} \frac{\partial B_\zeta}{\partial \theta_f} = 0 \ , \tag{2.96}$$

which reveals that the covariant ζ-component of $\mathbf{B}$ is a flux label, usually denoted $B_\zeta = I\left(r_f\right)$. The total magnetic field can therefore be written in the mixed representation form

$$\mathbf{B} = I \nabla \zeta + \nabla \zeta \times \nabla \Psi_P = I \nabla \zeta + B^{\theta_f} \frac{\nabla \zeta \times \nabla r_f}{J_f} \ , \tag{2.97}$$

whose magnitude evaluates to

$$B^2 = \frac{I^2}{R^2} \left[1 + \frac{1}{R^2 q^2} \left| \frac{\nabla \zeta \times \nabla r_f}{J_f} \right|^2 \right] \ . \tag{2.98}$$

Note that the covariant poloidal basis vector in toroidal systems typically satisfies

$$\left|\frac{\nabla\zeta\times\nabla r_f}{J_f}\right|\sim r_f\ , \tag{2.99}$$

Moreover, the flux label I is closely related to the total exterior current in the toroidal field coils, I_C, via the expression

$$I\left(r_f\right)=\frac{\mu_0}{2\pi}\Big[I_C+\big(I_P\left(a\right)-I_P\left(r_f\right)\big)\Big]\ . \tag{2.100}$$

Here, $I_P\left(r_f\right)$ is the total poloidal plasma current through a ribbon-like surface extending throughout the torus from the magnetic axis to the magnetic flux surface labeled with r_f, and a denotes the value of r_f at the outermost flux surface.

2.2.3 Large Aspect Ratio Approximation

The flux coordinates discussed in the preceding section have so far given many general results and provided useful information on toroidal plasmas. However, in order to actually determine r_f and θ_f for a specific axisymmetric tokamak equilibrium, one has to resort to numerical modeling. Such an analysis will not be presented here. Rather, we will proceed in an approximate fashion by invoking some idealized assumptions, the purposes of which are to obtain an approximate analytical formula for Ψ in terms of R. Such a relation is needed for the discussion of tokamak particle orbits in the following section.

We therefore restrict our analysis to the case of circular flux surfaces, all commonly centered at $R=R_0$. Under these assumptions, the toroidal coordinates (2.68) are almost flux-type. Indeed, r labels the flux surfaces, so we can set $r_f=r$ and $R_0=R_A$. The relation between θ_f and θ is more involved, and generally has to be solved for numerically. However, if we assume that the ratio of major to minor radius is large throughout the device, so that the *inverse aspect ratio* satisfies

$$\epsilon\equiv\frac{r}{R_A}\ll 1\ , \tag{2.101}$$

and that the plasma-β, the ratio of kinetic to magnetic pressure, is even smaller,

$$\beta\equiv\frac{2\mu_0 P}{B^2}\sim\epsilon^2\ , \tag{2.102}$$

then there is an analytical expression for θ_f in terms of θ that holds through first order in ϵ, namely

$$\theta_f=\theta-\epsilon\sin\theta\ . \tag{2.103}$$

The former assumptions are not particularly well justified in modern tokamaks. As previously discussed, the generic cross section is D-shaped rather than circular, with an aspect ratio of major to minor radius around 3.[4] Nevertheless, we will use the large aspect ratio, circular cross section approximation throughout this chapter in order to make analytical progress. The low β assumption is however far more accurate. Tokamak equilibrium pressures are indeed limited by stability regards to β-values of a few percent [16, 17].[5]

The next few calculations will be carried out perturbatively to first order in ϵ. That is, terms on the order of $\mathcal{O}(\epsilon^2)$ and smaller will be neglected. In this fashion, it can be shown that in a tokamak, $I_P/I_C \sim \beta$, so that

$$I(r_f) \approx \frac{\mu_0 I_C}{2\pi} = \text{Const.} \tag{2.104}$$

Since the second term inside the bracket on the right hand side of (2.98) is $\mathcal{O}(\epsilon^2)$ as compared to the first, we therefore have

$$B \approx \frac{\mu_0 I_C}{2\pi R} = \frac{B_A R_A}{R} \ , \tag{2.105}$$

where B_A is the magnitude of the total magnetic field evaluated at the magnetic axis. With (2.105), the poloidal and toroidal magnetic fluxes become, to first order in ϵ,

$$\Psi_P \approx B_A \int_0^r \frac{r'\,dr'}{q(r')} \ , \quad \Psi_T \approx \frac{B_A r^2}{2} \ , \tag{2.106}$$

and the expression (2.86) for the safety factor becomes

$$q = \frac{d\Psi_T/dr}{d\Psi_P/dr} = B_A \frac{r dr}{d\Psi_P} \ . \tag{2.107}$$

Viewing q as a function of Ψ_P rather than r, $q = q(r(\Psi_P))$, and expanding it in powers of Ψ_P, the solution to (2.107) reads

$$r^2 = \frac{2}{B_A}\left[q_A \Psi_p + \frac{1}{2}\left.\frac{dq}{d\Psi_p}\right|_{\Psi_p=0} \Psi_p^2 + \frac{1}{6}\left.\frac{d^2 q}{d\Psi_p^2}\right|_{\Psi_p=0} \Psi_p^3 + \dots \right] \ , \tag{2.108}$$

[4] As examples, JET has an aspect ratio of 3, whereas ITER will have the aspect ratio 3.1. There are also *spherical tokamaks*, with aspect ratios ~ 1. Such devices are certainly not covered by the present analysis.

[5] In recent years, tokamak experimentalists have nevertheless found ways to slightly stretch the limitations on β. Careful shaping of the plasma cross section by an elongation in the vertical direction and a bean-like, D-shaping of the flux surfaces have increased the conceivable values of β [18]. A more intriguing method of increasing β was found through the discovery of so called *advanced scenarios*, in which external heating schemes are applied as to create a non-monotonic radial current profile with a local minimum rather than a maximum at the magnetic axis. Such *current-hole* configurations exhibit potent transport barriers at mid-minor radius, within which the plasma confinement improves significantly.

where $q_A \equiv q\left(\Psi_p = 0\right)$. Although the safety factor in general varies throughout the tokamak, the constant model $q = q_A$ enables a simple qualitative description of the guiding center orbits. We then have

$$r^2 \approx \frac{2q_A}{B_A}\Psi_p \ , \tag{2.109}$$

which may be combined with the expression for z^2 in equation (2.68) to give

$$z^2 = \frac{2q_A}{B_A}\Psi_p - \left(R - R_A\right)^2 \ . \tag{2.110}$$

Note that the vertical midplane of the tokamak is then described by an equation of the form

$$\Psi_p = \frac{B_A}{2q_A}\left(R - R_A\right)^2 \ , \tag{2.111}$$

i.e. a parabola in (R, Ψ_p)-space.

The above calculations are not quite rigorous. A proper $\mathcal{O}\left(\epsilon\right)$-description of a large aspect ratio, low-β tokamak equilibrium should really include a small, gradual inward (towards smaller R) shift of the magnetic flux surfaces from the geometric center of the cross section, the so called *Shafranov shift*. While this shift itself is indeed $\mathcal{O}\left(\epsilon^2\right)$, and therefore most often rigorously neglected, its radial derivative is not quite that small. It actually enters the calculations already at $\mathcal{O}\left(\epsilon\right)$, and must therefore be taken properly into account e.g. in the description of toroidal Alfvén eigenmodes in Chapter 4, since the existence of such modes relies intrinsically on toroidal effects. For the following discussion of tokamak particle guiding center trajectories, however, the proposed "cylindrical" approximation with concentric flux surfaces suffices well.

2.2.4 Tokamak Guiding Center Trajectories

Guiding center motion in axisymmetric, toroidal equilibria is governed by the phase space Lagrangian (2.52). With magnetic flux coordinates (r_f, θ_f, ζ) the phase space coordinates are $\left(r_f, \theta_f, \zeta, v_\parallel, p_\alpha, \alpha\right)$, and one should substitute into the general form (2.52) the field structure discussed in the previous section, i.e. $\mathbf{A}$ and $\mathbf{B}$ as given in equations (2.89) and (2.97), and $\phi = 0$. However, as shown in [19], it is always possible to choose the flux coordinate θ_f so that the covariant component B_{r_f} vanishes (in addition to B^{r_f}, which vanishes as a means of how flux coordinates were defined in Section 2.2.2). Then, the guiding center Lagrangian (2.52) becomes particularly simple,

$$\mathcal{L}_{gc} = \left[Mv_\parallel \frac{B_{\theta_f}}{B} + e\Psi_T\right]\dot{\theta}_f + \left[Mv_\parallel \frac{B_\zeta}{B} - e\Psi_P\right]\dot{\zeta} + p_\alpha\dot{\alpha} - \mathcal{H}_{gc} \ , \tag{2.112}$$

with

$$\mathcal{H}_{gc} = \frac{M}{2} v_\parallel^2 \mp p_\alpha \omega_c \ . \tag{2.113}$$

From the symplectic part of (2.112), i.e. the first three terms $\mathcal{L}_{gc} + \mathcal{H}_{gc}$, it is clear that the angular coordinates θ_f, ζ and α are canonical, with conjugate momenta

$$p_{\theta_f} = M v_\parallel \frac{B_{\theta_f}}{B} + e\Psi_T \ , \quad p_\zeta = M v_\parallel \frac{B_\zeta}{B} - e\Psi_P \ , \quad p_\alpha = \frac{M}{e}\mu \ . \tag{2.114}$$

Generally, the ratio B_{θ_f}/B_ζ is small in axisymmetric toroidal devices,

$$\frac{B_{\theta_f}}{B_\zeta} = \frac{1}{qR^2} \left| \frac{\nabla\zeta \times \nabla r_f}{J_f} \right|^2 \sim \frac{r_f^2}{R^2} \ , \tag{2.115}$$

so the first term in p_{θ_f} is negligible as compared with the first term in p_ζ. On the other hand, the first term in p_ζ represents the effect of deviations in the guiding center orbits from the magnetic flux surfaces, due to the cross field drift velocity (2.61). As such, it is in itself small as compared to the second term in p_ζ, except for highly energetic particles (especially those close to the magnetic axis, with r_f small). With these remarks taken into account, the guiding center Lagrangian for particle motion in a large aspect ratio, low β tokamak becomes, to first order in ϵ,

$$\mathcal{L}_{gc} = p_\theta \dot{\theta} + p_\zeta \dot{\zeta} + p_\alpha \dot{\alpha} - \mathcal{H}_{gc} \ . \tag{2.116}$$

Here,

$$p_\theta = e\Psi_T(r) \ , \quad p_\zeta = MR(r,\theta)\, v_\parallel - e\Psi_P(r) \ , \quad p_\alpha = \frac{M}{e}\mu \ , \tag{2.117}$$

and the form of $\mathcal{H}$ remains as given in (2.113),

$$\mathcal{H}_{gc} = \frac{M}{2} v_\parallel^2 \mp p_\alpha \omega_c(r,\theta) \ . \tag{2.118}$$

We have written these expressions explicitly in terms of their dependencies on the guiding center coordinates, which have now been chosen as the usual toroidal coordinates (r, θ, ζ), assuming that the flux surfaces are circular and concentric. It is noteworthy that these simple coordinates indeed satisfy $\nabla r \cdot \nabla\theta = 0$, and thus have $B_r = 0$.

The equations of motion for the guiding centers are found via the Euler-Lagrange equations for each phase space coordinate. In reverse order, they give

$$\dot{p}_\alpha = 0 \ , \quad \dot{\alpha} = \mp\omega_c \ , \quad \dot{\zeta} = \frac{v_\parallel}{R} \ , \quad \dot{p}_\zeta = 0 \ , \tag{2.119}$$

$$e\frac{d\Psi_T}{dr}\dot{r} = -\frac{r\sin\theta}{R}\left[E + \frac{M}{2}v_\parallel^2\right] \ , \quad e\frac{d\Psi_P}{dr}\left[q\dot{\theta} - \dot{\zeta}\right] + \frac{\cos\theta}{R}\left[E + \frac{M}{2}v_\parallel^2\right] = 0 \ .$$

Here, E denotes the instantaneous value of the guiding center Hamiltonian $\mathcal{H}_{gc}$, which is a constant of motion since the time variable t is cyclic. Upon substitution of the magnetic fluxes (2.106), we obtain

$$\dot{r} = \mp \frac{\sin\theta}{\omega_{cA} R} \left[\frac{E}{M} + \frac{1}{2} v_\parallel^2 \right] , \tag{2.120a}$$

$$\dot{\theta} = \frac{v_\parallel}{qR} \mp \frac{\cos\theta}{\omega_{cA} r R} \left[\frac{E}{M} + \frac{1}{2} v_\parallel^2 \right] , \tag{2.120b}$$

$$\dot{\zeta} = \frac{v_\parallel}{R} . \tag{2.120c}$$

These equations can, in principle, be integrated to give expressions for the particle guiding center position. In practice, however, the integrations can only be carried out analytically if the right hand side of (2.120a) and the second term in (2.120b), representing the drifts across the magnetic field, are both small. Such an analysis is presented at the end of this section.

A more intuitive and direct approach, one that does not rely on the "small drift assumption", is to utilize directly the constancy of E, p_ζ and p_α, or rather $v \equiv \sqrt{2E/M}$, p_ζ and $\mu = -e p_\alpha / M$. To this end, we define the dimensionless invariants

$$\lambda \equiv \frac{\mu B_A}{E} = \frac{R}{R_A} \left[1 - \chi^2 \right] , \tag{2.121a}$$

$$J \equiv -\frac{p_\zeta}{M v R_A} = \psi - \frac{R}{R_A} \chi , \tag{2.121b}$$

$$w \equiv \pm \frac{2 q_A v}{\omega_{cA} R_A} , \tag{2.121c}$$

where $\chi \equiv v_\parallel / v \leq 1$ is the inverse ratio of total guiding center speed to that along the magnetic field, the dimensionless poloidal magnetic flux is $\psi \equiv e\Psi_P / M v R_A$ and the $\pm$ applies for ions/electrons, respectively. Note that the so called pitch-angle variable λ always satisfies $0 \leq \lambda \leq B_A / B_{\min}$, where $B_{\min}$ denotes the minimum magnitude of the magnetic field strength in the device, attained at the very outboard edge of the outermost flux surface, i.e. at $r = a$, $\theta = 0$. Hence, to first order in ϵ, $0 \leq \lambda \leq 1 + a/R_A$. If we now define the dimensionless radial variable $x \equiv R/R_A$, J and λ may be combined to give

$$\left(J - \psi \right)^2 = x \left(x - \lambda \right) , \tag{2.122}$$

which can be written as

$$\left(x - \lambda/2 \right)^2 - \left(\psi - J \right)^2 = \frac{\lambda^2}{4} . \tag{2.123}$$

Given values for J and λ, equation (2.123) describes a hyperbola in the (x, ψ)-plane. Examples of such hyperbolas are shown in Figures 2.4 – 2.6, alongside the parabola

$$\psi = \frac{1}{w}\left(x-1\right)^2 \ , \tag{2.124}$$

obtained from equation (2.111). Since equation (2.124) depicts values for ψ at which $z = 0$, the intersections of these two types of curves represent radii where particles pass the vertical midplane of the cross section. The corresponding guiding center orbits are given by solving (2.122) for ψ, and combining the result with equation (2.110). Solving for the dimensionless vertical coordinate $\xi = z/R_A$ gives

$$\xi = \pm\left\{w\left[J \pm \sqrt{x\left(x-\lambda\right)}\right] - \left(x-1\right)^2\right\}^{1/2} \ . \tag{2.125}$$

Such trajectories are plotted in the complementary, lower graphs in Figures 2.4 – 2.6.

As seen in Figures 2.4 – 2.6, there are several different types of orbits. The simplest category consists of particles that encircle both the toroidal and magnetic axis, so called *passing particles*. They are in majority in a large aspect ratio tokamak, and have a relatively small value of λ,[6]

$$0 \leq \lambda \leq \frac{B_A}{B_{\max}} = 1 - a/R_A + \mathcal{O}\left(\epsilon^2\right) \ . \tag{2.126}$$

Here, $B_{\max}$ is the maximum magnitude of the magnetic field strength, attained at $r = a$, $\theta = \pi$. A typical passing particle orbit is on display to the left in Figure 2.4. Note that the guiding center of a passing particle always remain fairly close to the same magnetic flux surface. Larger values of λ result in entirely different types of orbits. In particular, particles that satisfy

$$\frac{B_A}{B_{\max}} < \lambda \leq \frac{B_A}{B_{\min}} = 1 + a/R_A + \mathcal{O}\left(\epsilon^2\right) \tag{2.127}$$

do not revolve all the way around in the poloidal direction. As their guiding centers approach the inboard, large field side of the torus, they slow down due to the decelerating mirror force $-\mu\nabla_\parallel B$, much like the confined particle population in a mirror machine, cf. Section 2.1.3. They eventually come to a halt when $v_\parallel = 0$, at which point the motion parallel to the magnetic field reverses. Such *trapped* orbits are often called *bananas*, due to their characteristic shapes when projected on a cross section with constant toroidal angle ζ, see e.g. the graphs on the right in Figure 2.4. The parallel velocity $v_\parallel$ is positive (along $\nabla\zeta$ and $\nabla\theta$) on the outside and negative on the inside of the

[6] Alternatively, a relatively large ratio $v_\parallel/v$.

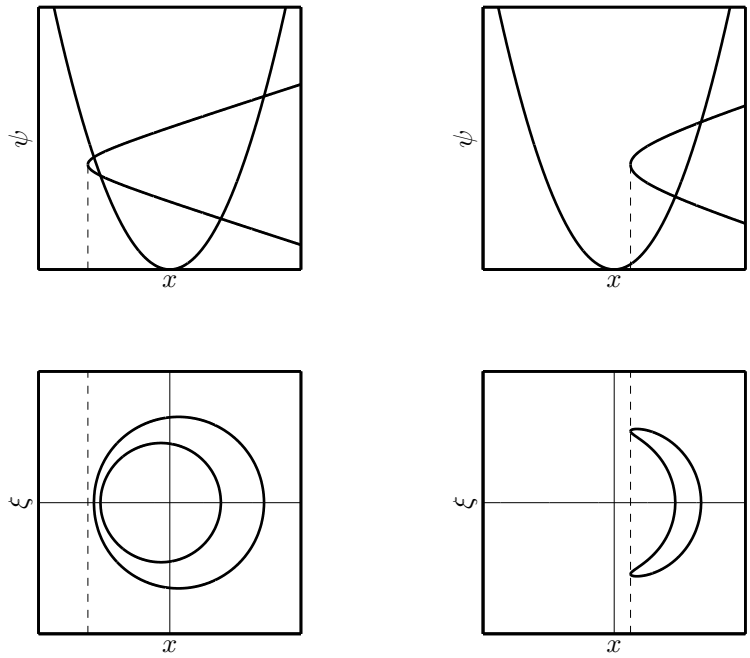

Figure 2.4: Left: Passing particle orbits with $J = 2$, $\lambda = 0.5$, $w = 0.1$. The upper branch of the hyperbola (2.123) bounded by the parabola (2.124) corresponds to a co-passing particle, whereas the lower branch is a counter-passing particle. The corresponding orbits in the (R, z)-plane encircle the magnetic axis anti-clockwise and clockwise, respectively. Right: Deeply trapped banana orbit with $J = 2$, $\lambda = 1.1$, $w = 0.1$.

orbit. Other examples of trapped orbits are shown in Figure 2.5: The orbit to the left corresponds to a moderately trapped particle, while the one on the right is just barely trapped (it has a value of λ very close to $B_A/B_{\max}$). It is noteworthy that, under normal conditions, the trapped particles constitute a minority fraction, $\mathcal{O}(\sqrt{\epsilon})$, of the total number of plasma particles, whose orbits most often exhibit a relatively small shift from the magnetic flux surfaces. However, for high-energy ions close to the magnetic axis, the *banana width* can become comparable to the average radius of the orbit, see e.g. Figure 2.6. The trajectory to the right in this figure has so large banana width that it encircles the magnetic axis.

The poloidal angles $\pm\theta_B$ at which trapped particles bounce (the banana tips) can be deduced by solving equation (2.121a) for the parallel velocity component χ as a function of r, θ and normalized adiabatic invariant λ. One

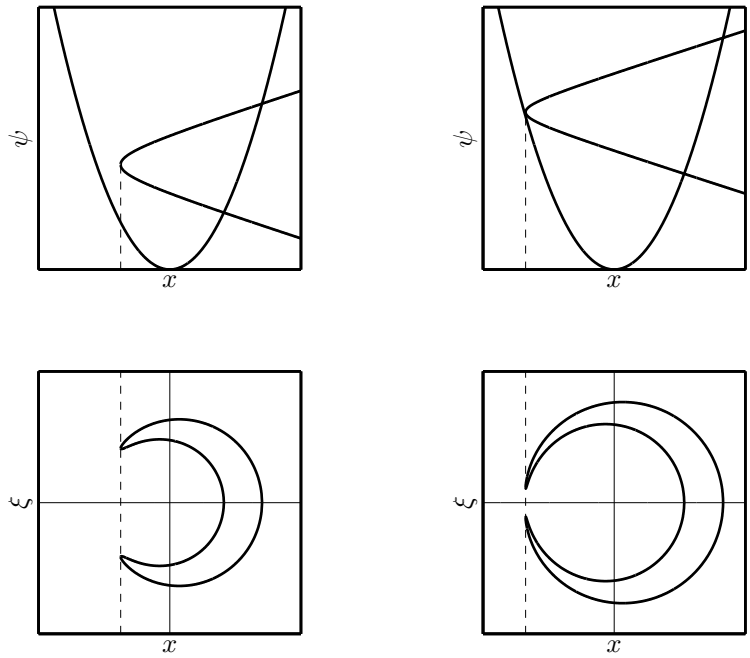

Figure 2.5: More examples of trapped orbits. Left: Moderately trapped banana particle with $J = 2$, $\lambda = 0.7$, $w = 0.1$. Right: Barely trapped orbit with $J = 3$, $\lambda = 0.46$, $w = 0.1$.

obtains, neglecting systematically terms $\mathcal{O}(\epsilon^2)$ and smaller,

$$\chi(r, \theta; \lambda) = \pm\sqrt{2\epsilon\lambda}\sqrt{\kappa^2(r; \lambda) - \sin^2(\theta/2)}\ , \tag{2.128}$$

where the *trapping parameter* is defined as

$$\kappa^2(r; \lambda) \equiv \frac{1 - \lambda(1 - \epsilon)}{2\epsilon\lambda}\ . \tag{2.129}$$

Trapped particles satisfy $0 < \kappa^2 < 1$, or, equivalently, $1/(1 + \epsilon) < \lambda < 1/(1 - \epsilon)$, which agrees with (2.126) and (2.127) to first order in ϵ. Thus, θ_B is found by setting $\chi = 0$ and solving for θ, giving

$$\theta_B = 2 \arcsin \kappa\ . \tag{2.130}$$

Note that equation (2.130) has no real roots for $\kappa > 1$. From now on, we will supress the argument λ in e.g. χ and κ, simply because it is an adiabatic invariant that does not change along the guiding center trajectory.

We now explore the complementary approach of directly integrating of equations (2.120a) - (2.120c). The method consists of rewriting equation

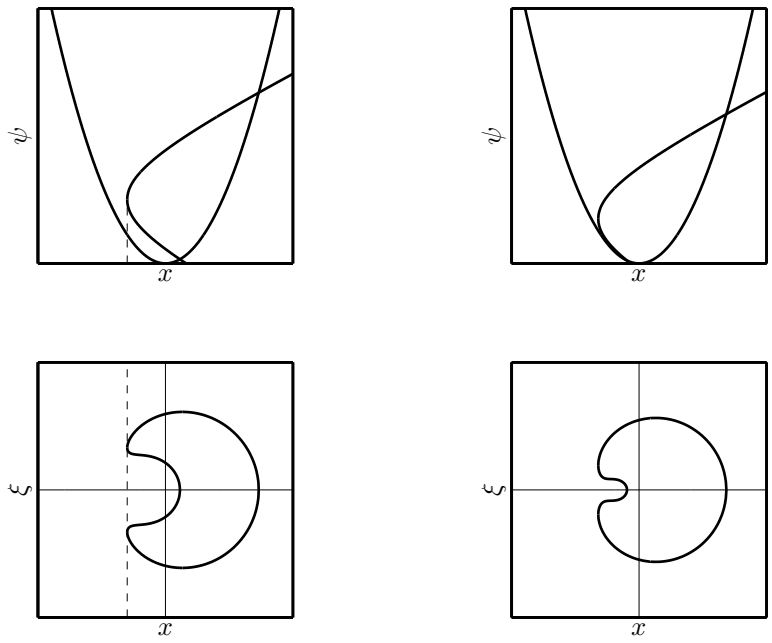

Figure 2.6: Trapped orbits sometimes exhibit large orbit widths, which may even encircle the magnetic axis. Left: So called *fat banana* with $J = 0.5$, $\lambda = 0.85$, $w = 0.1$. Right: So called *potato orbit* with $J = 0.35$, $\lambda = 0.84$, $w = 0.1$.

(2.120b) in terms of the dimensionless invariants λ, J and w, and the coordinates r and θ, as

$$dt = \frac{qR}{v\chi}\left[1 - \frac{w}{2\epsilon}\frac{q}{q_A}\frac{\cos\theta}{\chi}\left(1+\chi^2\right)\right]^{-1} d\theta \ , \tag{2.131}$$

so that time integrals may be transformed into integrals over θ. In principle, this means that averages over the poloidal orbits may be calculated as

$$\langle \dots \rangle_B = \frac{1}{\tau_B}\int_0^{\tau_B} (\dots)\, dt \tag{2.132}$$

$$= \frac{1}{\tau_B}\int_0^{2\pi} (\dots)\, \frac{qR}{v\chi}\left[1 - \frac{w}{2\epsilon}\frac{q}{q_A}\frac{\cos\theta}{\chi}\left(1+\chi^2\right)\right]^{-1} d\theta \ , \tag{2.133}$$

where

$$\tau_B = \int_0^{\tau_B} dt = \oint \frac{qR}{v\chi}\left[1 - \frac{w}{2\epsilon}\frac{q}{q_A}\frac{\cos\theta}{\chi}\left(1+\chi^2\right)\right]^{-1} d\theta \tag{2.134}$$

is the temporal period of the poloidal orbit and the θ-integrals are to be taken around one such period. A problem with these integrals is that q, R, χ and ϵ are all functions of r.[7] Since the guiding center radius varies over the poloidal orbit as the particles drift across the magnetic flux surfaces, we are therefore in need of an additional relation $r = r(\theta)$ in order to evaluate the integrals. Formally, such an equation can be derived by combining equations (2.120a) and (2.120b) into the following differential relation,

$$\frac{dr}{d\theta} = \frac{w}{2\epsilon}\frac{q}{q_A}\frac{\partial}{\partial\theta}(\chi R)\left[1 - \frac{w}{2\epsilon}\frac{q}{q_A}\frac{\partial}{\partial r}(\chi R)\right]^{-1} . \tag{2.135}$$

If the drift induced radial shift from the average orbital radius $\bar{r}$ is assumed small, one may perform an expansion in $(r - \bar{r}/)/\bar{r}$,

$$\epsilon \approx \bar{\epsilon} \equiv \bar{r}/R_A , \quad q \approx q(\bar{r})\left[1 + s(\bar{r})\frac{r - \bar{r}}{\bar{r}}\right] , \tag{2.136}$$

where the *magnetic shear* is defined as

$$s(r) \equiv \frac{r}{q}\frac{dq}{dr} . \tag{2.137}$$

To lowest order in the expansion parameters, the resulting expression for $dr/d\theta$ is given by

$$\frac{dr}{d\theta} \approx \frac{wR_A}{2\bar{\epsilon}}\frac{q(\bar{r})}{q_A}\left.\frac{\partial\chi}{\partial\theta}\right|_{r=\bar{r}} , \tag{2.138}$$

which may be directly integrated to give

$$r - \bar{r} \approx \frac{wR_A}{2\bar{\epsilon}}\frac{q(\bar{r})}{q_A}\Big[\chi(\bar{r},\theta) - \langle\chi(\bar{r},\theta)\rangle_B\Big] . \tag{2.139}$$

It is important to remember that equation (2.139) is lowest order in both ϵ and $(r - \bar{r})/\bar{r}$, and that a more accurate expression can be derived by going to next order in both parameters. Such a cumbersome analysis is most often avoided though, since, by assumption, the radial shift is already small. If not, the approximations used would simply be invalid. A fair question to ask, however, is how large the radial shift is allowed to be within the current framework. *A posteriori*, it can be shown from (2.139) that the expansion in $(r - \bar{r})/\bar{r}$ is valid whenever the Larmor radius is small enough, namely when $r_L \ll \sqrt{\bar{\epsilon}}$ holds. Therefore, a more accurate model (in the line of what was presented earlier in this section, but including a radial variation in the safety factor profile) is needed for realistic modeling of particle orbits with large radial excursions from their average flux surface, e.g. potatoes.

[7] Note that we no longer assume q to be constant.

In order to proceed, we need to evaluate the poloidal transit period (2.134) and learn how to calculate averages of the form (2.132). Starting with the former, one often neglects the drifts alltogether and simply writes

$$\tau_B = \int_0^{\tau_B} dt \approx \frac{q\left(\bar{r}\right) R_A}{v} \int_{\theta(0)}^{\theta(\tau_B)} \frac{d\theta}{\chi\left(\bar{r},\theta\right)} \ . \tag{2.140}$$

For passing particles, the integral should be taken from 0 to 2π. Then, one obtains

$$\begin{aligned}\tau_B &\approx \frac{q\left(\bar{r}\right) R_A}{v\sqrt{2\bar{\epsilon}\lambda}} \int_0^{2\pi} \frac{d\theta}{\sqrt{\kappa^2\left(\bar{r}\right) - \sin^2\frac{\theta}{2}}} = \frac{4q\left(\bar{r}\right) R_A}{v\kappa\left(\bar{r}\right)\sqrt{2\bar{\epsilon}\lambda}} \int_0^{\frac{\pi}{2}} \frac{d\phi}{\sqrt{1-\kappa^{-2}\left(\bar{r}\right)\sin^2\phi}} \\ &= \frac{4qR_A}{v\kappa\sqrt{2\epsilon\lambda}} K\left(1/\kappa\right) \ , \end{aligned} \tag{2.141}$$

where K is the complete elliptic integral of the first kind. In the final line, we have suppressed the argument $\bar{r}$. From now on it will be understood that q, κ, ϵ and s are to be evaluated at $r = \bar{r}$. The corresponding poloidal frequency then becomes

$$\omega_B = \frac{2\pi}{\tau_B} = \frac{\pi v\kappa\sqrt{2\epsilon\lambda}}{2qR_A K\left(1/\kappa\right)} \ . \tag{2.142}$$

For trapped particles that bounce at $\theta = \pm\theta_B$, the so called *bounce period* (the time it takes to complete a banana orbit) evaluates to

$$\begin{aligned}\tau_B &\approx \frac{qR_A}{v\sqrt{2\epsilon\lambda}} 2 \int_{-\theta_B}^{\theta_B} \frac{d\theta}{\sqrt{\kappa^2 - \sin^2\frac{\theta}{2}}} = \frac{8qR_A}{v\sqrt{2\epsilon\lambda}} \int_0^{\arcsin\kappa} \frac{d\phi}{\sqrt{\kappa^2 - \sin^2\phi}} = \\ &= \left\{\sin\phi = \kappa\sin\varphi\right\} = \frac{8qR_A}{v\sqrt{2\epsilon\lambda}} \int_0^{\frac{\pi}{2}} \frac{d\varphi}{\sqrt{1-\kappa^2\sin^2\varphi}} = \frac{8qR_A}{v\sqrt{2\epsilon\lambda}} K\left(\kappa\right) \ , \end{aligned} \tag{2.143}$$

and the associated *bounce frequency* becomes

$$\omega_B = \frac{2\pi}{\tau_B} \approx \frac{\pi v\sqrt{2\epsilon\lambda}}{4qR_A K\left(\kappa\right)} \ . \tag{2.144}$$

We are now in a position to evaluate the orbit average of the normalized parallel velocity component χ. Once again neglecting drift excursions and terms linear and higher order in ϵ, we obtain

$$\left\langle\chi\right\rangle_B \equiv \frac{1}{\tau_B} \int_0^{\tau_B} \chi\, dt \approx \frac{qR_A}{v\tau_B} \int_{\theta(0)}^{\theta(\tau_B)} d\theta = \begin{cases} \frac{\pi\kappa\sqrt{2\epsilon\lambda}}{2K(1/\kappa)} & \text{Passing particles} \\ 0 & \text{Trapped particles} \end{cases} \tag{2.145}$$

Thus, the midplane width of the banana orbit for trapped particles becomes

$$\Delta_t = 2\left|r\left(\theta=0\right)-\bar{r}\right| = \frac{2vq}{\omega_{cA}}\frac{\sqrt{1-\lambda\left(1-\epsilon\right)}}{\epsilon}\ . \tag{2.146}$$

This is an important quantity in so called neo-classical transport theory, where the step size of diffusing trapped particles is Δ_t (which is much larger than the ion Larmor radius r_L – the step size of diffusing passing particles).

We conclude this section by presenting expressions for the toroidal transit frequency, ω_ζ. Usually, such expressions include terms up to linear order in ϵ and $\left(r-\bar{r}\right)/\bar{r}$, the reason being that trapped particles would not circulate the toroidal axis, were it not due to the drifts that introduce a slow precession of the entire banana orbit. For passing particles, the relevant expression is

$$\begin{aligned}\omega_\zeta = q\omega_B + \omega_D\Bigg\{&1-2\kappa^2\left[1-\frac{E\left(1/\kappa\right)}{K\left(1/\kappa\right)}\right]\\ &+\frac{4}{3}\frac{\bar{\epsilon}\kappa^2}{1+2\bar{\epsilon}\kappa^2}\left[1-\kappa^2-\left(\frac{1}{2}-\kappa^2\right)\frac{E\left(1/\kappa\right)}{K\left(1/\kappa\right)}\right]\\ &+4s\frac{\kappa^2}{1+2\bar{\epsilon}\kappa^2}\frac{E\left(1/\kappa\right)}{K\left(1/\kappa\right)}\left[1-\frac{\pi^2}{4E\left(1/\kappa\right)K\left(1/\kappa\right)}\right]\Bigg\}\ ,\end{aligned} \tag{2.147}$$

where the toroidal drift frequency is

$$\omega_D = \frac{q\left(\bar{r}\right)v^2}{2\bar{r}\omega_{cA}R_A}\ . \tag{2.148}$$

The similar expression for trapped particles is given by

$$\begin{aligned}\omega_\zeta = \omega_D\Bigg\{&2\frac{E\left(\kappa\right)}{K\left(\kappa\right)}-1+\frac{2\epsilon}{3}\left[1-\kappa^2-\left(1-2\kappa^2\right)\frac{E\left(\kappa\right)}{K\left(\kappa\right)}\right]\\ &+4s\left[\kappa^2-1+\frac{E\left(\kappa\right)}{K\left(\kappa\right)}\right]\Bigg\}\ .\end{aligned} \tag{2.149}$$

As stated at the outset, this expression includes no components of the parallel transit velocity (which effectively averages out for the bouncing, trapped particles). Rather, it represents a slow precessional drift of the entire banana around the torus.

Finally, we note that the obtained orbital frequencies, ω_B and ω_ζ, are both functions only of the orbit invariants. That is, depending on ones taste, one of the sets (λ, J, v) or (μ, p_ζ, E). In the expressions given above, it may seem as if the relevant dependencies are λ, $\bar{r}$ and v rather than the ones just stated.

However, the average radius $\bar{r}$ is actually also a function of the orbit invariants, defined via the functional form of the toroidal momentum. For trapped particles, this relation is easily found simply by using for the orbit constant J (or p_ζ) its value at the banana tips $\pm\theta_B$, where χ vanishes and $r = \bar{r}$, i.e. $J = \psi(\bar{r})$. For passing particles, the relation is more involved. One has to use that the average of J during a poloidal transit (which of course equals its instantaneous, constant value) provides the desired relation. To very high accuracy, it reads

$$J = \psi(\bar{r}) - \sqrt{1 - \lambda(1 - \bar{\epsilon})}\ , \tag{2.150}$$

which should then be inverted to obtain the desired relation $\bar{r} = \bar{r}(\lambda, J, v)$.

2.3 Statistical Description of Energetic Particles

The single particle orbits considered so far do not properly describe tokamak plasmas. Their main deficiency lies in that the particle trajectories were derived for given magnetic fields, whereas in real plasmas the particles certainly alter the externally generated electromagnetic field structure. The ultimate description of plasmas would be one in which all particle orbits were calculated simultaneously, taking into account the electromagnetic interactions with all other charged particles as well as the externally applied fields. Such a description is not plausible, however, since it implies solving, simultaneously, the equations of motion for each particle together with Maxwell's equations for self-consistently evolving fields. The number of particles, and therefore equations, is simply way too large for that approach. A more realistic, but still very challenging, task, is to resort to statistical physics. In such theories, the plasma is modeled as a fluid in six-dimensional phase space, whose density function f is determined through the Boltzmann equation

$$\frac{\partial f}{\partial t} + \dot{\mathbf{q}}\frac{\partial f}{\partial \mathbf{q}} + \dot{\mathbf{p}}\frac{\partial f}{\partial \mathbf{p}} = \mathcal{C} + \mathcal{S} + \mathcal{L} \tag{2.151}$$

Here, $(\mathbf{p}, \mathbf{q})$ are generalized phase space coordinates, $\mathcal{C}$ is a collision operator that describes the effects of small-angle, binary Coulomb collisions and the terms $\mathcal{S}$ and $\mathcal{L}$ represent particle sources and losses. Note that in the absence of collisions, sources and losses (with the right hand side equal to zero), the Boltzmann equation is usually referred to as the Vlasov equation. The Vlasov equation is, in fact, a continuity equation that describes an incompressible phase space fluid (the plasma). It is easy to see that when the motion is integrable, any function that only depends on the constants of motion is a solution to the Vlasov equation. Consider, e.g., a set of action-angle variables $(\mathbf{J}, \boldsymbol{\Theta})$, designed as to satisfy

$$\dot{\mathbf{J}} = 0\ , \quad \dot{\boldsymbol{\Theta}} = \boldsymbol{\Omega}(\mathbf{J})\ . \tag{2.152}$$

Then, any function $g(\mathbf{J})$ satisfies

$$\frac{\partial g}{\partial t} = \frac{\partial g}{\partial \boldsymbol{\Theta}} = 0 \ , \tag{2.153}$$

which means that g is automatically a solution to the Vlasov equation.

Typical sources of fast particles include external heating schemes such as NBI and RF heating, but of course also thermonuclear fusion reactions, which feed the plasma with highly energetic alpha particles. Fusion generated alphas are born primarily in the tokamak core, where the density and temperature both peak. Their nominal birth energy is 3.5 MeV, around which a statistical spread is observed due to Doppler broadening. The two complementary categories of fast ions discussed here (NBI and RF generated ions) are quite different in that their distributions are strongly anisotropic. NBI produces energetic ions in the tokamak center, whose kinetic energies are primarily algined with the beam injection angle. On the contrary, RF heating can deposit power and heat ions at any chosen resonance layer, and the resulting acceleration of the particles occurs mainly perpendicularly to the magnetic field. Nevertheless, throughout this thesis we will (for reasons of simplicity) assume that the source of fast particles is isotropic, like it is for the alphas, and that the fast ions are generated at some definite velocity v_b, with little spread in energy. We therefore model the fast particle source as [20]

$$\mathcal{S} = \frac{S_0(r,t)}{4\pi v_\mathrm{b}^2}\,\delta(v - v_\mathrm{b}) \ , \tag{2.154}$$

where S_0 is the alpha particle birth rate per unit volume (which is allowed to vary with radius and time) and δ is the Dirac delta function.

Fast particle losses are usually modeled by an exponential loss time τ_L, which in principle should be regarded as a function of v and χ, but most often is taken as constant. Under these assumptions, the loss term becomes

$$\mathcal{L} = -\frac{f}{\tau_\mathrm{L}} \ . \tag{2.155}$$

The exponential loss time τ_L generally depends on a number of effects [21]. These include direct losses due to particle orbits that intersect the cavity wall, e.g. as a result of large Larmor radii or drift induced shifts, which may both vary when the equilibrium magnetic field is not perfectly axisymmetric. There is also a strong dependence in τ_L on so called indirect losses, arising as a result of nonlinear interaction between fast particles and thermonuclear instabilities. The latter have the capacity to redistribute and transport the fast particles in phase space, which in many situations is expected to enhance the losses [8]. Usually, however, τ_L is not calculated from first principle in the presence of

these effects, but rather the form (2.155) is assumed and used to evaluate τ_{L} from a measured distribution of fast ions.

The relevant collision operator for fast particles consists of a combination of a slowing-down term, a diffusive random walk in energy and so called pitch-angle scattering. It is given by [7, 20]

$$\mathcal{C} = \frac{1}{\tau_s}\left\{ \frac{1}{v^2}\frac{\partial}{\partial v}\left[\left(v^3 + v_c^3\right) f\right] + \frac{1}{2v^2}\frac{\partial}{\partial v}\left[v^2\left(v_e^2\frac{M_e}{M_\alpha} + v_i^2\frac{v_c^3}{v^3}\frac{M_i}{M_\alpha}\right)\frac{\partial f}{\partial v}\right] + \frac{M_i}{M_\alpha}\frac{v_c^3}{v^3}\frac{\partial}{\partial \chi}\left[\left(1-\chi^2\right)\frac{\partial f}{\partial \chi}\right]\right\}. \tag{2.156}$$

Here, v_i and v_e are the thermal speeds of the bulk ions and electrons. The characteristic collision frequency $1/\tau_s$, with τ_s the so called Spitzer slowing-down time, is that of drag-like collisions between the fast ions and thermal electrons. We shall not give an expression for τ_s here. It suffices to know that it is large as compared with the characteristic period τ_B of the particle orbits. The critical speed v_c defines the fast ion energy at which the friction forces due to collisions with thermal electrons and ions are equal. At velocities larger than v_c, electron drag predominates: The fast ions do not change their pitch-angles during such collisions, but like an elephant running through a sea of tennis balls, they experience a deceleration. The relevant collision operator for such energetic ions consists of merely the first piece in (2.156). At lower velocities, collisions with thermal ions are more likely. In this regime energy diffusion (the second term) and pitch-angle scattering (the third term) are both appreciable. It should be noted that the energy diffusion term includes contributions from collisions with both thermal electrons and fast ions.

A huge simplification is readily available if one notes that, in the guiding center approximation, the modifications of the fast ion distribution due to the right hand side of equation (2.151) usually occurs on a time scale much longer than the orbital periods of the particle motion. The Larmor gyration, e.g., is unquestionably much faster than the operational time of $\mathcal{C}$, $\mathcal{S}$ ad $\mathcal{L}$, and can therefore safely be averaged over.[8] Likewise, averaging over the poloidal and

[8]However, in the case of RF heating, one must take into account that the particles are accelerated via cyclotron resonances with externally generated wave fields that oscillate on the time scale of the Larmor rotation. Nevertheless, since the gyration frequency scales as one over the major radius, the resonant interaction will mainly occur in thin layers somewhere along the particles trajectories. Due to Coulomb collisions, the particles will enter each resonant layer with decorrelated gyration phases, so the interaction effectively results in random kicks in energy. Such wave-particle interaction is usually described in terms of so called *quasi-linear theory*, in which one simply adds to the gyro-averaged kinetic equation a quasi-linear operator Q that describes the overall effect of the kicks in terms of a diffusive random walk.

toroidal transit periods as well, eventually generates an equation of the form

$$\frac{\partial f}{\partial t} = \mathcal{C} + \mathcal{S} + \mathcal{L} \ . \tag{2.157}$$

Equation (2.157) seems almost too simple to be true, and indeed it represents an oversimplification. To be perfectly stringent, one should perform an analysis in which the time scales of the various periodic motions are ordered and then carefully averaged out by expanding the distribution function in associated small parameters, one for each pair of ordered time scales. In order to carry out such calculations, it is convenient to transform to action-angle coordinates for the guiding center motion, in which the averages are evaluated by simply integrating over one period of the angles. The result will differ slightly from that given in equation (2.157), but for our purposes the simpler model works just fine.

In the following, we will assume that the losses are negligibly slow, $\tau_{\mathrm{L}} \to \infty$, and derive the so called *slowing-down distribution* of a fast ion population that is so energetic that it evolves only under the influence of decelerating Coulomb collisions (mainly with thermal electrons) and the source term (2.154),

$$\frac{\partial f}{\partial t} = \frac{1}{\tau_s}\frac{1}{v^2}\frac{\partial}{\partial v}\left[\left(v^3 + v_c^3\right) f\right] + \frac{S_0\left(r,t\right)}{4\pi v_{\mathrm{b}}^2}\,\delta\left(v - v_{\mathrm{b}}\right) \ . \tag{2.158}$$

The long-term equilibrium solution to equation (2.158) is found by setting $\partial f/\partial t = 0$ and integrating the resulting equation

$$\frac{\partial}{\partial v}\left[\left(v^3 + v_c^3\right) f\right] = -\frac{S_0\left(r,t\right)\tau_s}{4\pi}\frac{v^2}{v_{\mathrm{b}}^2}\,\delta\left(v - v_{\mathrm{b}}\right) \tag{2.159}$$

from some $v < v_{\mathrm{b}}$ to ∞. Noting that $f = 0$ for $v > v_{\mathrm{b}}$, one obtains

$$f\left(r,v,t\right) = \frac{S_0\left(r,t\right)\tau_s\left(t\right)}{4\pi\left(v^3 + v_c^3\left(t\right)\right)} \ , \tag{2.160}$$

where we have included time dependencies in both τ_s and v_c, since, in principle, the outlined solution allows them to evolve (slowly) in time.

3

Plasma Waves and their Interaction with Particles

Plasma waves are oscillating perturbations from an equilibrium state that are usually described in terms of their electric and magnetic fields. On the other hand, these oscillating fields of course interact with the charged particles that constitute the plasma, so the perturbations persist in the charge density, current, pressure and temperature as well. Due to the long reaching range of the Coulomb potential, which effectively couples the motion of each plasma particle to that of many others, plasma waves are truly collective phenomena in which entire populations of particles oscillate coherently.

In general, plasmas support multiple types of waves, or *modes* of oscillation, which all correspond to some or another characteristic motion of the plasma particles. For example, there are high frequency waves in which only the electrons are rapid enough to partake in the oscillations, while lower frequency oscillations involve the ions as well. In magnetized plasmas, where particles gyrate around the magnetic field lines, the particles respond extra vividly to circularly polarized waves. It also makes a difference as to whether the plasma is warm or cold: Finite thermal speeds introduce dispersive effects where the oscillation frequency becomes dependent on the wave number (or, equivalently, the wavelength).

In the following section, we will first outline in Section 3.1 the general approach to kinetic linear wave theory in a uniform and static plasma. We will see that there is a certain group of particles, the resonant ones that move in sync with the wave field, that essentially dominate the wave-particle interaction. Next, we go on to study this intricate interaction in the simplest possible setup: A one-dimensional equilibrium, in which the bulk plasma supports a high frequency oscillation that only interacts with a small group of fast elec-

trons. Section 3.2 is devoted to this interaction, which is found to result in an exponential damping (or growth, depending on statistical aspects of the fast particles) of the wave amplitude that goes under the name *Landau damping*. In Section 3.3, we then generalize the geometry by considering linear wave-particle interaction in toroidal geometry. The final section is devoted to nonlinear wave-particle interaction, which is studied, once again, via the simple setup of a one-dimensional plasma.

3.1 Kinetic Theory of Linear Plasma Waves

At heart of the theoretical treatment of plasma waves lies the issue of relating the particle density and current to the electromagnetic wave field. The two Maxwell equations

$$\nabla \times \mathbf{E} = -\frac{\partial \mathbf{B}}{\partial t} \ , \quad \nabla \times \mathbf{B} = \mu_0 \mathbf{J} + \frac{1}{c^2}\frac{\partial \mathbf{E}}{\partial t} \tag{3.1}$$

can be combined into the wave equation

$$\nabla \cdot \nabla \mathbf{E} - \nabla \left(\nabla \cdot \mathbf{E} \right) - \frac{1}{c^2}\frac{\partial^2 \mathbf{E}}{\partial t^2} = \mu_0 \frac{\partial \mathbf{J}}{\partial t} \ . \tag{3.2}$$

In order to solve equation (3.1) for the electric field $\mathbf{E}$, we need first to somehow relate $\mathbf{J}$ to $\mathbf{E}$. Such a relation goes beyond Maxwell's equations. In principle, it involves solving, simultaneously, the equations of motion for many interacting plasma particles under the influence of the electric wave field $\mathbf{E}$. In reality, however, one resorts to simplified plasma models that describe the plasma in statistical terms. In that spirit, by far the easiest approach is to treat the plasma as a conducting fluid: Either a two-fluid model in which electrons and ions are modeled as separate entities, or a single-fluid model (like e.g. the magnetohydrodynamic model we will present in the following chapter) in which the ions and electrons are considered to comprise a single fluid. However, in the present chapter we will pursue the more ambitious task of treating the plasma as a six-dimensional phase space fluid rather than an ordinary, three-dimensional fluid, and tackle the problem by means of the kinetic equation given in Section 2.3 of Chapter 2.

Before embarking on a brute force kinetic calculation, we can make some simplifying observations. For small wave amplitudes, a linear approach is reasonable in which $\mathbf{J} \propto \mathbf{E}$. The motivation for this approximation comes from the particle equation of motion (2.7), repeated here in slightly different notation,

$$M\frac{d\mathbf{v}}{dt} = e\big[\mathbf{E} + \mathbf{v} \times \mathbf{B}\big] \ . \tag{3.3}$$

Equation (3.3) suggests that when $\mathbf{E}$ and $\mathbf{B}$ are both small, then $\mathbf{J} \propto \mathbf{v} \propto \mathbf{E}$, and the magnetic field enters only as a second order correction. If indeed $\mathbf{J} \propto \mathbf{E}$, then the wave equation is a linear PDE in space and time. Therefore, if we assume, as outlined in the chapter introduction, that the system is uniform and static, it is highly advantageous to Fourier transform $\mathbf{E}$ and $\mathbf{J}$ according to

$$Q_\alpha(\mathbf{x}, t) = \frac{1}{(2\pi)^2} \int\int \widetilde{Q}_\alpha(\mathbf{k}, \omega)\, \mathrm{e}^{i(\mathbf{k}\cdot\mathbf{x} - \omega t)}\, d^3\mathbf{k}\, d\omega \ . \tag{3.4}$$

Here, we have introduced Einstein's tensor notation in order to simplify the subsequent analysis. Upon application of (3.4), the wave equation (3.2) becomes

$$\left[\left(1 - \frac{k^2c^2}{\omega^2}\right)\delta_{\alpha\beta} + \frac{c^2}{\omega^2}k_{\alpha\beta}\right]\widetilde{E}_\beta = -i\frac{\mu_0}{c^2\omega}\tilde{J}_\alpha \ , \tag{3.5}$$

where repeated indices are to be summed over and $\delta_{\alpha\beta}$ is the Kronecker delta. Now, the most general linear response that can be imagined has the form

$$J_\alpha(\mathbf{x}, t) = \int\int \sigma_{\alpha\beta}(\mathbf{x}, t; \mathbf{x}', t')\, E_\beta(\mathbf{x}', t')\, d\mathbf{x}' dt' \ . \tag{3.6}$$

This expression allows the current at some space time position $(\mathbf{x}, t)$ to depend on the electric field at other space time locations $(\mathbf{x}', t')$, and is valid as long as causality and special relativity are not violated. In essence, therefore, solving the Fourier space wave equation (3.5) really comes down to the problem of evaluating the *conductivity tensor* $\sigma_{\alpha\beta}$. However, when the plasma is uniform and static, as assumed here, the conductivity tensor cannot be just any function of $\mathbf{x}$, $\mathbf{x}'$, t and t'. Rather, it must depend only on the differences $\mathbf{x} - \mathbf{x}'$ and $t - t'$,

$$\sigma(\mathbf{x}, t; \mathbf{x}', t') = \sigma(\mathbf{x} - \mathbf{x}'; t - t') \ . \tag{3.7}$$

Hence, equation (3.6) becomes a convolution, whose Fourier transform is simply the product

$$\tilde{J}_\alpha(\omega, \mathbf{k}) = \tilde{\sigma}_{\alpha\beta}(\omega, \mathbf{k})\, \widetilde{E}_\beta(\omega, \mathbf{k}) \ . \tag{3.8}$$

Substituting (3.8) into the Fourier transformed wave equation (3.5), one obtains

$$\left[\frac{c^2}{\omega^2}k_\alpha k_\beta - \frac{k^2c^2}{\omega^2}\delta_{\alpha\beta} + \epsilon_{\alpha\beta}\right]\widetilde{E}_\beta = 0 \ , \tag{3.9}$$

where the so called *dielectric tensor* relates to the conductivity tensor as

$$\epsilon_{\alpha\beta} = \delta_{\alpha\beta} + \frac{i}{\epsilon_0\omega}\tilde{\sigma}_{\alpha\beta} \ . \tag{3.10}$$

In general, therefore, finding $\tilde{\sigma}_{\alpha\beta}$ gives a so called dispersion relation, a functional relation of the form $\omega = \omega(\mathbf{k})$. Note that the dielectric tensor is essentially ic^2/ω times the Fourier transform of the right hand side of Ampére's law, $\partial\mathbf{E}/\partial t + \mathbf{J}/\epsilon_0$.

As already mentioned, various models can be employed for the evaluation of $\tilde{\sigma}_{\alpha\beta}$, and depending on what physics these models include, various modes of oscillations will be found. The current investigation focuses on the effects due to deviations in the particle distributions from their equilibrium velocity profiles. We therefore commence a study in which the conductivity tensor is calculated by means of kinetic theory. We describe the plasma particles in terms of a distribution function $f(\mathbf{x}, \mathbf{v}, t)$ that evolves in the 6-dimensional (non-canonical) phase space $(\mathbf{x}, \mathbf{v})$ according to the Vlasov equation

$$\frac{\partial f}{\partial t} + \mathbf{v} \cdot \frac{\partial f}{\partial \mathbf{x}} + \frac{d\mathbf{v}}{dt} \cdot \frac{\partial f}{\partial \mathbf{v}} = 0 \ , \tag{3.11}$$

and we restrict the investigation to the special case of an unmagnetized plasma whose particles are isotropically distributed in $\mathbf{v}$-space. The inclusion of an equilibrium magnetic field certainly complicates the analysis, but the underlying physics mechanism we want to highlight is present even in the simpler setup. Under these assumptions, we may substitute the particle equation of motion (3.3) into the Vlasov equation, yielding

$$\frac{\partial f}{\partial t} + \mathbf{v} \cdot \frac{\partial f}{\partial \mathbf{x}} + \frac{e}{M} \frac{\partial f}{\partial \mathbf{v}} \cdot \left[\mathbf{E} + \mathbf{v} \times \mathbf{B} \right] = 0 \ . \tag{3.12}$$

Here, it is understood that $\mathbf{E}$ and $\mathbf{B}$ are both wave quantities, and thus have no unperturbed components. On the contrary, the distribution function of course has an unperturbed equilibrium part, which we denote F_0. By definition, F_0 is taken to be static, $\partial F_0 / \partial t = 0$. Hence, it must satisfy $\partial F_0 / \partial \mathbf{x}$, which means that $F_0 = F_0(v)$, where $v = |\mathbf{v}|$ and we have invoked the assumption that the unperturbed equilibrium configuration is isotropic in velocity. We note that when the plasma is unmagnetized, there are only two second rank tensors available, $\delta_{\alpha\beta}$ and $k_\alpha k_\beta$. We therefore construct $\epsilon_{\alpha\beta}$ according to

$$\epsilon_{\alpha\beta} = \epsilon_\parallel \frac{k_\alpha k_\beta}{k^2} + \epsilon_\perp \left(\delta_{\alpha\beta} - \frac{k_\alpha k_\beta}{k^2} \right) \ , \tag{3.13}$$

where $\epsilon_\parallel$ and $\epsilon_\perp$ are defined as

$$\epsilon_\parallel \equiv \frac{k_\alpha k_\beta}{k^2} \epsilon_{\alpha\beta} \ , \quad \epsilon_\perp \equiv \frac{1}{2} \left(\delta_{\alpha\beta} - \frac{k_\alpha k_\beta}{k^2} \right) \epsilon_{\alpha\beta} \ . \tag{3.14}$$

Then, the wave equation becomes

$$\left[\epsilon_\parallel \frac{k_\alpha k_\beta}{k^2} + \left(\epsilon_\perp - \frac{k^2 c^2}{\omega^2} \right) \left(\delta_{\alpha\beta} - \frac{k_\alpha k_\beta}{k^2} \right) \right] \widetilde{E}_\beta = 0 \ . \tag{3.15}$$

From (3.15), we see that there are essentially two modes of oscillation: A longitudinal wave with $\mathbf{k} \parallel \mathbf{E}$ and a transverse wave with $\mathbf{k} \perp \mathbf{E}$. Their

respective dispersion relations read

$$\epsilon_{\parallel} = 0 \ , \quad \epsilon_{\perp} = \frac{k^2 c^2}{\omega^2} \ . \tag{3.16}$$

We shall only be concerned with the former type of wave, described by $\epsilon_{\parallel} = 0$. The treatment of the transverse wave is simply more complicated, but provides no further insights.

Since the amplitudes of $\mathbf{E}$ and $\mathbf{B}$ are both assumed small, we can construct a perturbative solution to the kinetic equation by expanding the distribution function according to

$$f = F_0 + \delta f \ , \tag{3.17}$$

where $\delta f \ll F_0$ represents a small deviation from the unperturbed equilibrium distribution F_0. Due to the isotropy, we have that $dF_0/d\mathbf{v}$ is parallel to $\mathbf{v}$, so

$$\frac{dF_0}{d\mathbf{v}} \cdot \mathbf{v} \times \mathbf{B} = 0 \ . \tag{3.18}$$

We then obtain

$$\frac{\partial \delta f}{\partial t} + \mathbf{v} \cdot \frac{\partial \delta f}{\partial \mathbf{x}} = -\frac{e\mathbf{E}}{M} \cdot \frac{dF_0}{d\mathbf{v}} + \mathcal{O}\left(\mathbf{E}^2\right) \ , \tag{3.19}$$

where the final term on the right hand side represents terms that are doubly small in the wave amplitude. In the present linear approach, with the goal to establish a linear connection $\tilde{J}_\alpha = \tilde{\sigma}_{\alpha\beta}\widetilde{E}_\beta$, we completely neglect such corrections and write

$$\frac{\partial \delta f}{\partial t} + \mathbf{v} \cdot \frac{\partial \delta f}{\partial \mathbf{x}} = -\frac{e\mathbf{E}}{M} \cdot \frac{dF_0}{d\mathbf{v}} \ . \tag{3.20}$$

Just like the wave equation, equation (3.20) also constitutes a linear PDE in space and time, and can therefore be similarly Fourier transformed according to the recipe in (3.4). The procedure results in a simple algebraic expression for $\widetilde{\delta f}$ in terms of $\widetilde{\mathbf{E}}$,

$$\widetilde{\delta f} = i\frac{e}{M}\frac{\widetilde{\mathbf{E}} \cdot dF_0/d\mathbf{v}}{\mathbf{k} \cdot \mathbf{v} - \omega} \ . \tag{3.21}$$

Hence, the total current and the conductivity tensor become

$$\begin{aligned} \tilde{J}_\alpha &= \sum_{\text{Species}} e \int v_\alpha \tilde{f} \, d^3\mathbf{v} = \sum_{\text{Species}} e \int v_\alpha \widetilde{\delta f} \, d^3\mathbf{v} \\ &= i \sum_{\text{Species}} \frac{e^2}{M} \int \frac{v_\alpha dF_0/dv_\beta}{\mathbf{k} \cdot \mathbf{v} - \omega} \, \widetilde{E}_\beta \, d^3\mathbf{v} \end{aligned} \tag{3.22}$$

and

$$\tilde{\sigma}_{\alpha\beta} = i \sum_{\text{Species}} \frac{e^2}{M} \int \frac{v_\alpha dF_0/dv_\beta}{\mathbf{k}\cdot\mathbf{v} - \omega}\, d^3\mathbf{v} \ . \tag{3.23}$$

With the solution (3.23), the dispersion relation $\epsilon_{\|} = 0$ for the longitudinal wave becomes

$$1 - \frac{1}{\epsilon_0 \omega k^2} \sum_{\text{Species}} \frac{e^2}{M} \int \frac{(\mathbf{k}\cdot\mathbf{v})\,(\mathbf{k}\cdot dF_0/d\mathbf{v})}{\mathbf{k}\cdot\mathbf{v} - \omega}\, d^3\mathbf{v} = 0 \ . \tag{3.24}$$

We note that the integrand in (3.24) has a singularity at $\omega = \mathbf{k}\cdot\mathbf{v}$. The singularity reflects the fact that only a small fraction of the total number of particles interact heavily with the wave, namely those that move in resonance with the wave and therefore have velocities close to the *resonant velocity* defined by $\mathbf{k}\cdot\mathbf{v} = \omega$.

From a quantum point of view, similar conclusions can be drawn. In such theories, charged particles interact with waves via emission and absorption of light quanta: Massless particles, called photons, that move with the speed of light c. Consider, e.g., the interaction between a wave (with angular oscillation frequency ω and wave vector $\mathbf{k}$) and a charged particle via the emission of a photon, the energy and linear momentum of which are given by

$$E_{\text{ph}} = \hbar\omega \ , \quad \mathbf{p}_{\text{ph}} = \hbar\mathbf{k} \ . \tag{3.25}$$

Conservation of energy and momentum during the emission gives

$$\frac{Mv^2}{2} = \frac{Mv'^2}{2} + \hbar\omega \ , \quad M\mathbf{v} = M\mathbf{v}' + \hbar\mathbf{k} \ , \tag{3.26}$$

where $\mathbf{v}$ and $\mathbf{v}'$ are the particle velocities before and after the emission, respectively. The second relation immediately reveals that

$$|\mathbf{v} - \mathbf{v}'| = |\mathbf{k}|\, \frac{\hbar}{M} \ , \tag{3.27}$$

so that, due to the smallness of the ratio $\hbar/M$, $\mathbf{v}$ must be close to $\mathbf{v}'$. Then, the energy conservation relation can be rewritten as

$$\omega = \frac{M}{2\hbar}\left(v^2 - v'^2\right) = \frac{M}{2\hbar}\,(\mathbf{v} + \mathbf{v}')\cdot(\mathbf{v} - \mathbf{v}') = \frac{\mathbf{v} + \mathbf{v}'}{2}\cdot\mathbf{k} \approx \mathbf{v}\cdot\mathbf{k} \ , \tag{3.28}$$

which shows that, indeed, the interacting particles are those that move in sync with the wave oscillations, i.e. the resonant ones for which $\omega \sim \mathbf{k}\cdot\mathbf{v}$.

3.2 Landau Damping

The natural question that arises is how, exactly, the resonant particles move in the presence of the wave, and how they affect, in return, the wave field. It turns out that within the linear framework presented above, the effect of the particles is to damp (or drive) the wave amplitude exponentially via so called Landau damping. Although a formal derivation of the Landau damping rate is complicated, [22], qualitative understanding can be gained through the following picture: In essence, the resonant particles are nothing but a large set of coupled objects that oscillate back and forth in the wave field. Therefore, as the energy initially contained in the wave spreads in time, via resonant interaction, over the coupled oscillators, it is extremely unlikely that it can ever be extracted again.

As an illustration of the Landau damping phenomenon, we consider a simple one-dimensional plasma, and investigate the effect of a group of resonant electrons on an electrostatic plasma wave that oscillates with angular frequency $\omega = \omega_p$. We assume that the resonant velocity $v = \omega_p/k$ is high in the tail of the electron distribution and that the ions are essentially immobile. The wave can then be viewed as being established by the non-resonant majority of the plasma, the so called bulk, whereas the resonant interaction involves a much smaller electron population. Within the linear theory presented in the preceding section, we can take the wave field as given,

$$E = E_0 \cos\left(kx - \omega_p t\right) \ , \tag{3.29}$$

whereas the distribution $f\left(x, v; t\right)$ of resonant electrons must be evolved by means of a one-dimensional version of (3.20),

$$\frac{\partial \delta f}{\partial t} + v \frac{\partial \delta f}{\partial x} = \frac{|e|\, E_0}{M} \cos\left(kx - \omega_p t\right) \frac{dF_0}{dv} \ . \tag{3.30}$$

In what follows, we present a real space solution to equation (3.30) rather than the sort of Fourier space solution outlined in the previous section. The particular solution to (3.30) is

$$\delta f_P\left(x, v; t\right) = \frac{|e|\, E_0}{M} \frac{\sin\left(kx - \omega_p t\right)}{kv - \omega_p} \frac{dF_0}{dv} \ . \tag{3.31}$$

It is however singular for highly resonant particles with $\omega_p = kv$. For that reason, we choose the homogeneous solution as to cancel the singularity,

$$\delta f_H\left(x, v; t\right) = -\frac{|e|\, E_0}{M} \frac{\sin\left[k\left(x - vt\right)\right]}{kv - \omega_p} \frac{dF_0}{dv} \ , \tag{3.32}$$

so that the total solution becomes

$$\delta f\left(x, v; t\right) = \frac{|e|\, E_0}{M} \frac{\sin\left(kx - \omega_p t\right) - \sin\left[k\left(x - vt\right)\right]}{kv - \omega_p} \frac{dF_0}{dv} \ . \tag{3.33}$$

Note that δf is bounded at $v = \omega_p/k$.

With the composite solution in equation (3.33), we can go on and evaluate the average work done *on* the particles *by* the wave, per wavelength λ. It is given by

$$Q = \frac{1}{\lambda} \int_0^\lambda JE \, dx \ , \tag{3.34}$$

where the current reads

$$\begin{aligned} J &= -|e| \int_{-\infty}^{\infty} v f(v) \, dv = -|e| \int_{-\infty}^{\infty} v \left[F_0(v) + \delta f(v) \right] dv = -|e| \int_{-\infty}^{\infty} v \, \delta f(v) \, dv \\ &= -\frac{e^2 E_0}{M} \int_{-\infty}^{\infty} v \, \frac{\sin(kx - \omega_p t) - \sin\left[k(x - vt)\right]}{kv - \omega_p} \frac{dF_0}{dv} \, dv \ . \end{aligned} \tag{3.35}$$

Note that the one-dimensional equivalent of the velocity space isotropy assumed in the preceding section is to let F_0 be even with respect to v, thus allowing the final step on the first line in the calculation above. Inserting this J into Q, it can be shown that

$$Q = -\frac{e^2 E_0^2}{2M} \int_{-\infty}^{\infty} v \, \frac{dF_0}{dv} \frac{\sin\left[(kv - \omega_p)\, t\right]}{kv - \omega_p} \, dv \ . \tag{3.36}$$

For $t > 0$, the factor $\sin\left[[kv - \omega_p)\, t\right] / (kv - \omega_p)$ in the integrand oscillates rapidly. Then, since $v \, dF_0/dv$ is assumed smooth, the main portion of the integral will average to zero, the exception being for those v in the very proximity of ω_p/k. In the spirit of the stationary phase method, we therefore approximate $v dF_0/dv$ as constant over the narrow interval that actually contributes to the integral, so that

$$Q \approx -\frac{e^2 E_0^2}{2M} \left[v \frac{dF_0}{dv} \right]_{v=\omega_p/k} \int_{-\infty}^{\infty} \frac{\sin\left[(kv - \omega_p)\, t\right]}{kv - \omega_p} \, dv \ . \tag{3.37}$$

Since ω_p/k is finite, the substitution $x = v - \omega_p/k$ is helpful. It gives

$$Q = -\frac{e^2 E_0^2}{2Mk} \left[v \frac{dF_0}{dv} \right]_{v=\omega_p/k} I \ , \tag{3.38}$$

where

$$I = \int_{-\infty}^{\infty} \frac{\sin xt}{x} \, dx = 2 \int_0^{\infty} \frac{\sin z}{z} \, dz = \pi \ . \tag{3.39}$$

Hence,

$$Q \approx -\pi\omega_p \frac{e^2 E_0^2}{2Mk^2} \frac{dF_0}{dv}\bigg|_{v=\omega_p/k} \tag{3.40}$$

is our final expression for the work done on the resonant particles by the wave.

We now consider Poynting's theorem, which states that in media with no dispersion, the total energy density of an electromagnetic field,

$$W = \frac{\epsilon_0}{2} |\mathbf{E}|^2 + \frac{1}{2\mu_0} |\mathbf{B}|^2 \ , \tag{3.41}$$

changes due to the energy density flux carried by the Poynting vector

$$\mathbf{S} = \mathbf{E} \times \mathbf{B} \tag{3.42}$$

and as a result of dissipation according to

$$\frac{\partial W}{\partial t} + \nabla \cdot \mathbf{S} = -\mathbf{E} \cdot \mathbf{J} \ . \tag{3.43}$$

In our simple 1D example, $\mathbf{S} = 0$ and $W = \epsilon_0 E^2/2$, so we find that

$$\frac{1}{\lambda} \int_0^\lambda \frac{\partial W}{\partial t}\, dx = -\frac{1}{\lambda} \int_0^\lambda JE\, dx = -Q \ , \tag{3.44}$$

where

$$\frac{\partial W}{\partial t} = \frac{\epsilon_0}{2} \Bigg[2E_0 \frac{dE_0}{dt} \cos^2(kx - \omega_p t) + \omega_p E_0^2 \cos(kx - \omega_p t) \sin(kx - \omega_p t) \Bigg] \ . \tag{3.45}$$

The second term within the bracket averages to zero when performing the integration in (3.44). Hence,

$$\frac{\epsilon_0}{2} E_0 \frac{dE_0}{dt} = -Q \ , \tag{3.46}$$

so that

$$\frac{dE_0}{dt} = \gamma_L E_0 \ , \tag{3.47}$$

with

$$\gamma_L \equiv -\frac{2Q}{\epsilon_0 E_0^2} = \frac{\pi e^2 \omega_p}{M\epsilon_0 k^2} \frac{dF_0}{dv}\bigg|_{v=\omega_p/k} \ . \tag{3.48}$$

The solution for the amplitude is thus an exponential increase/decay in time, depending on the sign of dF_0/dv at the resonance $v = \omega_p/k$. E.g., if the resonant velocity is high in the tail of a Maxwellian distribution, the fast electrons will give an exponentially weak linear damping. On the other hand, if the wave resonates with a low density electron beam, i.e. a small population of fast electrons with a distribution centered around a maximum at some speed $v_{\max}$, the linear interaction will depend on whether $v_{\max}$ is larger or smaller than the resonant velocity. When $\omega_p/k < v_{\max}$, the gradient dF_0/dv is positive at the resonance, so the wave will be linearly driven by the beam electrons rather than damped.

A more intuitive understanding of the Landau damping/drive can be gained through studying the motion of single particles in the given wave field (3.29). The charged particle equation of motion is

$$M\ddot{x} = eE_0 \cos\left(kx - \omega_p t\right) \ , \tag{3.49}$$

but a change of variables can transform it into the pendulum equation. Indeed, the following dimensionless wave frame variables,

$$z = kx - \omega_p t - \frac{\pi}{2} \ , \quad \tau = \frac{t}{\tau_B} \ , \tag{3.50}$$

defined as to remove the rapid oscillations described by the argument $kx - \omega_p t$, give

$$\frac{d^2 z}{d\tau^2} = 2\pi \sin 2\pi z \ . \tag{3.51}$$

Here, the bounce period τ_B is defined in terms of the bounce frequency ω_B as

$$\omega_B^2 = \frac{(2\pi)^2}{\tau_B^2} \equiv \frac{ekE_0}{M} \ . \tag{3.52}$$

The analytic solution to equation (3.51) is well known, and is best visualized as a phase space plot of the particle trajectories, cf. Figure 3.1. In this figure, the gray trajectories with $dz/d\tau > 0$, i.e. those in the upper half plane, describe phase space flows in the direction of increasing z, i.e. to the right in the figure. Such trajectories are called co-passing, whereas the gray ones in the lower half plane, with $dz/d\tau < 0$, are called counter-passing. The black trajectories inside the so called *separatrix* (the red curve) are called trapped. They correspond to bounded oscillations.

Consider first the siutation with $dF_0/dv < 0$ at the resonant velocity $v = \omega_p/k$ at time $t = 0$. Initially, there are more particles in the lower half of the phase space plot, where $dz/d\tau < 0$, so as the trapped particles start to circulate within the separatrix, there is a net transport of particles to higher

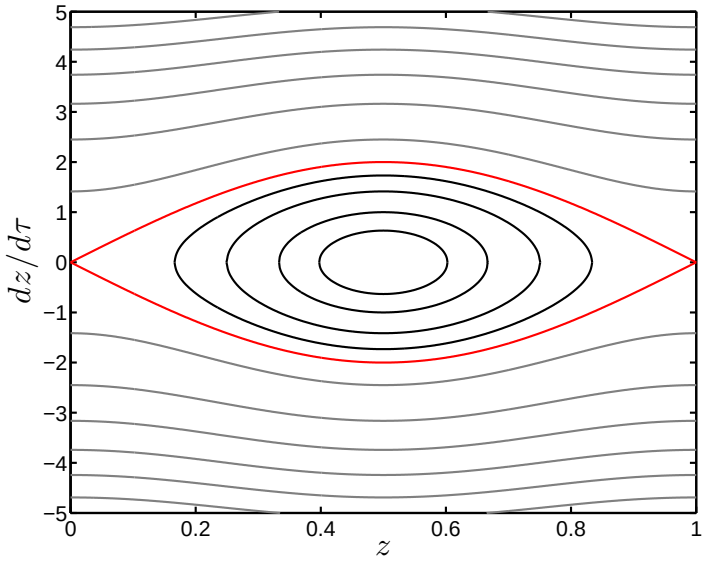

Figure 3.1: Phase space trajectories for the pendulum equation (3.51). The separatrix is highlighted in red.

velocities, or a flux of energy from the wave to the particles. This is the physical reason for the initial, exponential amplitude decrease presented above, and it is known as *linear Landau damping*. Of course, since the trapped particle motion in the wave field is periodic, the particles will eventually deposit the gained energy back into the wave as their velocities decrease. Therefore, linear Landau damping refers to the very initial phase, during the first or so bounce period. On the other hand, if the trapped particles manage to momentarily steal enough energy during the linear phase, there is the possibility of extinguishing the wave entirely. Such an obliteration requires that the wave lifetime τ_L during the linear damping phase is essentially shorter than one half bounce period,

$$\tau_L < \tau_B/2 = \pi/\omega_B \ . \tag{3.53}$$

Hence, it is at least required that

$$\omega_B^2 < \gamma_L^2 \ . \tag{3.54}$$

However, by looking at deeply trapped particles with small z, we see that

$$\ddot{z} = \frac{eE_0}{M} \sin kz \approx \frac{eE_0 k}{M} z \ , \tag{3.55}$$

so that the bounce frequency of such particles is simply

$$\omega_B^2 = \frac{eE_0 k}{M} \ . \tag{3.56}$$

Thus, wave effacement via linear Landau damping is only relevant when E_0 is small enough,

$$E_0 < \frac{M}{ek}\gamma_L^2 \ . \tag{3.57}$$

If, on the contrary, E_0 is so large that the wave outlives the first bounce period, linear Landau damping is no longer applicable and a nonlinear investigation will have to be carried out. Such an analysis has been performed by several authors [23–25], but is way outside the scope of this section. The general conclusions, however, are that the wave amplitude is indeed exponentially damped when $t \ll \tau_B$, but oscillates for $t \sim \tau_B$ and finally saturates as t becomes large. The saturation mechanism in the long run is due to so called *phase mixing*: Since trapped particles that bounce back and forth within the separatrix move at different speeds, the distribution inside the trapping area will eventually have stirred to a smooth plateau, upon which energy can no longer be extracted from, nor deposited into, the trapped particle population.

3.3 Kinetic Instabilities in Tokamak Plasmas

In toroidal systems, the situation is somewhat similar to what was presented above, but the fully three-dimensional, curved geometry complicates the analysis. As before, we will consider the case when the resonant interaction involves only a small group of particles (energetic ions) whose density is small compared to that of the bulk plasma. The situation thus involves a true eigenmode of the background plasma, with an eigenfrequency that is insensitive to the total number of fast particles. On the other hand, the fast particles interact resonantly with tiny seeds of such eigenmodes, and if there is free energy available among the fast particles, a flow of energy from the particles to the eigenmode can be expected to drive the modes unstable. Initially, the resulting exponential growth of the wave amplitude must naturally occur on time scales much longer than that of the mode oscillations (otherwise the fast particles would influence the eigenmode existence and structure as well), which means that the imaginary part of the total linear frequency $\omega = \omega_r + i\gamma_L$ satisfies $\gamma_L \ll \omega_r$.

The excitation of a plane, electromagnetic wave, driven unstable by fast ions in a large aspect ratio, low-β tokamak with circular flux surfaces was considered in [26]. It was shown that, quite generally, the linear growth rate is given by an expression of the form

$$\gamma_L \propto \int (\dots)\, \delta\left(\Omega - \omega_r\right) \left[\omega_r \frac{\partial}{\partial E} + \frac{l\omega_{cA}}{B_A}\frac{\partial}{\partial \mu} + \frac{m}{r\omega_{cA}}\frac{\partial}{\partial r}\right] F_0 \, dE \, d\mu \ . \tag{3.58}$$

Here, F_0 is the unperturbed distribution of energetic ions, i.e. their statistical distribution in the absence of any wave, which has been taken as a function of

the orbit invariants E, μ and p_ζ. The $\partial/\partial r$-term stems from the r-dependence in p_ζ. The delta-function ensures that only resonant particles, those with

$$\Omega \equiv n \langle \omega_\zeta \rangle_B - (m+p)\,\omega_B + l \langle \omega_c \rangle_B \approx \omega \ , \tag{3.59}$$

contribute significantly to the wave excitation. Note that n and m are the toroidal and poloidal mode numbers, while p is just an integer. Much like the Landau damping discussed in Section 3.2, we see that the linear growth rate (3.58) depends on the slope of the unperturbed energetic particle distribution. However, in the present, three-dimensional geometry, three slopes has to be evaluated in three different directions across the resonance, and then averaged over the entire resonance, which in three spatial dimensions is a surface in velocity space rather than a single point.

3.4 Nonlinear Wave-Particle Interaction within a One-Dimensional Bump-On-Tail Model

The nonlinear evolution of fast particle driven modes is important for many reasons. For starters, much like diagnostic tools based on linear mode and frequency determination, measurements of nonlinear mode behavior can serve as probes and yield information about the equilibrium conditions in the inaccessible hot core of a burning plasma environment. Moreover, fast particle losses [27] and redistribution due to such wave-particle interaction are essentially nonlinear features that are currently far from understood. Of course, global calculations of particle and energy transport would require general multimode models that incorporate the full tokamak geometry. Nevertheless, the evolution of single, isolated fast particle driven instabilities[1] remains an important concept on its own (as well as for the general understanding of nonlinear wave-particle physics).

It has been suggested that in the proximity of such isolated resonances, particle motion is effectively 1D, once expressed in proper action-angle variables [28]. Therefore, a simple one-dimensional model, much like the one presented in Section 3.2, with a low density fast electron beam destabilizing an electrostatic plasma wave by means of the free energy available in its positive velocity gradient, should give at least qualitative understanding of nonlinear

[1] With the term *isolated*, we refer to waves that are sufficiently separated in phase space that their regions of influence on the particle orbits do not significantly overlap. In such situations, mode-mode interactions may be safely neglected, and the impact of the fields may be independently treated in the particle trajectory analysis. In fact, when the spectrum of modes is not too dense, small wave amplitudes usually suffices: The electric field amplitude can really be used as a measure of the phase space separatrix width, which roughly indicates the extensions of the resonances.

wave-particle interaction in more general configurations. In fact, if one extends such a simple configuration just slightly to include a phenomenological linear damping rate γ_d, due to dissipation in the background plasma, the system turns out to show great disparity with regards to the relative rates of drive and dissipation.

Away from the excitation threshold (i.e., when the linear drive γ_L from the fast electrons by far exceeds the linear damping rate γ_d), the nonlinear wave evolution consists of an initial linear phase with exponential growth of the mode amplitude, during which a finite width plateau is formed in the driving species distribution function. The fast growth is followed by an oscillatory saturation stage, and then a gradual decay due to the dissipation in the background plasma. However, just above the instability threshold, when

$$0 < \gamma_L - \gamma_d \ll \gamma_d \lesssim \gamma_L \ , \tag{3.60}$$

the characteristic initial growth time $1/\gamma$, with $\gamma \equiv \gamma_L - \gamma_d$ the effective, near-threshold linear growth rate, may become comparable to the relaxation time of the driving species distribution due to collisions and particle sources. The resulting wave evolution unveils a rich spectrum of interesting nonlinear scenarios [29, 30].

Experimentally, there have been many observations of nonlinear mode evolution in the weakly driven regime (3.60). On JET, ICRH accelerated ions excite TAEs that display so called *soft* nonlinear behavior, in the sense that their wave fields quickly evolve into one of several possible steady states. The Fourier signals of the steady states range from nicely saturated, well-defined spectral lines that evolve merely with the plasma equilibrium, to modulated signals that include closely situated sidebands (so called *pitchfork splitting*) [**?**] and blurry indications of chaotic wave evolution [31]. On the contrary, on the spherical tokamak MAST, NBI generated fast ions drive the TAEs into a strongly nonlinear, *hard* regime, with bursting mode amplitudes and rapid frequency chirping [32]. Modes with extended frequency sweeping have also been observed [33], sometimes actually covering frequency ranges several orders of magnitude larger than their initial, linear eigenfrequencies [34].

The model considered in this section describes an electrostatic plasma wave, with prescribed wavelength λ (so that the wave number is $k = 2\pi/\lambda$) and linear frequency ω_p, in a uniform, one-dimensional plasma that contains three different particle species:

- A population of static ions that do not contribute to the dynamics, except that they keep the unperturbed plasma neutral.

- A fluid background of cold electrons that respond linearly to the wave field. These electrons are taken to be subject to a phenomenological

linear friction force, which provides a definition for the linear damping rate γ_d in terms of an unspecified dissipation among the cold electrons. In essence, however, γ_d is nothing but an adjustable input parameter with the purpose of mocking up whatever ways real plasma configurations damp their eigenmodes.

- A low density beam of highly energetic electrons. The fast electrons are described kinetically in terms of their phase space distribution $f(x, v; t)$, whose equilibrium part $F_0(v)$ has a positive slope at the initial resonant velocity $v = \omega_p/k$. The fast electrons thus provide free energy that drives the eigenmode with a linear growth rate $\gamma_L \propto dF_0/dv$. Moreover, they are subject to weak collisions, which act to relax f to F_0 on a time scale long compared to that of the dissipation in the bulk plasma.

The particle species interact with each other and the wave field nonlinearly through the following set of equations for f, the electrostatic potential $\phi(x; t)$ and the cold electron perturbed fluid velocity and density, v_e and δn_e:

- A kinetic equation for the fast electrons,

$$\frac{\partial f}{\partial t} + v\frac{\partial f}{\partial x} + \frac{|e|}{M_e}\frac{\partial \phi}{\partial x}\frac{\partial f}{\partial v} = \mathcal{C}(f) \ . \tag{3.61a}$$

- Linearized fluid momentum and continuity equations for the cold electrons,

$$\frac{\partial v_e}{\partial t} = \frac{|e|}{M_e}\frac{\partial \phi}{\partial x} - 2\gamma_d v_e \tag{3.61b}$$

and

$$\frac{\partial \delta n_e}{\partial t} + n_{e0}\frac{\partial v_e}{\partial x} = 0 \ . \tag{3.61c}$$

- The Poisson equation,

$$\frac{\partial^2 \phi}{\partial x^2} = -\frac{|e|}{\epsilon_0}\left[\delta n_e + \int (f - F_0)\, dv\right] \ . \tag{3.61d}$$

In these expressions, n_{e0} is the unperturbed cold electron density and the phenomenological linear friction force on the cold electrons, due to the dissipation in the background, is $-2\gamma_d v_e$. Note that most authors have preferred to describe the wave in terms of its electric field $E(x; t) = -\partial\phi/\partial x$ rather than the electrostatic potential, and used, instead of the cold electron linearized continuity equation and the Poisson equation, the one-dimensional Ampére's law

$$\frac{\partial E}{\partial t} = \frac{|e|}{\epsilon_0}\left[n_{e0} v_e + \int v\,(f - F_0)\, dv\right] \ . \tag{3.62}$$

The fast electron collision operator $\mathcal{C}(f)$ is written as superposition of three idealized operators, namely:

- **Velocity space diffusion**: These collisions generate a diffusive random walk process in velocity space, and they act to smoothen out any gradients in the perturbed fast particle distribution $f - F_0$. The diffusion operator is given by

$$\mathcal{C}_{\text{Diffusion}}(f) = \frac{\partial^2}{\partial v^2}(f - F_0) \ . \tag{3.63}$$

- **Krook type collisions**: Krook collisions act to relax f into the unperturbed distribution F_0 via the simple operator

$$\mathcal{C}_{\text{Krook}}(f) = -(f - F_0) \ . \tag{3.64}$$

  Such collisions are often employed as a simpler alternative capable of mimicking the more realistic, but also more demanding, diffusion operator. Krook collisions can however be of true interest, e.g. to model large-angle Coulomb collisions that immediately scatter fast particles out of resonance.

- **Drag**: The drag operator is given by

$$\mathcal{C}_{\text{Drag}}(f) = \frac{\partial}{\partial v}(f - F_0) \ , \tag{3.65}$$

  and it represents the effect of slowing-down due to small-angle Coulomb collisions with the slower particle species. From the perspective of the kinetic equation (3.61a), the first term acts as a constant, DC, electric field that generates a flow of fast electrons towards lower velocities, whereas the second term constitutes a sink that preserves the equilibrium distribution function F_0.

The total fast electron collision operator is thus given by

$$\mathcal{C}(f) = -\beta(f - F_0) + \frac{\alpha^2}{k}\frac{\partial}{\partial v}(f - F_0) + \frac{\nu^3}{k^2}\frac{\partial^2}{\partial v^2}(f - F_0) \ , \tag{3.66}$$

where $k = 2\pi/\lambda$ is the wave number and β, α and ν are effective rates for the various types of collisions considered. Note that, quite generically, all authors have assumed that α, β, and ν are small as compared to γ_d.

The near threshold limit of the presented model has been thoroughly investigated throughout the years. Under the assumption of a small nonlinearity, which enables the construction of an analytical perturbative solution, it was

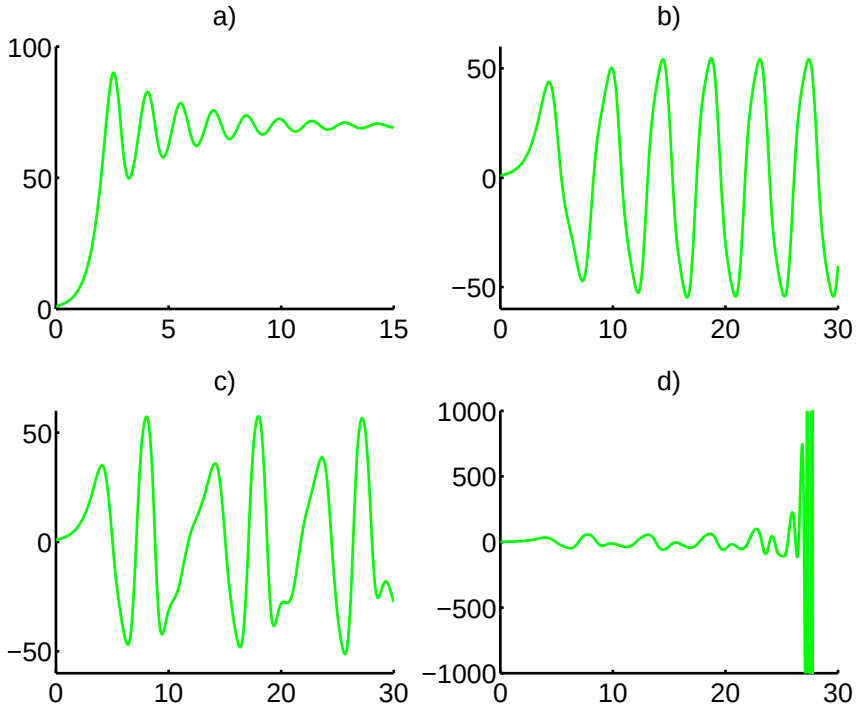

Figure 3.2: Amplitude evolution as predicted by the weakly nonlinear, perturbative solution. The effective collision rate is decreased in the sequence of figures a) - d). Axis labels have been omitted for simplicity. They should read 'γt' (x-axis) and 'Normalized amplitude' (y-axis).

found that the fast particle effective collision rate determines the wave evolution in a manner that essentially replicates the observations from JET and MAST discussed previously: In the presence of the idealized Krook operator (3.64), [29], and/or the velocity space diffusion operator (3.63), [35], the electric field amplitude evolves into one of four possible regimes, depending on the ratio between the effective linear growth rate $\gamma \equiv \gamma_L - \gamma_d$ and the relexation time of the fast particle distribution. With a sufficient rate of fast electron collisions, the amplitude evolves into a nicely saturated steady state. Then, as the collisionality is gradually lowered, the amplitude evolution is characterized by the following sequence (cf. Figure 3.2): A steady state regime with a periodic amplitude modulation that generates closely situated sidebands (pitchfork splitting); a regime with chaotic, but bounded, amplitude evolution; a regime characterized by a fast, explosive blow-up of the electric field amplitude in a finite time. On the contrary, with enough drag collisions the initial amplitude evolution was found to be unavoidably explosive [36]. Within this framework, the bursting tendency for TAEs observed on MAST was explained in terms of a relatively higher fraction of slowing-down collisions experienced by NBI gen-

erated fast ions as compared to those in ICRH heated JET discharges, which undergo a quasilinear, diffusive random walk due to the interaction with the RF field.

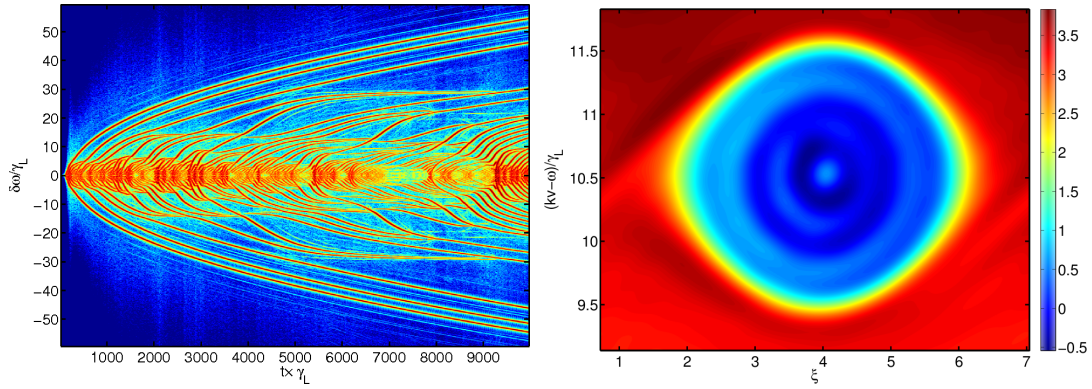

Figure 3.3: Left: Spectrogram obtained from the BOT code [38] in the collisionless limit. Right: Phase space plot of the hole corresponding to the first excited mode on the left. The snapshot is taken at the end of the simulation. Note how well phase mixed the fast electron distribution function is. This is in fact a robust statement which applies to almost the entire hole evolution, with the actual formation of the hole as the only exception.

The amplitude blow-up in the explosive regime leads to a breakdown of the perturbative approach and clearly motivates a nonlinear numerical investigation. In fact, a fully nonlinear analysis is needed, since during the blow-up, nonlinearities of all orders can be shown to be equally large. The nonlinear regime was probed in [30,37,38], where it was established that the initial explosive stage in the drag dominated and weakly collisional scenarios is associated with the formation of coherent structures in the fast particle distribution, so called hole-clump pairs. These entities extend in configuration as well as velocity space, and their Fourier signals correspond to slightly up- and down-shifted sidebands (with respect to the linearly unstable frequency). During the subsequent evolution, the holes and clumps undertake a voyage through fast particle phase space as they seek lower energy states in order to compensate for the dissipation in the background plasma. Quite generically (at least for the initial evolution), this implies that the holes shifts towards larger velocities, whereas the clump shifts towards lower velocities. Meanwhile, the associated nonlinear frequencies of the sidebands shift up and down, respectively, as seen in the spectrogram in Figure 3.3. Analytically, it can be shown that the initial frequency shift evolves according to

$$\delta\omega \propto \pm\sqrt{t} \ . \tag{3.67}$$

On a somewhat longer time scale, fast particle collisions can actually influence the frequency shift. For instance, interesting hole sweeping patterns, including

so called *hooks* and steady states holes (see Figure 3.4), were obtained for certain combinations of drag and diffusion collision rates. Similar features have, in fact, been observed experimentally [39].

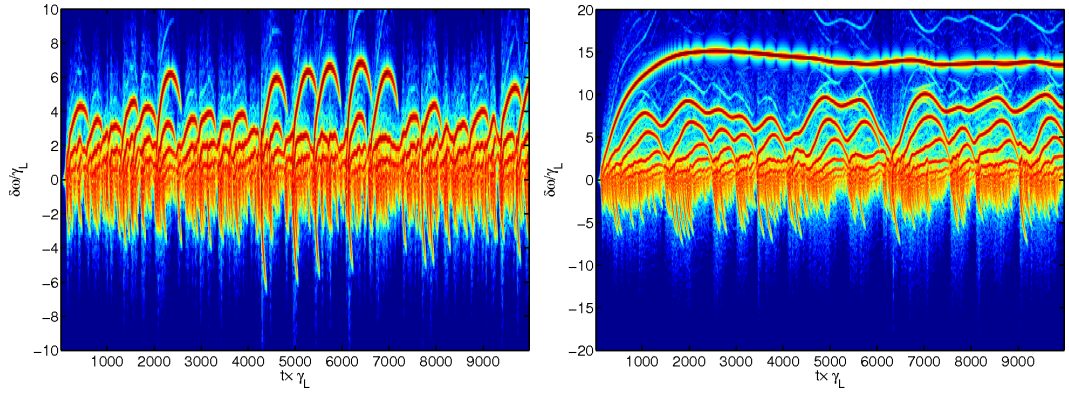

Figure 3.4: Left: Spectrogram displaying so called hooked frequency sweeping. Right: Spectrogram showing a hole reaching a steady state frequency. Note the assymetry between holes and clumps in these simulations, which is due to the presence of drag. These plots were both obtained using the BOT code [38].

4

Toroidal Alfvén Eigenmodes

Alfvén waves are the basic low frequency modes of magnetized plasmas [40]. They were discovered theoretically in 1942 by Hannes Alfvén [41], and are of high importance in tokamak, space and astrophysical plasmas. In toroidal devices, there is an entire zoo of Alfvén waves. There are toroidicity, ellipticity and triangularity induced Alfvénic eigenmodes supported by the device geometry itself, as well as global modes associated with off-axis currents and current holes in the lplasma core. In addition, a spectrum of non-ideal modes exists, which can be found theoretically only once small wavelengths on the order of the thermal ion Larmor radius are taken into account.

In typical tokamak experiments, Alfvén waves oscillate with frequencies in the range of a few hundred kHz. As already discussed in Chapter 1, they are therefore very prone to interact resonantly with super-thermal ions, and accordingly earned much attention during the 1980s and 1990s, when tokamaks first started to probe regimes with non-negligible populations of energetic ions. Early on, global Alfvénic modes were found to be destabilized by circulating, NBI produced fast ions in the Wendelstein W7-AS stellarator. Somewhat later, NBI [42,43] and ICRH [44,45] generated fast ions proved capable of destabilizing so called *toroidal Alfvén eigenmodes* (TAEs) on TFTR, JET and DIII-D. These observations led to the widespread notion that Alfvénic activity may result in large radial fluxes of fast ions due to increased transport. Indeed, a 70 % loss of the total beam power was observed, and attributed to the TAEs, on DIII-D during the experiments with high-power NBI [43]. However, even during the D-T campaigns, where record high concentrations of alpha particles were produced in experiments on JET and TFTR, unambiguous identification of alpha particle-driven TAEs proved difficult. The most succesful attempts occured on TFTR. They include indirect measurements of the alpha particle contribution to the TAE linear growth rate [46], and direct observations of

TAEs during the so called *afterglow* phase, 100 - 200 ms following the end of NBI [47]. An additional remark on the future importance of Alfvénic eigenmodes concerns their stability in future, high-β devices: Alfvén waves tend to become more stable as the plasma pressure rises.

In this chapter, we start by introducing in Section 4.1 the magnetohydrodynamic (MHD) model usually employed to analyze plasma equilibrium configurations and linear perturbations with low oscillation frequencies. Then, in Section 4.2, we apply this model to derive and comment on the Alfvén wave dispersion relation in a static and uniform plasma. In Section 4.3, we generalize the geometry and consider Alfvénic waves in cylidrical and toroidal plasmas. We also discuss the role of non-ideal effects, in particular those associated with first order finite thermal ion Larmor radius and parallel electron dynamics corrections to the MHD equations.

4.1 The Magnetohydrodynamic Model

Low frequency plasma waves are usually treated within the framework of MHD, a single-fluid description of two-species plasmas that contain ions with mass M_i and charge number Z_i, and electrons with mass M_e. The model equations are obtained by combining Maxwell's equations with velocity moments of the kinetic equations for each plasma species. First, a two-fluid model is formed by truncating the series of moments with an equation of state, arising from the second velocity moment by neglecting heat conduction and heat exchange between the plasma species. Second, the two-fluid model is reduced to a one-fluid description via the introduction of the following quantities:

- The total mass density

$$\rho = M_i n_i + M_e n_e \approx M_i n_i \tag{4.1}$$

- The overall charge density

$$\rho_c = (Z_i n_i - n_e) \tag{4.2}$$

- The centre-of-mass velocity

$$\mathbf{v} = \frac{M_i n_i \mathbf{v}_i + M_e n_e \mathbf{v}_e}{\rho} \approx \mathbf{v}_i \tag{4.3}$$

- The total current

$$\mathbf{J} = e\,(Z_i n_i \mathbf{v}_i - n_e \mathbf{v}_e) \tag{4.4}$$

- The total scalar pressure
$$P = P_e + P_i \tag{4.5}$$

In these expressions, n_i, n_e, $\mathbf{v}_i$ and $\mathbf{v}_e$ are the number densities and individual fluid velocities of the ions and electrons, respectively, and we have changed the notation so that e now denotes the magnitude of the electron charge rather than the overall charge of a particle. Finally, under the assumption of quasineutrality, meaning that $Z_i n_i = n_e = n$ and $\rho_c = 0$, the MHD set of equations can be summarized as follows:

- The equation of continuity (expressing mass density conservation)
$$\frac{\partial \rho}{\partial t} + \nabla \cdot (\rho \mathbf{v}) = 0 \ , \tag{4.6a}$$

- The momentum equation
$$\rho \frac{d\mathbf{v}}{dt} = \mathbf{J} \times \mathbf{B} - \nabla P \ , \tag{4.6b}$$

- The adiabatic equation of state
$$\frac{d}{dt}\left(\frac{P}{\rho^\gamma}\right) = 0 \ , \tag{4.6c}$$

- The resistive Ohm's law
$$\mathbf{E} + \mathbf{v} \times \mathbf{B} = \eta \mathbf{J} \ , \tag{4.6d}$$

- The non-relativistic Ampére's law
$$\nabla \times \mathbf{B} = \mu_0 \mathbf{J} \tag{4.6e}$$

- Faraday's law
$$\nabla \times \mathbf{E} = -\frac{\partial \mathbf{B}}{\partial t} \ . \tag{4.6f}$$

Here, $\mathbf{E}$ and $\mathbf{B}$ are the electric and magnetic fields, η is the plasma resistivity and the adiabatic index γ is the ratio of specific heats, or heat capacities, taken at constant pressure and volume. Note that the Ampére's law (4.6e) implies that
$$\nabla \cdot \mathbf{J} = 0 \ . \tag{4.7}$$
Therefore, multiplying both sides of the continuity equation (4.6a) with the charges of the respective particle species, and subsequently adding the resulting equations gives the charge conservation condition
$$\frac{\partial \rho_c}{\partial t} = -\nabla \cdot \mathbf{J} = 0 \ , \tag{4.8}$$

which is a reminder that MHD describes a quasineutral system.

Since the displacement current is neglected in the non-relativistic version (4.6e) of Ampére's law, the MHD equations presented above are restricted to describe phenomena that occur on time scales much longer than the time it takes light to traverse the plasma. Indeed, the dominant fluid velocity in equations (4.6) is that of the $\mathbf{E} \times \mathbf{B}$-drift, which means that MHD theory describes relatively low frequency oscillations. In many cases, the MHD set of equations can be simplified even further by assuming that the plasma conducitivity is so high that the right hand side of Ohm's law (4.6d) can be neglected. The resulting model is called *ideal* MHD, and it contains no parallel electric field. In that spirit, the equations given above are sometimes called *resistive* MHD. It has been pointed out that tokamak fusion plasmas actually do not satisfy all the criteria for ideal MHD theory to be valid. In particular, they are not sufficiently collisional to relax the various plasma species distribution functions into local Maxwellians on a fast enough time scale. Nevertheless, ideal MHD seems to provide an accurate description of macroscopic fusion plasma behavior [48], and has been extensively used in the modeling of plasma equilibria and for stability predictions. For those reasons, we will use ideal MHD for the basic analysis of low frequency Alfvén waves throughout this thesis. When parallel dynamics and non-ideal effects are needed, we will simply introduce *a posteriori* a parallel current via the quasineutrality condition $\nabla \cdot \mathbf{J} = 0$.

4.1.1 Equilibrium Analysis

The ideal MHD framework is well suited for the description of static plasma equilibria. That is, time independent configurations (whose one-fluid quantities all satisfy $\partial/\partial t = 0$) with no overall plasma flow ($\mathbf{v} = 0$). Under these assumptions, the remaining, non-trivial ideal MHD equations (4.6) are

$$\mathbf{J} \times \mathbf{B} = \nabla P \ , \quad \nabla \times \mathbf{B} = \mu_0 \mathbf{J} \ , \quad \nabla \cdot \mathbf{B} = 0 \ , \tag{4.9}$$

where the $\nabla \cdot \mathbf{B} = 0$ has been added by hand to the usual ideal MHD set in order to close the system of equilibrium equations. We will not say more about MHD equilibria here. However, we note that (4.9) is the set that was used for the equilibrium analysis in Section 2.2.2 of Chapter 2.

4.1.2 Linear Stability

In order to assess the stability of ideal MHD configurations, we consider small perturbations from static equilibria of the type described in the preceding section. In the analysis, equilibrium quantities are denoted with the subscript 0, while the perturbations are denoted with the subscript 1,

$$\mathbf{B} = \mathbf{B}_0 + \mathbf{B}_1 \ , \quad \mathbf{J} = \mathbf{J}_0 + \mathbf{J}_1 \ , \quad \mathbf{v} = \mathbf{v}_1 \ , \quad \mathbf{E} = \mathbf{E}_1 \ ,$$
$$P = P_0 + P_1 \ , \quad \rho = \rho_0 + \rho_1 \ . \tag{4.10}$$

The set of ideal MHD equations can then be expanded order by order in the perturbed quantities. To lowest order, the equations that describe the equilibrium configuration are those in (4.9),

$$\mathbf{J}_0 \times \mathbf{B}_0 = \nabla P_0 \ , \quad \nabla \times \mathbf{B}_0 = \mu_0 \mathbf{J}_0 \ , \quad \nabla \cdot \mathbf{B}_0 = 0 \ . \tag{4.11}$$

The next order equations, linear in the perturbations, are given by

$$\frac{\partial \rho_1}{\partial t} + \nabla \cdot (\rho_0 \mathbf{v}_1) = 0 \ , \tag{4.12a}$$
$$\rho_0 \frac{\partial \mathbf{v}_1}{\partial t} = \mathbf{J}_0 \times \mathbf{B}_1 + \mathbf{J}_1 \times \mathbf{B}_0 - \nabla P_1 \ , \tag{4.12b}$$
$$\frac{\partial P_1}{\partial t} + \mathbf{v}_1 \cdot \nabla P_0 - \gamma \frac{P_0}{\rho_0} \left(\frac{\partial \rho_1}{\partial t} + \mathbf{v}_1 \cdot \nabla \rho_0 \right) = 0 \ , \tag{4.12c}$$
$$\mathbf{E}_1 + \mathbf{v}_1 \times \mathbf{B}_0 = 0 \ , \tag{4.12d}$$
$$\nabla \times \mathbf{B}_1 = \mu_0 \mathbf{J}_1 \ , \tag{4.12e}$$
$$\frac{\partial \mathbf{B}_1}{\partial t} + \nabla \times \mathbf{E}_1 = 0 \ . \tag{4.12f}$$

Since the equilibrium quantities are independent of time and the stability equations (4.12) are linear, we can represent the perturbations as normal modes,

$$Q_1 (\mathbf{r}, t) = Q_1 (\mathbf{r}) \, \mathrm{e}^{-i\omega t} \ , \tag{4.13}$$

where the frequency ω may be complex. If we now introduce the perturbed displacement $\mathbf{x}$ via the definition

$$\mathbf{v}_1 = \frac{\partial \mathbf{x}}{\partial t} = -i\omega \mathbf{x} \ , \tag{4.14}$$

the perturbed quantities may be eliminated one by one, until the system (4.12) has been reduced to a single, vectorial equation for $\mathbf{x}$:

$$-\omega^2 \rho_0 \mathbf{x} = \mathbf{F} (\mathbf{x}) \ , \tag{4.15}$$

where the so called *force operator* $\mathbf{F}$ has the form

$$\mathbf{F}(\mathbf{x}) = \frac{1}{\mu_0}(\nabla \times \mathbf{B}_0) \times \Big[\nabla \times (\mathbf{x} \times \mathbf{B}_0)\Big] + \frac{1}{\mu_0}\Big\{\nabla \times \Big[\nabla \times (\mathbf{x} \times \mathbf{B}_0)\Big]\Big\} \times \mathbf{B}_0 + \nabla(\mathbf{x} \cdot \nabla P_0 + \gamma P_0 \nabla \cdot \mathbf{x}) \ . \tag{4.16}$$

Equation (4.15) consitutes an eigenvalue problem for ω, to be solved in a certain equilibrium configuration (magnetic field structure and geometry), given initial values for and boundary conditions on $\mathbf{x}$. It is important to note that $\mathbf{F}$ is Hermitian. This means that $\omega^2 \in \mathfrak{R}$, which allows for two types of solutions: When $\omega^2 > 0$, the perturbation is an eigenmode with frequency $\omega \in \mathfrak{R}$. On the contrary, when $\omega^2 < 0$, then $i\omega \in \mathfrak{R}$, and the perturbation is a pure instability with $\mathrm{Re}(\omega) = 0$ that grows exponentially.

4.2 Alfvén Waves in a Uniform Plasma

As a first application of ideal MHD stability analysis, we derive the dispersion relation for Alfvén waves in the simplest possible setup: An infinite, static and homogeneous plasma. In such a configuration, there are only two non-zero terms in $\mathbf{F}$: That in the middle and the second within the bracket. The mode equation can then be put on the form

$$-\omega^2 \mathbf{x} = v_A^2 \left\{\nabla \times \Big[\nabla \times \big(\mathbf{x} \times \mathbf{b}\big)\Big]\right\} \times \mathbf{b} + c_s^2 \nabla(\nabla \cdot \mathbf{x}) \ , \tag{4.17}$$

where we have defined the Alfvén and sound speeds as

$$v_A^2 \equiv \frac{B_0^2}{\mu_0 \rho_0} \ , \quad c_s^2 \equiv \frac{\gamma P_0}{\rho_0} \ . \tag{4.18}$$

Equation (4.17) is a second order, linear ODE with constant coefficients. It is therefore advantageous to normal mode expand $\mathbf{x}$ in space too, all in all giving

$$\mathbf{x}(\mathbf{r}, t) = \mathbf{x} \exp\left[i(\mathbf{k} \cdot \mathbf{r} - \omega t)\right] \ , \tag{4.19}$$

where $\mathbf{k}$ is the wave vector. We then get

$$\omega^2 \mathbf{x} = v_A^2 \left\{\mathbf{k} \times \Big[\mathbf{k} \times \big(\mathbf{x} \times \mathbf{b}\big)\Big]\right\} \times \mathbf{b} + c_s^2 \mathbf{k}\big(\mathbf{k} \cdot \mathbf{x}\big) \ . \tag{4.20}$$

Aligning the coordinate system so that the perpendicular wave vector $\mathbf{k}_\perp$ points along a certain direction with unit vector $\mathbf{e}_\perp$ (and with $\mathbf{e}_a = \mathbf{e}_\perp \times \mathbf{e}_\parallel$), equation (4.20) can be represented as

$$\begin{bmatrix} \omega^2 - k_\parallel^2 v_A^2 & 0 & 0 \\ 0 & \omega^2 - k^2 v_A^2 - k_\perp^2 c_s^2 & -k_\perp k_\parallel c_s^2 \\ 0 & -k_\perp k_\parallel c_s^2 & \omega^2 - k_\parallel^2 c_s^2 \end{bmatrix} \begin{bmatrix} x_a \\ x_\perp \\ x_\parallel \end{bmatrix} = 0 \ . \tag{4.21}$$

Two nontrivial solutions exists to this matrix equation:

- The *shear* Alfvén wave has $x_\perp = x_\parallel = 0$, with $x_a \neq 0$, and it satisfies the dispersion relation
$$\omega^2 = k_\parallel^2 v_A^2 \ . \tag{4.22}$$
Since $k_a = 0$, we have $\nabla \cdot \mathbf{x} = 0$, meaning that $P_1 = \rho_1 = 0$. Hence, the shear Alfvén wave is said to be incompressible: It has neither density nor pressure fluctuations. Furthermore, Faraday's law combined with the ideal Ohm's law shows that $\mathbf{B}_1 \parallel x_a$, so that $\mathbf{B}_1 \perp \mathbf{B}_0$, which is the reason it is called the shear wave.

- The *compressional* Alfvén wave has $x_a = 0$, and its dispersion relation is found by setting the bottom right 2×2 subdeterminant of the matrix in (4.21) to zero. After some algebra, one obtains
$$\omega^2 = \frac{k^2}{2}\left(v_A^2 + c_s^2\right)\left\{1 \pm \left[1 - \frac{4k_\parallel^2 v_A^2 c_s^2}{k^2\left(v_A^2 + c_s^2\right)^2}\right]^{\frac{1}{2}}\right\} \ , \tag{4.23}$$
where $k^2 = k_\perp^2 + k_\parallel^2$. The plus sign in (4.23) corresponds to the so called fast magnetosonic wave, which involves perturbed motion perpendicular to the equilibrium magnetic field, while the minus sign corresponds to the slow magnetosonic wave, which in the limit $c_s \ll v_A$ is a sound wave whose perturbed motion is dominated by pressure fluctuations along the equilibrium magnetic field.

4.3 Alfvén Waves in Toroidal Plasmas

In toroidal configurations, the experimental geometry requires the Alfvén waves to be periodic with respect to the poloidal and toroidal angles θ and ζ. The modes are therefore characterized poloidally and toroidally by some integer wave numbers m and n, while the radial mode structure must be solved for by means of the ideal MHD equations. The linearization procedure depicted in the previous section leads to the equation [49]

$$\nabla \cdot \left[\frac{\omega^2}{v_A^2}\nabla_\perp \phi\right] + \mathbf{B}_0 \cdot \nabla\left[\frac{1}{B_0^2}\nabla \cdot \left\{B_0^2 \nabla_\perp \left[\frac{\mathbf{B}_0 \cdot \nabla\phi}{B_0^2}\right]\right\}\right] = 0 \ , \tag{4.24}$$

for normal modes with high toroidal mode number, n, of the shear Alfvén wave electrostatic potential. Here, the zero pressure limit $\beta \to 0$ has been adopted in order to simplify the analysis.

An essential ingredient in the derivation of equation (4.24) is that the shear waves are assumed to be described by a single scalar potential $\Phi(\mathbf{r}; t) =$

$\phi(\mathbf{r})\,\mathrm{e}^{-i\omega t}$. This is somewhat counter-intuitive, since, quite generally, all three types of modes described in Section 4.2 couple when the magnetic field is non-uniform [50]. However, when the equilibrium flow is subsonic and $v_A \gg c_s$, displacements along the magnetic field, the slow magnetosonic mode, effectively decouple from the shear and fast magnetosonic modes, and moreover do not interact with the equilibrium flow. In fact, we are assuming throughout the present section that there is no equilibrium flow at all, $\mathbf{v}_0 = 0$, which means that we can certainly neglect the parallel component $x_\parallel$. Moreover, in the limit of low β, it can be shown, [51], that the shear and compressional waves also, more or less, decouple. The resulting equation for the shear wave takes exactly the form (4.24) when written in terms of the scalar potential ϕ. However, one must remember that shear waves in non-uniform plasmas always have a small compressional part with a small but finite group velocity across the magnetic field lines.

Equation (4.24) is most easily analyzed by assuming that the aspect ratio is large and that the flux surfaces are circular. However, as previously mentioned, we can no longer rely on the further simplifying assumption that the flux surfaces are also concentric. A consistent treatment of toroidal effects must necessarily include the Shafranov shift discussed in Section 2.2.2, simply because the effects of the shift enter the calculations at $\mathcal{O}(\epsilon)$, and are therefore equally important as purely toroidal effects due to the scaling $B \propto 1/R$. From now on, we will use the term "toroidal effects" as a common label for both the Shafranov shift and the poloidal variation in the magnetic field strength. If we introduce straight field line, flux-type coordinates (r, θ_f, ζ), cf. Section 2.2.3 and [52],[1] and Fourier expand the periodic function ϕ in the variables θ_f and ζ according to

$$\phi(r, \theta_f, \zeta, t) = \sum_{m,n} \phi_{mn}(r)\,\mathrm{e}^{i\left(n\zeta - m\theta_f - \omega t\right)}\,, \tag{4.25}$$

we can form a set of equations for ϕ_{mn} by multiplying (4.24) with orthogonal phase functions of the type appearing in (4.25), and integrating in both θ_f and ζ from 0 to 2π. In these calculations, the toroidal mode number n is a good "quantum number" due to the symmetry along the ζ direction, so toroidal harmonics of ϕ, i.e. ϕ_{mn} with different n, never mix in the resulting equations. On the contrary, due to the toroidal effects, there is no analogous symmetry along the θ_f direction, which results in couplings between the poloidal harmonics of ϕ, i.e. ϕ_{mn} with different m. In general, many such harmonics are involved

[1] Here, r and ζ are the radial coordinate and toroidal angle in the usual toroidal coordinate system. However, θ_f does not equal the usual poloidal angle θ. Instead, it is a function of r and θ, much similar to equation (2.103), but also including the effects of the Shafranov shift.

and the situation is most difficult to assess analytically. However, under certain conditions (which we will come back to and discuss more exhaustively later on), the modes are well localized around certain radial positions in the plasma, and involve mainly two neighboring poloidal harmonics, say the m:th and $m-1$:th. To first order in ϵ, the set of equations that describe such modes consists of two coupled, second order ODEs for ϕ_m and ϕ_{m-1}, [53],

$$\begin{bmatrix} \mathfrak{L}_m & \mathfrak{L}_1 \\ \mathfrak{L}_1 & \mathfrak{L}_{m-1} \end{bmatrix} \begin{bmatrix} \phi_m \\ \phi_{m-1} \end{bmatrix} = 0 \ , \tag{4.26}$$

with

$$\mathfrak{L}_m = \frac{d}{dr}\left[\left(\frac{\omega^2}{v_A^2} - k_{\parallel m}^2\right)\frac{d}{dr}\right] - \frac{m^2}{r^2}\left(\frac{\omega^2}{v_A^2} - k_{\parallel m}^2\right) \ , \tag{4.27a}$$

$$\mathfrak{L}_1 = \frac{\hat{\epsilon}}{4q^2R_A^2}\frac{d^2}{dr^2} \ . \tag{4.27b}$$

Here, the Alfvén speed is defined as to contain no toroidal effects and therefore acquires its radial dependence merely through the equilibrium density profile,

$$v_A^2(r) = \frac{B_A^2}{\mu_0\rho_0(r)} \ , \tag{4.28}$$

the parallel wave number is given by

$$k_{\parallel m}(r) = \frac{nq(r) - m}{q(r)R_0} \tag{4.29}$$

and the parameter $\hat{\epsilon}$ is a small, $\hat{\epsilon} \ll 1$, effective coupling coefficient that includes contributions due to both types of toroidal effects in our analysis. In [52], it is shown that $\hat{\epsilon} \approx 5r/2R_0$. Note that since equation (4.26) holds for any large enough toroidal mode number n, we have changed the notation by suppressing n in ϕ_{mn}. Similarly, $k_{\parallel m}$ is labeled only with m, although its definition (4.29) contains an n.

4.3.1 Cylindrical Limit

In the cylindrical limit $r/R_0 \to 0$, the magnetic field strength can be approximated as constant throughout the plasma. There is then an additional translational symmetry along the poloidal direction, and the equations (4.26) that describe the neighboring poloidal harmonics effectively decouple into

$$\mathfrak{L}_m\phi_m = \frac{d}{dr}\left[\left(\frac{\omega^2}{v_A^2} - k_{\parallel m}^2\right)\frac{d\phi_m}{dr}\right] - \frac{m^2}{r^2}\left(\frac{\omega^2}{v_A^2} - k_{\parallel m}^2\right)\phi_m = 0 \tag{4.30}$$

for each poloidal harmonic. For a wave that oscillates with a fixed frequency ω, the solutions to (4.30) are logarithmically divergent along the curves defined by $\omega = \pm k_{\parallel m}(r)\, v_A(r)$ in (r, ω)-space. The solutions on each side of such a singularity are related by analytic continuation, which results in complex solutions whose imaginary parts represent resonant absorption. Therefore, such modes are resonantly damped throughout the plasma, and the damping has been shown to be almost complete [54]. The logarithmically divergent modes are called *continuum modes* and the associated damping is known as *continuum damping*. The radial spectrum of the continuum modes, called the *Alfvén continuum*, coincides with the positive branch of $\omega = \pm k_{\parallel m}(r)\, v_A(r)$ in the cylindrical limit, cf. Figure 4.1. As seen in the figure, these cylindrical Alfvén continua typically decrease along the branch $\omega = -k_{\parallel m}(r)\, v_A(r)$ from $r = 0$ until $k_{\parallel m} = 0$, upon which they increase monotonically along $\omega = k_{\parallel m}(r)\, v_A(r)$ all the way to the plasma edge.

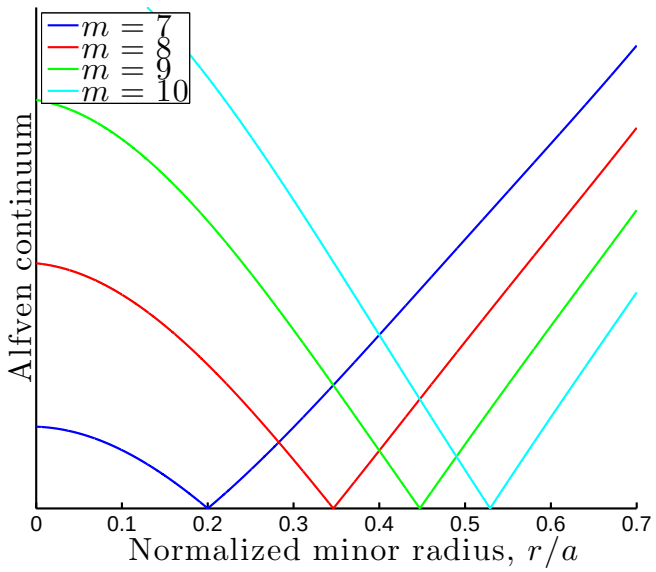

Figure 4.1: Qualitative radial profiles for Alfvén continua, the positive branch of $\pm k_{\parallel m}(r)\, v_A(r)$, in the cylindrical limit. The toroidal mode number is $n = 5$ and m ranges from 7 to 10.

To investigate in detail what happens when a wave resonates with the local Alfvén frequency, finite ion Larmor radius effects and parallel electron dynamics need to be added [55]. As already noted, ideal MHD theory on its own does not allow the shear wave to propagate across the equilibrium magnetic field. But as the logarithmically singular solution to the MHD mode equation (4.30) starts to blow up, the radial gradients will eventually hit the

ion Larmor radius scale where the ions can no longer be viewed as tied to the magnetic field lines. The MHD singularity is thus resolved in the very proximity of the resonance via mode conversion of the MHD wave into a kinetic wave that is allowed to propagate across the equilibrium magnetic field. The propagating kinetic wave is then absorbed by the plasma through both linear and nonlinear, collisional and collisionless damping processes. In Section 4.3.4, we will discuss kinetic Alfvén waves in more detail and show specifically how to make the mode equations account for first order finite ion Larmor radius effects and parallel electron dynamics.

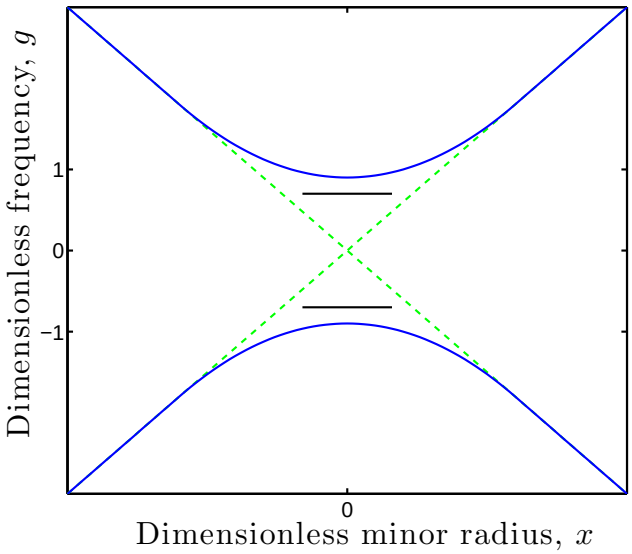

Figure 4.2: The toroidal effects induce gaps in the cylindrical Alfvén continuum, which is given by the dashed green lines. For definitions of g and x, see equations (4.38) and (4.37). The solid, black lines represent eigenmodes: The lower is the usual TAE; The upper is an analogue of the lower TAE, found in the very low shear limit.

4.3.2 Toroidal Alfvén Eigenmodes

When the toroidal coupling terms in (4.26) are taken into account, the continuum modes will no longer diverge exactly along the cylindrical continua. Instead, what happens is that close to the radial positions r_m where the cylindrical continua for neighboring poloidal modes cross, defined by setting $k_{\parallel m-1} = -k_{\parallel m}$, so that the safety factor satisfies

$$q\left(r_m\right) = \frac{2m-1}{2n} \ , \tag{4.31}$$

gaps appear that remove the crossings and therefore resolve the degeneracies with respect to neighboring poloidal mode numbers. A qualitative example of such a *toroidicity induced Alfvén gap* is shown in Figure 4.2, whereas Figure 4.3 shows the global continuum in an actual experiment. The frequency span of the gap can be calculated by rewriting (4.26) in a form where the second radial derivative of each poloidal harmonic is given as a function of only lower order derivatives, r and ω,

$$G(\omega;r)\frac{d^2\phi_m}{dr^2} = f_m\left(\omega;\phi_m,\phi_{m-1},\frac{d\phi_m}{dr},\frac{d\phi_{m-1}}{dr},r\right) , \tag{4.32a}$$

$$G(\omega;r)\frac{d^2\phi_{m-1}}{dr^2} = f_{m-1}\left(\omega;\phi_m,\phi_{m-1},\frac{d\phi_m}{dr},\frac{d\phi_{m-1}}{dr},r\right) , \tag{4.32b}$$

with

$$G(\omega;r) \equiv \left[\frac{\omega^2}{v_A^2} - k_{\|m}^2\right]\left[\frac{\omega^2}{v_A^2} - k_{\|m-1}^2\right] - \left(\frac{\hat{\epsilon}}{4q^2R_A^2}\right)^2 . \tag{4.33}$$

The actual form of the functions f_m and f_{m-1} is irrelevant. It simply suffices to observe that the characteristic sign of the Alfvén continuum is the logarithmic divergence of the poloidal harmonics ϕ_m. In equations (4.32), such singularities occur when the function G that multiplies the second order derivatives vanishes. At the radial positions r_m, where $k_{\|m-1} = -k_{\|m}$ holds, the condition $G = 0$ gives the continuum frequencies

$$\omega_\pm \approx \frac{v_A(r_m)}{2q(r_m)R_A}\left[1 \pm \hat{\epsilon}/2\right] . \tag{4.34}$$

Therefore, the gap width is given by

$$\Delta\omega = \omega_+ - \omega_- \approx \hat{\epsilon}\frac{v_A(r_m)}{2q(r_m)R_A} , \tag{4.35}$$

which is seen to vanish in the cylindrical limit $\epsilon \to 0$.

The occurence of gaps in the Alfvén continuum enables the possibility of cavity eigenmodes with frequencies in the gap [57], since such modes would not experience any continuum damping. In principle, the extrema at the continuum tips allows for the formation of wells in the effective potentials of equations (4.32), [58], so that radially standing waves with discrete eigenfrequencies can be set up. Conceptually, the existence of such potentials relies on the small compressional components of the shear wave (that are always present in non-uniform magnetic fields), which allows the plasma at different radial positions to communicate and synchronize enough to endorse standing waves.

In order to analyze analytically whether eigenmodes are present or not, the system (4.26) must be tackled in a boundary layer manner, [59]. In the

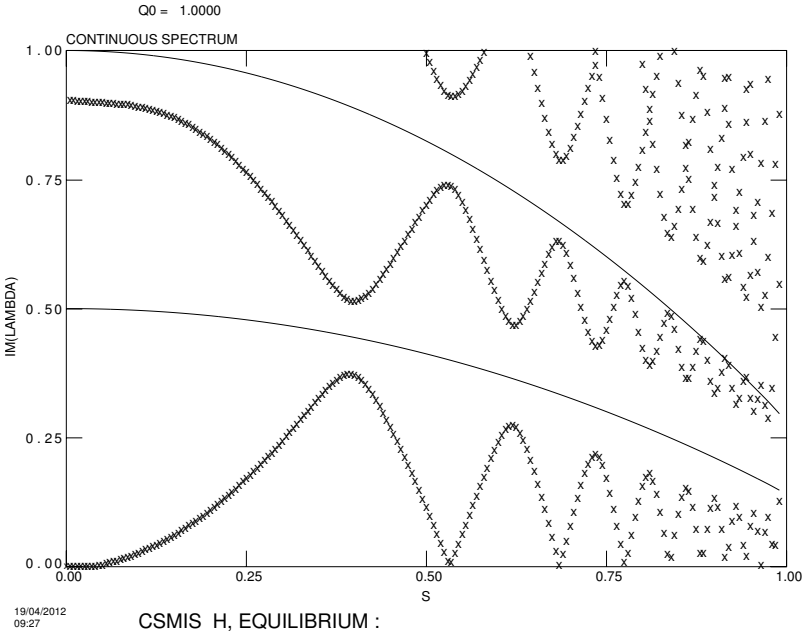

Figure 4.3: Alfvén continuum (spectrum of logarithmically divergent, ideal MHD modes) for $n = 4$, shot 42976 on JET. The equilibrium was reproduced by means of the MHD equilibrium code HELENA [56] and the continuum was calculated with the stability code CSCAS. The x-axis label is $S \propto \sqrt{\psi}$.

so called *outer region*, far from the radial positions r_m where the main part of the mode interaction takes place, the toroidal coupling is negligable and each poloidal mode satisfies the cylindrical mode equation (4.30). On the other hand, close to r_m, there are narrow *inner layers* in which the radial derivatives in (4.26) are so large that the coupling terms between neighboring poloidal harmonics cannot be neglected but the terms proportional to m^2/r^2 can.

We now have enough knowledge to go back and motivate the omission of non-nearest neighbor couplings in the mode equations (4.26). The mode radial width is determined by the outer region equation (4.30). Approximately, it is given by the characteristic radial scale length in the outer region, $\Delta_{\text{out}} \sim r_m/m$. Similarly, the distance between neighboring r_m is approximately

$$|r_m - r_{m-1}| \sim \frac{dr}{dq} |q_m - q_{m-1}| \sim \frac{r_m}{nq\,(r_m)\, s\,(r_m)} \ , \tag{4.36}$$

where s is the magnetic shear, given by equation (2.137) in Section 2.2.4, Chapter 2. We note that when the shear is small, $s \ll 1$, the distance $|r_m - r_{m-1}|$ is much larger than the mode radial extension Δ_{out}, which means that merely two poloidal harmonics couple at each r_m. Therefore, validity of the reduced set (4.26) of *two* coupled equations for the *two* nearest neighbors ϕ_m and ϕ_{m-1}

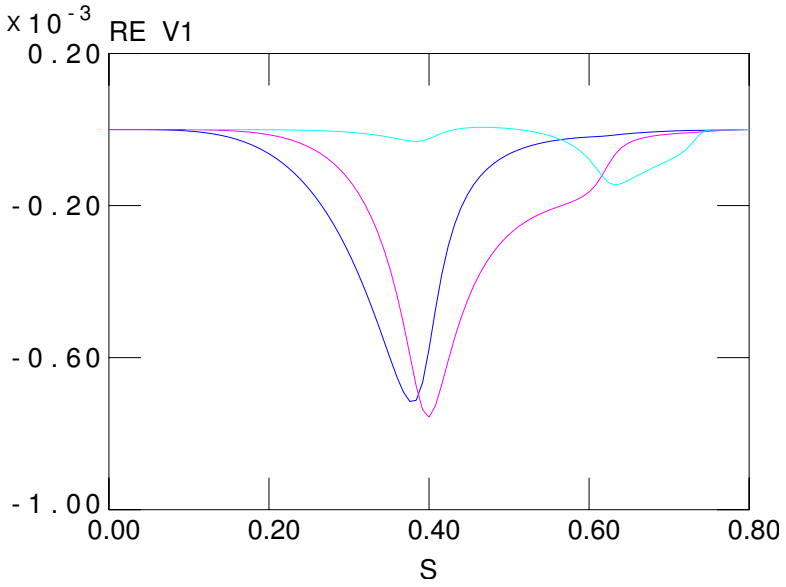

Figure 4.4: TAE mode structure for $n = 4$, as calculated by the stability code MISHKA [60] for the equilibrium that corresponds to the continuum in Figure 4.3. The mode is localized around the first radial gap, but the tail of one of the poloidal harmonics reaches into the next gap where it interacts with another neighboring harmonic.

requires not only high n, but also low shear, $s \ll 1$. If the latter requirement were not met, more couplings would need to be accounted for, which would result in more than two equations involving more than two poloidal harmonics.

The natural question that arises is, of course, how low s must be in relation to the other small parameter, ϵ, involved in the problem? The answer is that there are several possibilities, which have all been investigated analytically:

i. In the limit $\epsilon \ll s^2$, *one* eigenmode exists per gap. This mode is the well known toroidal Alfvén eigenmode (TAE). It has an eigenfrequency close to the bottom of the gap and it consists of a symmetric, or *even*, combination of the neighboring poloidal harmonics ϕ_m and ϕ_{m-1}, i.e. $\phi = |\phi_m| + |\phi_{m-1}|$. An example is on display in Figure 4.4.

ii. When the shear is sufficiently low, $s^2 \leq \epsilon$, *two* modes are present in the gap: One with frequency close to the bottom of the gap, corresponding to the previously discussed TAE, and one whose frequency lies close to the top end of the gap. In contrast to the lower frequency, even mode, the upper mode consists of an antisymmetric, or *odd*, combination of the poloidal harmonics, i.e. $\phi = |\phi_m| - |\phi_{m-1}|$. These modes are sometimes referred to as low shear toroidal Alfvén eigenmodes (LSTAEs).

iii. In the very low shear limit $s \ll \epsilon$ spectra of multiple TAEs are predicted to exist within the gap. Evidence of such modes are yet to be found, and it is very likely that their existence will be confirmed in a spherical, rather than conventional, tokamak, since such machines have tighter aspect ratios.

In what follows, we will adress merely the first case with $\epsilon \ll s^2$, just because it is the simplest to analyze and provides most insight per equation. The second ordering is treated in PAPER D, and the interesting multiple TAEs are thoroughly discussed in [49].

In order to simplify the subsequent analysis, we observe that since the mode numbers are high, by far the strongest radial variation in the coefficients of equations (4.26) is that in the numerator of $k_{\parallel m}$ due to the variation in q. Therefore, we simply evaluate all other functions of r in the coefficients of equations (4.26) at $r = r_m$. We also introduce a dimensionless radial variable according to

$$x \equiv n\left[q\left(r\right) - q\left(r_m\right)\right] \approx ms\left(r_m\right)\frac{r - r_m}{r_m} \ , \tag{4.37}$$

and the dimensionless frequency parameter

$$g \equiv \frac{\omega^2 - \omega_0^2}{\hat{\epsilon}\omega_0^2} \ , \tag{4.38}$$

conveniently shifted so that $g = 0$ at the center of the gap, where

$$\omega = k_{\parallel m}\left(r_m\right) v_A\left(r_m\right) = \frac{v_A\left(r_m\right)}{2q\left(r_m\right) R_A} \equiv \omega_0 \ , \tag{4.39}$$

and normalized so that $g = \pm 1$ at the upper/lower tips of the continuum. With these transformations, the mode equations become

$$\begin{aligned} &\frac{d}{dx}\left[\left(\frac{\hat{\epsilon}g}{4} + x - x^2\right)\frac{d\phi_m}{dx}\right] \\ &\qquad - \frac{1}{s^2}\left(\frac{\hat{\epsilon}g}{4} + x - x^2\right)\phi_m + \frac{\hat{\epsilon}}{4}\frac{d^2\phi_{m-1}}{dx^2} = 0 \end{aligned} \tag{4.40a}$$

$$\begin{aligned} &\frac{d}{dx}\left[\left(\frac{\hat{\epsilon}g}{4} - x - x^2\right)\frac{d\phi_{m-1}}{dx}\right] \\ &\qquad - \frac{1}{s^2}\left(\frac{\hat{\epsilon}g}{4} - x - x^2\right)\phi_{m-1} + \frac{\hat{\epsilon}}{4}\frac{d^2\phi_m}{dx^2} = 0 \ , \end{aligned} \tag{4.40b}$$

where it is understood that $\hat{\epsilon}$ and s are evaluated at $r = r_m$.

In the outer region, $r - r_m \sim \Delta_{\text{out}} \sim r_m/m$, so there $x \sim s$. We therefore introduce a new dimensionless variable $y = x/s$, which is $\mathcal{O}\left(1\right)$ in the outer

region, and rewrite equations (4.40) so that the ordering becomes manifest:

$$\mathcal{L}_0\phi_m = s\left[y\mathcal{L}_0 + y\frac{d}{dy}\right]\phi_m \ , \quad \mathcal{L}_0\phi_{m-1} = -s\left[y\mathcal{L}_0 + y\frac{d}{dy}\right]\phi_{m-1} \ , \tag{4.41}$$

where

$$\mathcal{L}_0 \equiv \frac{d}{dy}\left(y\frac{d}{dy}\right) - y \ . \tag{4.42}$$

Note that we have neglected terms proportional to $\hat{\epsilon}/s^2$, which is equivalent to neglecting the coupling terms in equations (4.26). Thus, equations (4.41) are simply the cylindrical mode equation (4.30) for ϕ_m and ϕ_{m-1} written in terms of a new radial variable centered at $r = r_m$. To lowest order in s, the solutions that decay at $|y| \to \infty$ have even parity,

$$\phi_m^0 = -C_m K_0\left(|y|\right) \ , \tag{4.43}$$

where C_m are constants and K_0 is the zeroth order modified Bessel function of the second kind. The first order correction ϕ_m^1 turns out to have odd parity, which results in a small jump in ϕ_m across the origin. To lowest order in s, the jump can be calculated as

$$\Delta\phi_m \equiv \lim_{\delta\to 0}\left[\phi_m\left(\delta\right) - \phi_m\left(-\delta\right)\right] = -s\int_{-\infty}^{\infty} yK_0\left(|y|\right)\mathcal{L}_0\phi_m^1\, dy \ , \tag{4.44}$$

which leads to

$$\Delta\phi_m = -\frac{\pi^2 s}{4}C_m \ , \quad \Delta\phi_{m-1} = \frac{\pi^2 s}{4}C_{m-1} \tag{4.45}$$

if one substitutes the lowest order solutions ϕ_m^0.

In the inner layer, the poloidal harmonics are highly peaked, so we keep only the derivative terms in the mode equations (4.32). The equations can then be integrated once, and thus become algebraic in $U = d\phi_m/dz$ and $V = d\phi_{m-1}/dz$, where we have defined $z \equiv 4x/\hat{\epsilon}$. If we also neglect the terms x^2, we have

$$\left(g + z\right)U + V = C_m \ , \tag{4.46a}$$

$$\left(g - z\right)V + U = -C_{m-1} \ , \tag{4.46b}$$

where the integration constants have been chosen so that the large z asymptotes matches onto the $y \ll 1$, lowest order in s solutions in the outer regions.

Solving for U and V, and integrating once gives the inner layer solutions

$$\phi_m = -\frac{gC_m + C_{m-1}}{\sqrt{1-g^2}} \tan^{-1}\left[\frac{z}{\sqrt{1-g^2}}\right] + \frac{C_m}{2}\ln\left|z^2 + \left(1-g^2\right)\right| + \text{Const.} \tag{4.47a}$$

$$\phi_{m-1} = \frac{C_m + gC_{m-1}}{\sqrt{1-g^2}} \tan^{-1}\left[\frac{z}{\sqrt{1-g^2}}\right] + \frac{C_{m-1}}{2}\ln\left|z^2 + \left(1-g^2\right)\right| + \text{Const.} \tag{4.47b}$$

The second pieces in these two expressions are even, and they are the ones that match onto the lowest order, outer region solutions (4.43). The first pieces are odd, and much smaller than the logarithmic terms. Therefore, they generate small jumps in ϕ_m and ϕ_{m-1} across the inner layer, given by

$$\Delta\phi_m = -\pi\frac{gC_m + C_{m-1}}{\sqrt{1-g^2}} \ , \quad \Delta\phi_{m-1} = \pi\frac{C_m + gC_{m-1}}{\sqrt{1-g^2}} \ . \tag{4.48}$$

The TAE dispersion relation is now found by matching the jumps across the inner layer with those across the origin of the outer regions. Thus, equating the expressions for $\Delta\phi_m$ and $\Delta\phi_{m-1}$ in the outer region, i.e. equations (4.45), with those from the inner layers in equations (4.48), and subsequently adding and subtracting the results gives

$$(C_m + C_{m-1})\left[\sqrt{\frac{1+g}{1-g}} - \frac{\pi s}{4}\right] = 0 \ , \tag{4.49}$$

$$(C_m - C_{m-1})\left[\sqrt{\frac{1-g}{1+g}} + \frac{\pi s}{4}\right] = 0 \ . \tag{4.50}$$

In order for the square root to be positive, the only consistent solution to this system is to have $C_m = C_{m-1}$ and $\sqrt{(1+g)/(1-g)} = \pi s/4$, which gives the eigenvalue

$$g = -\frac{1-\pi^2 s^2/16}{1+\pi^2 s^2/16} \approx -1 + \frac{\pi^2 s^2}{8} \ . \tag{4.51}$$

In dimensional units, the eigenfrequency becomes

$$\omega = \omega_0\left[1 - \hat{\epsilon}\left(1 - \frac{\pi^2 s^2}{8}\right)\right] \ , \tag{4.52}$$

which is recognized to lie just above the bottom of the gap when $s \ll 1$. We also note that, as anticipated, the mode consists of an even combination of the

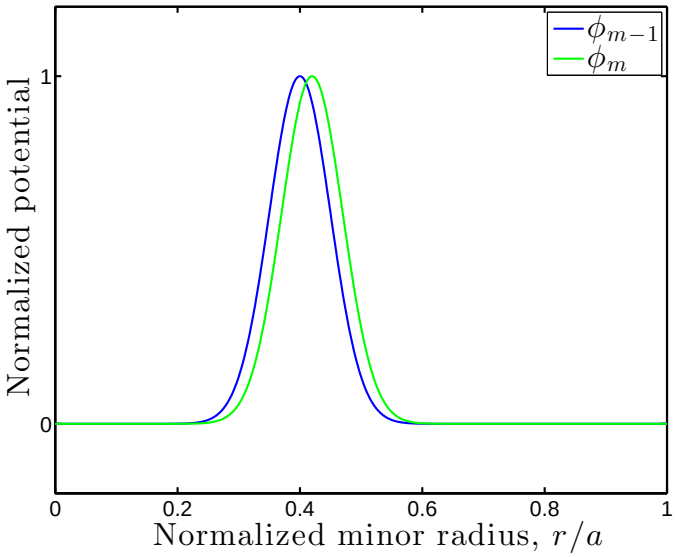

Figure 4.5: Qualitative behavior of the neighboring poloidal harmonics constituting the usual TAE that can be found theoretically in the limit $\epsilon \ll s^2$. The profiles have been normalized to their maximum values.

coupled neighboring poloidal harmonics. Qualitative plots of the profiles for the individual poloidal harmonics of a TAE is shown in Figure 4.5.

It should be noted that the LSTAEs mentioned prior to the TAE analysis presented above, i.e. the eigenmode content when the ordering is taken to be $s^2 \lesssim \epsilon$, requires a more systematic approach in which terms of order $\hat{\epsilon}/s^2$ are not dropped from the outer equation. The dispersion relation in this case is trickier to solve, but the results are easily interpreted with the knowledge already gained from the TAE analysis: Apart from the usual TAE with eigenfrequency (4.52), which persists in the LSTAE limit as well, an additional mode can now be found whose eigenfrequency lies at the top end of the gap,

$$\omega = \omega_0 \left[1 + \hat{\epsilon} \left(1 - \frac{\pi^2 s^2}{8} \right) \right] . \tag{4.53}$$

The upper mode resembles the usual TAE, with a similar eigenmode structure, but it has $C_m = -C_{m-1}$ rather than $C_m = C_{m-1}$, so the poloidal harmonics that couple have amplitudes of different signs, cf. Figure 4.6. A proper treatment of the LSTAEs is developed and presented in Paper D.

We finally note that similar theories have been developed for the experimentally observed ellipticity and triangularity induced modes, where the coupling between modes with mode numbers m and $m \pm 2$ and $m \pm 3$, respectively, creates a similar gap structure capable of supporting eigenmodes.

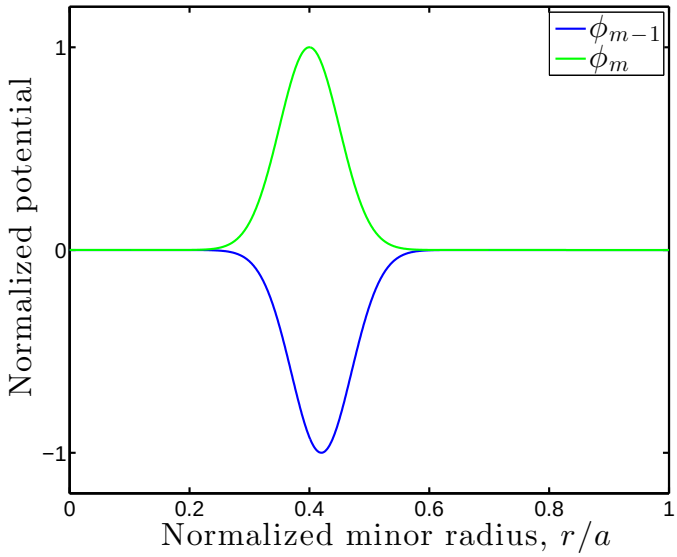

Figure 4.6: Qualitative behavior of neighboring poloidal harmonics for an odd LSTAE, with frequency close to the top of the Alfvén gap. The profiles have been normalized to their maximum values.

4.3.3 Alfvén Cascades

In advanced scenarios, the introduction of an off-axis minimum in the safety factor q (reversed shear) induces an extremum in the Alfvén continuum capable of supporting a localized eigenmode that avoids continuum damping and consists of a single poloidal harmonic, centered at the point of shear reversal. The eigenmodes are constructed theoretically by adding to equation (4.30) second order toroidal corrections [58], and their frequencies are found to lie just above the tip of the Alfvén continuum, once the shear-reversal has been taken into account. Thus, the temporal evolution of these modes and their frequencies follow the continuum, and the experimentally observed sweeping rates shown in Figure 4.7 are reproduced by the evolution of $k_{\|m}$ as q changes in time. These modes are called Alfvén cascades (ACs) due to the characteristic sweeping pattern they produce in the spectrograms.

4.3.4 Kinetic TAEs and Radiative Damping

To account for small scale effects (on the order of the thermal ion gyroradius) arising e.g. in the vicinity of singular points of the cylindrical Alfvén mode equation, first order finite ion Larmor radius (FLR) effects and parallel electron dynamics are introduced in the MHD mode equations (4.26) by adding a fourth order radial derivative to the operator $\mathfrak{L}_m$. In its simplest form, $\mathfrak{L}_m$ can then

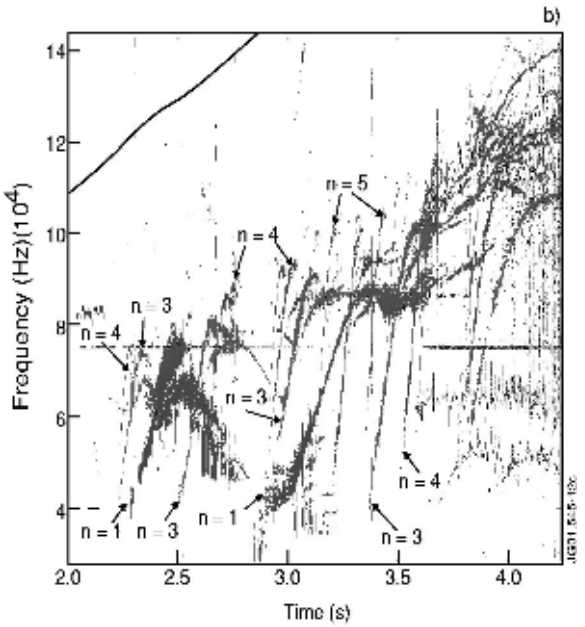

Figure 4.7: Magnetic spectrum of JET shot # 49382 as presented in [61]. Multiple AC branches are observed well below the TAE frequency range. The modes sweep up in frequency with sweeping rates proportional to their toroidal mode numbers, which range from $n = 1$ to $n = 6$.

be written as

$$\mathfrak{L}_m = \omega^2\rho^2\frac{d^4}{dr^4} + \frac{d}{dr}\left[\left(\omega^2 - \omega_A^2\right)\frac{d}{dr}\right] - \frac{m^2}{r^2}\left(\omega^2 - \omega_A^2\right) \ , \tag{4.54}$$

where

$$\rho^2 = \rho_i^2\left(\frac{3}{4} + \frac{T_e}{T_i}\right) \ , \tag{4.55}$$

and ρ_i is the ion Larmor radius. The additional term in (4.54) was first taken into account by Rosenbluth and Rutherford, [62], and has since then been used frequently throughout the litterature , cf. [63, 64].

The introduction of the fourth order derivative FLR term has two major effects on the Alfvénic spectrum in a tokamak. First and foremost, it modifies the Alfvén continuum as to support an entire set of radially standing waves with eigenfrequencies *above* the top of the toroidicity induced Alfvén gap. These modes are usually referred to as kinetic TAEs. Note that there are no equivalent modes below the bottom of the gap.

Secondly, the FLR term modifies slightly the toroidicity induced modes that already exist within the gap, by mediating a coupling to radially propagating, short wave length kinetic waves of the type discussed in Section 4.3.1.

Much like the mechanism discussed there, it turns out that these kinetic waves actually carry a non-negligible fraction of the energy content away from main mode body at the center of the gap, which is then irretrievably lost from the eigenmode. Therefore, for TAEs, the FLR term is really nothing but collisionless, linear damping. It goes under the name *radiative damping* and is the main focus of PAPER D.

4.4 Interaction between TAEs and Fast Ions

The theory presented above only gives criteria for the possibility, or *existence*, of TAEs. The actual excitation, and subsequent evolution, of such waves is an entirely different story, for which some type of driving force must be considered that can pump energy into and destabilize the modes. As already pointed out, the Alfvén speed in tokamaks lies between the thermal velocities of the bulk ions and electrons, i.e. in the range attained by the various types of energetic ions discussed in this thesis. Such particles are therefore very prone to interact resonantly with Alfvénic modes. The interaction is usually discussed under the assumption that the wave amplitude is relatively small, so that the fluid response remains linear. The effect of the fast particles can then be taken into account by adding to the linearized MHD mode equation (4.24) a drive term in the shape of a fast particle current [65], which needs to be calculated within the framework of kinetic theory. Nonlinearly, however, quantitative knowledge is lacking and most progress has been made via extensively reduced models, such as e.g. the one-dimensional toy model presented in Section 3.4.

4.4.1 Energetic Particle Drive

The most discussed, and by far best understood, aspect of resonant fast ion-wave interaction is the process whereupon TAEs are linearly destabilized due to the free energy available for the modes to tap from fast ion distributions that are not in thermodynamic equilibrium. Energy transfer between an ion and a wave generally requires that the ion velocity and wave electric field satisfy $\mathbf{v} \cdot \mathbf{E} \neq 0$. However, shear Alfvén waves have no component of $\mathbf{E}$ along the background magnetic field. Therefore, in tokamaks, the change in the ion kinetic energy is essentially

$$\frac{dE}{dt} = e\mathbf{v}_D \cdot \mathbf{E} \ , \tag{4.56}$$

where $\mathbf{v}_D$ is the drift across the magnetic surfaces due to the field inhomogeneity and curvature. For eigenmodes in the TAE frequency range, the energy transfer rate set by equation (4.56) is very small compared to the wave oscillation frequency. Therefore, it is appropriate to consider the net energy change

ΔE after many periods of the fast ion orbits. As depicted in the formal treatment presented in PAPER A, it turns out that due to the oscillating nature of $\mathbf{E}$, the integral on the right hand side of equation (4.56) essentially averages to zero, except for particles in orbital motion such that the harmonics of their poloidal and toroidal transit frequencies resonate with the phase velocity of the wave. That is, only highly resonant particles satisfying

$$\omega = n \left\langle \omega_\zeta \right\rangle_B - (m+p)\,\omega_B \tag{4.57}$$

contribute to the wave excitation. Here, n and m are the toroidal and poloidal wave numbers, whereas p can be any integer. Most often, however, the only appreciable harmonics are the $p = \pm 1$-terms. Note that the resonance condition (4.57) contains no cyclotron resonance ($l = 0$). In general, shear Alfvén waves have too low oscillation frequencies to resonate with the rapid gyromotion, which has important consequences that will be discussed in more depth in the following section.

A general expression for the linear growth rate of fast particle driven instabilities in toroidal plasmas was given in Section 3.3. With $l = 0$, therefore, Alfvén waves destabilize with a growth rate that scales as

$$[\gamma_L]_{\mathrm{TAE}} \propto \omega \frac{\partial F_0}{\partial E} + \frac{m}{r\omega_{cA}} \frac{\partial F_0}{\partial r} \ . \tag{4.58}$$

However, most energetic particle distributions actually decrease with E (cf., e.g., the slowing down distribution (2.160)), so the first term in the linear drive (4.58) usually damps the wave rather than driving it. Therefore, Alfvénic modes are most often destabilized by the free energy available in the radial gradient, the second term on the right hand side of equation (4.58).

Instability is due to occur when the linear drive exceeds the rate of total damping due to the background plasma. The latter include contributions from several processes, including e.g. Landau damping on passing, thermal electrons; continuum damping (if the tail of the mode anywhere extends into the Alfvén continuum); collisional damping due to pitch-angle scattering of passing thermal electrons onto trapped orbits; and the previously mentioned radiative damping, which is the subject of PAPER D. The relevant paradigm is that of the near-threshold situation discussed in Section 3.4, i.e. when γ_L just barely exceeds γ_d. The idea is that the energetic ion population builds up gradually, due to auxiliary heating schemes or thermonuclear fusion reactions, until eventually the radial gradient of their distribution is large enough to render an overall positive effective growth rate $\gamma = \gamma_L - \gamma_d$ that can destabilize small perturbations from the equilibrium. The excitations tap energy from the fast ions and relaxes their distribution towards the threshold gradient, at which $\gamma_L = \gamma_d$ and the power transfer ceases. On the other hand, while active, the

fast particle sources act to maintain the fast particle population and thereby steepen the radial gradient beyond the threshold. The competition between the two is expected to keep the gradient close to, but just above, the threshold, so that the modes are always weakly driven. Stated differently, the modes simply can not be strongly driven, just because such violent excitation would inevitably lead to large amplitude, bursting events, which is in strong constrast to the relatively serene excitation most often observed experimentally.

4.4.2 Nonlinear Mode Evolution

The assertion in Section 3.4 of Chapter 3 that resonant wave-particle interaction is essentially one-dimensional, once expressed in variables that clearly display that feature, is well motivated in the case of toroidal Alfvén eigenmodes, since the motion of a resonant fast ion in the wave field of a single TAE can be shown to preserve two constants of motion. These invariants are most easily derived via a canonical action-angle description of the unperturbed guiding center orbits. We therefore construct the set of action variables

$$J_1 = p_\alpha \ , \quad J_2 = p_\zeta \ , \quad J_3 = \frac{1}{2\pi} \oint p_\theta \, d\theta \ , \tag{4.59}$$

from the canonical momenta p_α, p_ζ and p_θ given in equation (2.114). Here, it is understood that p_θ can be solved for, at least implicitly (i.e., numerically), as a function of the action variables J_1 and J_2, the particle kinetic energy E, whose value can be evaluated by means of the Hamiltonian $\mathcal{H}_0$ for the unperturbed system, and the poloidal flux angle θ. Therefore, the integration in the definition of J_3 removes all dependencies on variables that evolve along the orbits, and what remains is an invariant of the (unperturbed) particle motion. The canonical angles $\mathbf{\Theta}$ conjugate to these actions are more cumbersome to find, and we shall neither use them nor derive them. However, we shall use their corresponding orbital frequencies,

$$\dot{\mathbf{\Theta}} = \frac{\partial \mathcal{H}_0}{\partial \mathbf{J}} = \mathbf{\Omega}\left(\mathbf{J}\right) \ , \tag{4.60}$$

which in fact are nothing but the bounce averaged orbital frequencies

$$\Omega_1 = \langle \omega_c \rangle_B \ , \quad \Omega_2 = \langle \omega_\zeta \rangle_B \ , \quad \Omega_3 = \omega_B \tag{4.61}$$

for the unperturbed particle trajectories. Here, we have used that since $\mathbf{J}$ are constants of the unperturbed motion, the Hamiltonian for the unperturbed system depends only on $\mathbf{J}$.

The actions are, however, not preserved in the presence of the wave field. Nevertheless, due to their low oscillation frequencies, shear Alfvén waves do

not resonate with the rapid Larmor gyration. As a result, the action variable corresponding to the adiabatic invariant remains constant,

$$\dot{J}_1 = 0 \ , \tag{4.62}$$

even in the presence of the Alfvénic wave field, and the resonant particles lock with the modes merely via their guiding center motion,

$$\omega = l_2\Omega_2 + l_3\Omega_3 \ . \tag{4.63}$$

Moreover, when individual Alfvén waves do not interact, i.e., when their phase space resonances do not overlap, the perturbed Hamiltonian that governs the wave-particle interaction can be shown to consist of a sum of individual potentials,

$$\delta\mathcal{H} = \sum_{l_1,l_2,l_3} U_{l_1l_2l_3}\left(\mathbf{J};\mathbf{\Theta};t\right) \ , \tag{4.64}$$

which, in general, depend on all the actions, but only on a certain combination of the angle variables,

$$U_{l_1l_2l_3}\left(\mathbf{J};\mathbf{\Theta};t\right) = U_{l_1l_2l_3}\left(\mathbf{J}; l_1\Theta_1 + l_2\Theta_2 + l_3\Theta_3 - \int^t \omega\left(t'\right)dt'; t\right) \ . \tag{4.65}$$

However, in view of the low frequency resonance condition (4.63), in which no cyclotron resonances occur, the relevant expression must have $l_1 = 0$, and therefore simplifies to

$$\delta\mathcal{H} = \sum_{l_2,l_3} U_{l_2l_3}\left(\mathbf{J}; l_2\Theta_2 + l_3\Theta_3 - \int^t \omega\left(t'\right)dt'; t\right) \ . \tag{4.66}$$

The sum over the various resonances in equation (4.66) is actually superfluous. In fact, a single pair (l_2, l_3) is enough to describe the resonant particle motion in the potential $U \equiv U_{l_2l_3}$ of an isolated resonance, in which case the total Hamiltonian reads

$$\mathcal{H}\left(\mathbf{J};\mathbf{\Theta};t\right) = \mathcal{H}_0\left(\mathbf{J}\right) + U\left(\mathbf{J}; l_2\Theta_2 + l_3\Theta_3 - \int^t \omega\left(t'\right)dt'; t\right) \ . \tag{4.67}$$

It is then easy to see that

$$l_3\frac{\partial\mathcal{H}}{\partial\Theta_2} = l_2\frac{\partial\mathcal{H}}{\partial\Theta_3} \ , \tag{4.68}$$

which, in the light of Hamilton's equations (2.17), gives

$$l_3\dot{J}_2 = l_2\dot{J}_3 \ , \tag{4.69}$$

i.e. a second conservation law.

The existence of the two invariants J_1 and $J_3 - l_3 J_2/l_2$ certainly indicates that low frequency Alfvén oscillations, at least qualitatively, can be described in one-dimensional terms. However, we can do better than that, and actually show that the kinetic equation for the fast ions is effectively one-dimensional. For that purpose, we perform a canonical transformation from $(\boldsymbol{\Theta}, \mathbf{J})$ to a new set of action-angle variables $(\boldsymbol{\Phi}, \mathbf{I})$, by means of the following generating function of the second kind,

$$F_2\left(\boldsymbol{\Theta}; \mathbf{I}; t\right) = \Theta_1 I_1 + \left[l_2 \Theta_2 + l_3 \Theta_3 - \int^t \omega\left(t'\right) dt' \right] I_2 + \Theta_3 I_3 \ . \tag{4.70}$$

From the transformation laws

$$\mathbf{J} = \frac{\partial F_2}{\partial \boldsymbol{\Theta}} \ , \quad \boldsymbol{\Phi} = \frac{\partial F_2}{\partial \mathbf{I}} \ , \tag{4.71}$$

we find

$$J_1 = I_1 \ , \quad J_2 = l_2 I_2 \ , \quad J_3 = l_3 I_2 + I_3 \ , \tag{4.72}$$

or, equivalently,

$$I_1 = J_1 \ , \quad I_2 = \frac{1}{l_2} J_2 \ , \quad I_3 = J_3 - \frac{l_3}{l_2} J_2 \ , \tag{4.73}$$

and

$$\Phi_1 = \Theta_1 \ , \quad \Phi_2 = l_2 \Theta_2 + l_3 \Theta_3 - \int_t \omega\left(t'\right) dt' \ , \quad \Phi_3 = \Theta_3 \ . \tag{4.74}$$

The transformed Hamiltonian becomes

$$\mathcal{K}\left(\mathbf{I}; \Phi_2; t\right) = \mathcal{K}_0\left(\mathbf{I}\right) + \delta\mathcal{K}\left(\mathbf{I}; \Phi_2; t\right) \ , \tag{4.75}$$

with

$$\mathcal{K}_0\left(\mathbf{I}\right) \equiv \mathcal{H}_0\left(\mathbf{J}\left(\mathbf{I}\right)\right) + \frac{\partial F_2}{\partial t} = \mathcal{H}_0\left(\mathbf{J}\left(\mathbf{I}\right)\right) - \omega I_2 \tag{4.76a}$$

and

$$\delta\mathcal{K}\left(\mathbf{I}; \Phi_2; t\right) \equiv U\left(\mathbf{J}\left(\mathbf{I}\right); \Phi_2; t\right) \ , \tag{4.76b}$$

so that Hamilton's equations give

$$\dot{I}_1 = 0 \ , \quad \dot{I}_2 = -\frac{\partial \mathcal{K}}{\partial \Phi_2} \ , \quad \dot{I}_3 = 0 \ , \tag{4.77}$$

and

$$\dot{\Phi}_1 = \Omega_1 + \frac{\partial \delta\mathcal{K}}{\partial I_1} \ , \quad \dot{\Phi}_2 = \Omega\left(\mathbf{I}\right) - \omega + \frac{\partial \delta\mathcal{K}}{\partial I_2} \ , \quad \dot{\Phi}_3 = \Omega_3 + \frac{\partial \delta\mathcal{K}}{\partial I_3} \ , \tag{4.78}$$

where

$$\Omega(\mathbf{I}) \equiv \partial\mathcal{H}_0/\partial I_2 = (l_2\partial/\partial J_2 + l_3\partial/\partial J_3)\,\mathcal{H}_0 = l_2\Omega_2 + l_3\Omega_3 \tag{4.79}$$

We thus see that the new action variables have been cleverly chosen so that two of them are, in fact, the two constants of motion that exist even in the presence of the Alfvénic wave. We also note that in the presence of the wave field, the angle variables are no longer linear functions of time. Their frequencies are instead shifted by functions that depend on the actions $\mathbf{I}$, the angle Φ_2 and time. On the other hand, the shifts are very small for a small wave amplitude, $\max[\partial\delta\mathcal{K}/\partial I_i] \ll \min[\Omega_i]$. As a first approximation, they can therefore be neglected in the Hamilton equations for Φ_1 and Φ_3, which means that the particle motion is constrained to straight lines in the (Φ_1, Φ_3)-plane. As a result, the effective impact of the Alfvénic wave field is one-dimensional, with the interactional particle motion in the Φ_2-direction, while the invariant actions I_1 and I_3 merely enter the problem as a pair of parameters that determine the linear motion transverse to Φ_2.

The Hamilton equation for Φ_2 is very different from those for Φ_1 and Φ_3. It involves the difference $\Omega - \omega$, which for the most interactive particles is comparable to, or even smaller than, the shift $\partial\delta\mathcal{K}/\partial I_2$ of the orbital frequency in the Φ_2-direction. Given a pair (I_1, I_3), the motion in the Φ_2-direction of such highly resonant particles is therefore most easily treated by Taylor expanding $\mathcal{K}$ around the resonant surface given by the equation $I_2 = I_{2r}$, where the constant I_{2r} can be calculated in terms of I_1, I_3 and ω via the resonance condition

$$\Omega(I_1, I_{2r}, I_3) = \omega\ . \tag{4.80}$$

We expand the unperturbed part $\mathcal{K}_0$ to second order in $\delta I \equiv I_2 - I_{2r}$, but we keep only the lowest order term in the perturbation $\delta\mathcal{K}$, simply because that term is already small due to the assumption of a small wave amplitude. We then obtain

$$\mathcal{K} \approx \frac{1}{2}F(I_1, I_3)\,\delta I^2 + U(I_1, I_3; \Phi_2; t)\ , \tag{4.81}$$

where

$$F(I_1, I_3) \equiv \left.\frac{\partial\Omega}{\partial\delta I}\right|_{\delta I=0}\ , \tag{4.82}$$

and the lowest order approximation for U no longer depends on I_2. Note that some constant terms have been dropped from the resonant particle Hamiltonian (4.81). It is easily seen that Hamilton's equations for Φ_2 and δI indeed correspond to those of a particle that moves under the influence of an evolving electric field $E(I_1, I_3; \Phi_2; t) = -\partial U/\partial\Phi_2$:

$$\dot{\Phi}_2 = \frac{\partial\mathcal{K}}{\partial\delta I} = F(I_1, I_3)\,\delta I\ , \quad \dot{\delta I} = -\frac{\partial\mathcal{K}}{\partial\Phi_2} = -\frac{\partial U}{\partial\Phi_2}\ , \tag{4.83}$$

which combine to give

$$\ddot{\Phi}_2 = F\left(I_1, I_3\right) E \ . \tag{4.84}$$

In view of equation (4.84), the parameter function $F\left(I_1, I_3\right)$ plays an important role: It effectively fixes the value of the local bounce frequency on each resonant surface for the particles trapped in the Alfvénic wave.

We now proceed with the final steps in the reduction from a three- to a one-dimensional Boltzmann equation for the resonant fast ions. By means of equations (4.78) and (4.83), we can immediately write down an approximate kinetic equation. It is given by

$$\begin{aligned} &\frac{\partial f}{\partial t} + F\left(I_1, I_3\right) \delta I \frac{\partial f}{\partial \Phi_2} - \frac{\partial U}{\partial \Phi_2}\frac{\partial f}{\partial \delta I} \\ &\qquad + \left[\Omega_1 + \frac{\partial U}{\partial I_1}\right] \frac{\partial f}{\partial \Phi_1} + \left[\Omega_3 + \frac{\partial U}{\partial I_3}\right] \frac{\partial f}{\partial \Phi_3} = \mathcal{C} + \mathcal{S} \ . \end{aligned} \tag{4.85}$$

As before, $\mathcal{C}$ and $\mathcal{S}$ denotes fast particles collisions and sources. An immediate observeration is that none of the coefficients on the left hand side depend on Φ_1 nor Φ_3. On the other hand, the nature of these angles is such that f must be periodic in both. Therefore, simply integrating equation (4.85) from 0 to 2π in both Φ_1 and Φ_3 eliminates the fourth and fifth terms on the left hand side, and generates a kinetic equation of the form

$$\frac{\partial g}{\partial t} + F\left(I_1, I_3\right) \delta I \frac{\partial g}{\partial \Phi_2} - \frac{\partial U}{\partial \Phi_2}\frac{\partial g}{\partial \delta I} = \frac{1}{4\pi^2} \oint \left[\mathcal{C} + \mathcal{S}\right] d\Phi_1 d\Phi_3 \tag{4.86}$$

for the function

$$g\left(\delta I, \Phi_2, t; I_1, I_3\right) \equiv \frac{1}{4\pi^2} \oint f\left(\mathbf{I}; \mathbf{\Phi}; t\right) \, d\Phi_1 d\Phi_3 \ . \tag{4.87}$$

Note that I_1 and I_3 enters g only in the form of parameters. Equation (4.86) is obviously in one-dimensional form, except for the right hand side terms $\mathcal{C}$ and $\mathcal{S}$, which, in general, can have components that lie in the resonant surface (and therefore are orthogonal to I_2 and δI). However, one can show, [37], that the dominant contribution from $\mathcal{C} + \mathcal{S}$ points along the I_2-direction, i.e. directly across the resonance. Therefore, a conceptually simple projection of $\mathcal{C}+\mathcal{S}$ onto I_2 constitutes a good approximation that makes the kinetic equation truly one-dimensional. The actual projection is not carried out in this thesis, however, due to its technically complicated nature.

Finally, we note that a one-dimensional kinetic equation is not enough to draw the analogue between the nonlinear wave-particle interaction for shear Alfvén waves and the one-dimensional model of Section 3.4. One also needs to put the linearized MHD equations for the perturbation in a suitable form, and then couple that description with the one given above for the fast ions.

The complete framework is not presented here. We merely point out that the way to go is to add the fast particle contribution in the form of a current to the right hand side of equation (4.24).

5

Brief Summary of the Included Articles

This thesis contains four articles on electromagnetic waves and their interaction with fast ions in tokamak plasmas. The present chapter summarizes briefly the content of each article. The role of the thesis author remained essentially constant throughout the four included publications: I performed, or took part, in all analytical and numerical calculations and wrote the main part of the articles, the exceptions being parts of Section IV of PAPER A, Section I of PAPER B, Section VI of PAPER C and Section I of PAPER D, which where written by the co-authors.

5.1 Paper A

In PAPER A, we investigate a single tokamak particle orbit in the presence of a plane, electromagnetic wave field. In particular, we derive a value for the wave amplitude, above which the resonances along the particle trajectories overlap and the motion becomes stochastic. In the stochastic regime, three-dimensional phase space diffusion dominates the dynamics, and an appropriate Fokker-Planck equation can be formulated and used to model the transport of particles due to the wave-particle interaction.

The analysis is performed by examining how the vector of invariants $\mathbf{I} = (E, \mu, p_\zeta)$ changes in the presence of the wave field

$$(\mathbf{E}_1\,,\,\mathbf{B}_1) = (\mathbf{E}_k\,,\,\mathbf{B}_k)\,\mathrm{e}^{-i\omega t + i\mathbf{k}\cdot\mathbf{r}}\,, \tag{5.1}$$

where the Fourier amplitudes $\mathbf{E}_k$ and $\mathbf{B}_k$ are assumed small. We relate $\mathbf{I}$ to its value one poloidal transit earlier by calculating the average change $\Delta\mathbf{I}$

induced by the wave (5.1) during the orbit. The evaluation of $\Delta\mathbf{I}$ is carried out by expanding the equations for $d\mathbf{I}/dt$ to first order in the wave amplitude,

$$\frac{dE}{dt} = e\,\mathbf{v}\cdot\mathbf{E}_k\,\mathrm{e}^{-i(\omega t-\mathbf{k}\cdot\mathbf{r})}\ , \tag{5.2a}$$

$$\frac{d}{dt}\left(\mu B\right) = \frac{e}{\omega}\Big[\left(\omega - k_\parallel v_\parallel\right)\mathbf{v}\cdot\mathbf{E}_k - \left(\omega-\mathbf{k}\cdot\mathbf{v}\right)v_\parallel E_\parallel\Big]\mathrm{e}^{-i(\omega t-\mathbf{k}\cdot\mathbf{r})}\ , \tag{5.2b}$$

$$\frac{dp_\zeta}{dt} = e\frac{k_\varphi R}{\omega}\left[\mathbf{v}\cdot\mathbf{E}_k + \left(\omega-\mathbf{k}\cdot\mathbf{v}\right)\frac{\mathbf{k}\cdot\mathbf{E}_k}{k^2}\right]\mathrm{e}^{-i(\omega t-\mathbf{k}\cdot\mathbf{r})}\ . \tag{5.2c}$$

The set (5.2) is integrated over the unperturbed particle orbits by transforming from time to the poloidal angle θ according to (2.131). Due to the rapid oscillations in equations (5.2), the interaction predominantly occurs when the phase in the exponentials has a minimum (at the wave-particle resonances). The integrals can then be evaluated approximately by means of a stationary phase method in which the multiplying factors in (5.2) are assumed constant throughout the resonant region. The resulting set of equations for $\mathbf{I}$ and the phase are cast in the form of the Chirikov standard map [28]:

$$A_{j+1} = A_j + K\mathrm{e}^{i\psi_j}\ , \tag{5.3a}$$

$$\psi_{j+1} = \psi_j + A_{j+1}\ . \tag{5.3b}$$

The system (5.3) constitutes an intensively studied area preserving map for two variables, whose dynamics corresponds to a sequence of free propagations interleaved by periodic kicks. In the present case, the kicks are being executed as the particle traverses the resonant regions where the phase ψ (corresponding to the phase in the exponentials of (5.2)) is stationary, and the free propagation corresponds to the rest of the orbit. The parameter K indicates the level of chaos: For $K < K_c \simeq 1$, the variation of A is bounded, while for $K > K_c$, A is characterized by a diffusive growth. In the article, we formulate K as a function of the wave field amplitude, and we express A as a function of the components of $\mathbf{I}$, thus providing a condition on the wave to cause stochastic particle motion in $\mathbf{I}$-space. We also estimate the associated diffusion coefficients in the two cases of waves interacting with passing and trapped ions by means of the cyclotron and bounce resonance, respectively, and compare our results with those obtained in [66] and [67].

5.2 Papers B and C

Taken together, PAPERS B and C comprise a suite that aims at describing long range frequency sweeping of single events in terms of evolving phase space holes and clumps. The viewpoint taken is that of the one-dimensional bump-on-tail model presented in Section 3.4, and the focus lies on developing a detailed, reduced model for single hole/clump modes with frequencies that shift over large ranges (comparable to the mode oscillation frequency). Such modeling is bound to include a procedure to solve for the mode amplitude and spatial structure as a function of the fast particle response, since frequency sweeping modes quickly evolve from the sinusoidal structure of the linear instability as their carrier frequencies shift from the original resonance, [68]. In fact, most previous theory has assumed the mode structure to remain sinusoidal, which limits their application to the description of small shifts.

PAPER B deals with the basics of the problem. Evolution equations are derived and motivated for slowly evolving holes/clumps. The equations are valid during the so called *adiabatic* phase, when the holes and clumps are already firmly established and evolve on time scales much longer than the bounce periods of particles trapped in the wave field. A few example solutions are presented that highlight many generic features of long range frequency sweeping. The considered effects include the dependence of the mode structure and amplitude on the frequency shift, the impact of fast particle slowing down and idealized Krook collisions on the mode evolution and frequency sweep and the strong dependence of the mode structure and amplitude on the velocity space shape of the unperturbed distribution of the fast particles, $F_0(v)$. However, the presented solution is based on an analytic approximation, a so called *waterbag* or *top-hat* model, in which the distribution of fast particles remains well phase mixed at a constant level throughout the trapping area. Therefore, the solution is only valid when no ambient particles enter the separatrix, i.e. when the trapping area does not expand (which it does when the wave amplitude increases) and when the fast particles are not subject to velocity space diffusion (which may kick ambient particles through the separatrix). On the other hand, the analytic top-hat model has no similar restriction on particle detrapping, even though shrinkage of the trapping area tends to generate a strong discontinuity in the fast particle distribution at the separatrix. In fact, interesting sweeping patterns may result when the mode amplitude decays and particles detach from the trapping area, in particular when the rate of fast particle slowing down due to Coulomb collisions is substantial. As a rule of thumb, there is a critical slope for the unperturbed distribution of fast particles such that the trapping area remains constant within the given solution. Any lesser slope results in particle detrapping, and can therefore be used with confidence in the modeling. Finally, PAPER B discusses, perturbatively,

the effect of particle trapping as a result of separatrix expansion. Somewhat surprisingly, it is found that modest particle trapping actually amplifies the amplitude increase and accelerates the separatrix expansion. In fact, an appreciable number of passing particles need to enter the trapping area in order to generate an amplitude decrease.

PAPER C goes futher than PAPER B and presents the complete solution to the adiabatic equations that govern the evolution of single holes and clumps. Unlike the semi-analytic theory in PAPER B, the presented tool solves numerically for the profile of the fast particle distribution inside the separatrix, which generally may evolve under the influence of three types of fast particle collisions and sources (the previously discussed slowing down and Krook operators, plus a more realistic velocity space diffusion operator) and as a result of a dynamically evolving separatrix. Consequently, the presented solutions handles perfectly well both types of particle trapping in the wave field (due to separatrix expansion and diffusive collisions), and the effect is shown to have an order of unity impact on the sweeping patterns. As already noted in PAPER B, the inclusion of a small number of passing particles, deposited close to the separatrix, tends to increase the wave amplitude (and therefore results in even more trapping), whereas a larger number of particles, distributed more uniformly throughout the trapping area, results in an amplitude decrease.

With regards to the relaxation rates of the fast particle distribution due to the various types of collisions and sources considered, clumps are found to behave exactly as one would naively expect. They simply disappear quicker and at smaller frequency shifts with higher collision rates, regardless of the type of operator. Holes, on the other hand, display a rich variety of interesting behaviors as the collision rates are scanned. As an example, three types of distinct sweeping patterns can be identified in the simultaneous presence of velocity space diffusion and slowing down of the fast particles: Indefinite, monotonic up-sweeping, asymptotic steady states and transient, hooked sweeping. Numerically, steady holes are found to be linear functions of fast particle energy inside the separatrix, which enables an analytic solution to be constructed. Within the analytical steady state model, it turns out that monotonic sweeping events correspond to values of the slowing down and diffusion rates for which no steady states exist. Further, the short-lived hooks are shown to arise when the steady states go unstable.

5.3 Paper D

PAPER D concerns so called *radiative damping* of TAEs, which arises as a result of small, but finite, non-ideal coupling to propagating, short wave length, *radiative* waves that carry away parts of the TAE amplitude from the main mode body. Radiative damping is thought to dominate the total damping rate of TAEs in most cases, a view which is supported by observations of kinetic Alfvén waves during TAE experiments on TFTR, [69], and numerical simulations of radiative damping rates on JET, [70]. It has previously been discussed by several authors, [71, 72], but the lack of convincing theory is striking. E.g., previous theory predicts a scaling with the ion gyroradius, [71], that does not agree quantitatively with experimental measurements, [73].

In PAPER D, appropriate TAE mode equations, including first order FLR effects and parallel electron dynamics, are presented, and motivated, in the case of an idealized large aspect ratio, low-β tokamak with circular flux surfaces. As discussed in Section 4.3.4, the non-ideal coupling takes the form of a fourth order radial derivative term, multiplied by a small number related to the thermal ion gyroradius. Much like in Section 4.3.2, the mode localization domain is divided into outer and inner regions: In the outer domain, the mode structure is slowly varying with respect to radius, and can be described in terms of reduced equations that do not include the non-ideal terms. It is recognized that the outer solution has a small, odd part (proportional to s) that generates a jump across the origin. However, due to the ordering $\hat{\epsilon} \gtrsim s^2$ rather than $\hat{\epsilon} \ll s^2$, the actual evaluation of the jump is more complicated than in Section 4.3.2, since the pertinent outer equations include toroidal coupling terms between neighboring poloidal harmonics. In the inner layer, the mode varies much faster, so all higher derivative terms must be kept, whereas non-derivative terms may be neglected. In contrast to the purely ideal derivation in Section 4.3.2, the inner equations then take the form

$$\lambda^2 \frac{d^2U}{dz^2} + (g+z)\,U + V = C_m \tag{5.4a}$$

$$\lambda^2 \frac{d^2V}{dz^2} + (g-z)\,V + U = C_{m-1}\ , \tag{5.4b}$$

where λ is a small dimensionless parameter that measures the strength of the non-ideal coupling.

Equations (5.4) are much harder to solve than the algebraic set (4.46). Nevertheless, since λ is small, the solutions are close to those given in Section 4.3.2, with a large even part that matches onto the asymptotes of the outer solutions, and a much smaller odd part that generates a jump across the inner layer (including an exponentially small correction that represents the radiative damping due to the second order derivatives in equation (5.4)). A convenient

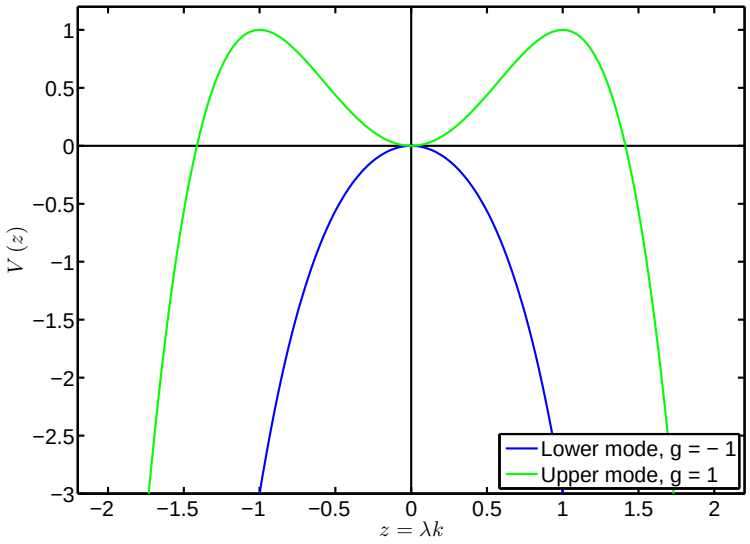

Figure 5.1: Effective potentials $V(k) = \lambda^4 k^4 - 2g\lambda^2 k^2$ for $g \sim \pm 1$.

method to calculate the inner layer jump in the presence of the second order derivatives is to Fourier transform with regards to z. The details of the calculation are given in PAPER D. Here, we just briefly mention that the damping corresponds to the fractional amplitude that escapes, via tunneling, from the potential hill in the Fourier space Schrödinger equation

$$\frac{d^2u}{dk^2} + \left[\left(g^2 - 1\right) - \left(\lambda^4 k^4 - 2g\lambda^2 k^2\right)\right] = 0 \,, \tag{5.5}$$

and becomes propagating, high-k non-ideal waves. The effective potential $V(k) = \lambda^4 k^4 - 2g\lambda^2 k^2$ is shown for $g \sim \pm 1$ in Figure 5.1. Note that the eigenvalue $g^2 - 1$ is negative for modes in the gap. It is obvious that the tunneling of modes with $g \lesssim 1$ must prevail longer, so that a smaller fraction of their total amplitude escapes to high k:s. The same conclusion is drawn from the actual calculations, namely that the upper (odd) TAE is much more weakly damped than the more commonly observed, lower (even) TAE.

6

Summary and Conclusion

The aim of the preceding five chapters has been to prepare and enthuse the reader for the research presented in PAPERS A – D. The text has contained selected parts of fusion and plasma physics theory needed for the understanding of the amended papers, but it also aspires to motivate the presented research and put it into context. It can further be viewed as a general introduction to the field, the referenced articles and the work in CONTRIBUTIONS 1 – 20. Unlike Chapters 1 –5, the present one does not simply contain mathematical or physical facts. Rather, it has been written with the intention to communicate the author's personal thoughts on the research in PAPERS A – D, including possible spin-offs and future outlooks.

To some extent, the investigation in PAPER A is more of an educational exercise. Although the actual end formulae and parts of the mathematical method, or actually the combination of methods, are novel, the general conclusions have long since been known to the theoretical community. On the other hand, at the moment of conduction, the calculations presented in PAPER A were intended to form the basis for a study of high frequency, compressional Alfvén waves observed on the spherical tokamaks MAST and NSTX, [74]. Since then, long discussions with experts within the field led the authors to the conclusion that the guiding center framework used for the description of the particle orbits in PAPER A is not sufficiently accurate in the presence of cyclotron resonances. Nevertheless, the study was not carried out in vain. The calculations are currently being reused in order to apply, quantitatively, the one-dimensional bump-on-tail model of Section 3.4 to frequency sweeping Alfvén waves on MAST.

The development of the adiabatic framework in PAPER B and the numerical tool presented in PAPER C were indeed necessary steps in the process of adding quantitative credibility to the simple one-dimensional bump-on-tail

model, which, throughout the years, has come to be regarded as a highly successful paradigm for predictions of general trends and qualitative explanations of the underlying physics of kinetic instabilities. Previous bump-on-tail theory was constrained to small frequency shifts, in which the mode amplitude remains close to that of the linear instability. In contrast, the work in PAPERS B and C sheds light on long range effects that require the mode structure to evolve from its initial form. The modeling also demonstrates the advantages of the adiabatic approach, in which only time scales longer than that of the trapped particle bounce motion need to be resolved. The presented work definitely forms the basis for quantitative, nonlinear modeling of Alfvénic eigenmodes driven by energetic particles. In fact, an effort is currently made to include the effects of realistic tokamak geometry and magnetic field topology, as well as proper fast particle orbits, into the reduced modeling.

Currently, not much is known on the dynamics of holes and clumps in realistic, three-dimensional toroidal geometries, even though wave-particle interaction in the presence of shear Alfvén waves becomes particularly simple, essentially one-dimensional. Some early, general comments were made in [75], and the numerical, gyrokinetic study in [76] can be interpreted as an indication of the presence of evolving, but coherent, structures in fast particle phase space. In the language of Section 4.4, many of the difficulties stem from the usage of the natural variables for the analysis, the action-angle set (4.73), which are complicated functions of the plasma equilibrium quantities that generally need to be evaluated numerically. As a first step, a reasonable and interesting question to ask concerns the radial locations of the modes, which change as the frequencies shift and the holes and clumps travel through phase space. Since radial profiles for the fast ion distribution, and thereby profiles for the linear drive/damping, are readily available via standard modeling tools, information on the evolution of the hole/clump average radii would certainly indicate, e.g., the preferential direction of the frequency shifts. A first attempt towards such an analysis was presented in CONTRIBUTION 20, where the usual idealized-tokamak assumptions (low β, large aspect ratio etc.) were employed for the investigation. The report largely reproduces some of the results in [75], but also suggest a general route towards the determination of the frequency sweeping directivity in tokamaks.

Another great challenge, but also an interesting feature, of realistic TAE modeling is the possibility of interaction with the continuum as the modes shift their frequencies. As discussed in Section 4.3.1, the ideal mode structure peaks logarithmically at the position of the continuum resonance. Although the divergence is ultimately resolved via the inclusion of small scale effects such as, e.g., first order FLR corrections, the local amplitude increase is very likely to go beyond linearized MHD perturbation theory. Therefore, a more careful, nonlinear fluid treatment of the mode structure, along the lines of [77],

might be needed in order to account for continuum crossings.

The appoximate radiative damping rates calculated in Paper D suggest that the odd LSTAE, with frequency close to the upper tip of the continuum, is, in fact, undamped. The result stands in stark contrast to observations on real experiments, where the conventional, even TAE is almost always solely observed, without so much as a trace of its odd companion, even during discharges with extended regions of low shear. However, the odd mode has antiballooning mode structure, and therefore resides on the inboard side of the torus. As a result, it interacts weakly with trapped, energetic ions, which constitute a major fraction of the super-Alfvénic population on, e.g., JET. The calculated result does, nevertheless, have waste implications for the future tokamak flagship ITER, since D-T experiments on ITER will ultimately contain significant numbers of super-Alfvénic alpha particles, capable of exciting such antiballooning modes via parallel resonances. In fact, it is very likely that the odd mode will destabilize prior to, and at lower fast particle pressure than, the conventional TAE.

For the time being, however, experimental verification (or falsification) of the suggested asymmetry in the damping rate must be regarded as highly desired. In fact, even clear and unambiguous identification of the odd mode would constitute an important step towards a complete understanding of the Alfvénic spectrum. The upper mode was actually observed once alongside the conventional mode, during discharges with extended low shear regions on JET, [78]. In the relevant spectrograms, the odd modes have narrower spectral lines and therefore seem more weakly driven than the even modes, but the asymmetry was attributed to the small number of trapped, ICRH generated ions available to drive the odd modes, even though the resonance layer had been shifted to the high field side of the magnetic axis. However, a clear asymmetry was observed in the temporal evolution of the saturated mode frequencies. Whereas the lower modes evolved according to a "tornado" pattern, [79], the upper spectral lines were almost linear functions of time. These results cry out for more, and similar, experiments to be performed, in which the apparent asymmetry between the even and odd LSTAEs can be studied in detail.

The calculations in Paper D actually rely on a questionable assumption, namely that the fraction of the TAE amplitude that is carried away by the radially propagating non-ideal waves becomes irretrievably lost. More careful modeling should really include the effects of possible reflection of the non-ideal waves towards the plasma edge.

Other conceivable ways to extend the work presented in Paper D includes formulating a real space solution that yields the obtained results, and then applying such a solution to calculate radiative damping rates in the limit of lower and lower shear, where entire spectra of upper and lower TAEs emerge

inside the Alfvénic gap, cf. [49]. Along similar lines, another interesting feature is the interaction of TAEs due to the formation of two radially neighboring potential wells, as sweeping ACs reach the Alfvén frequency range and are transformed into TAEs. Radiative damping rates for such a, more general, system should definitely be the aim of future research.

Bibliography

[1] U. S. Energy Information Administration, *www.eia.doe.gov*, May 2, 2011.

[2] J. D. Lawson, *Some Criteria for a Power Producing Thermonuclear Reactor*, Proc. Phys. Soc. B **70**, 6 (1957).

[3] European Fusion Development Agreement, *www.efda.org*, May 3, 2011.

[4] J. Wesson, *Tokamaks*, Oxford University Press, Oxford, 3rd edition (2004).

[5] International Thermonuclear Experimental Reactor, *www.iter.org*, May 3, 2011.

[6] M. Shimada, D. J. Campbell, V. Mukhovatov, M. Fujiwara, N. Kirneva, K. Lackner, M. Nagami, V. D. Pustovitov, N. Uckan, J. Wesley, N. Asakura, A. E. Costley, A. J. H. Donn, E. J. Doyle, A. Fasoli, C. Gormezano, Y. Gribov, O. Gruber, T. C. Hender, W. Houlberg, S. Ide, Y. Kamada, A. Leonard, B. Lipschultz, A. Loarte, K. Miyamoto, V. Mukhovatov, T. H. Osborne, A. Polevoi and A. C. C. Sips, *Progress in the ITER Physics Basis, Chapter 1: Overview and summary*, Nucl. Fusion **47**, S1 (2007).

[7] W. W. Heidbrink and G. J. Sadler, *The Behavior of Fast Ions in Tokamak Experiments*, Nucl. Fusion **34** (4), 535 (1994).

[8] A. Fasoli, C. Gormenzano, H. L. Berk, B. N. Breizman, S. Briguglio, D. S. Darrow, N. N. Gorelenkov, W. W. Heidbrink, A. Juan, S. V. Konovalov, R. Nazikian, J. M. Noterdaeme, S. E. Sharapov, D. Testa, K. Tobita, Y. Todo, G. Vlad and F. Zonca, *Progress in the ITER Physics Basis, Chapter 5: Physics of energetic ions*, Nucl. Fusion **47**, S264 (2007).

[9] H. Goldstein, C. Poole and J. Safko, *Classical Mechanics*, Addison-Wesley, San Fransisco, 3rd (international) edition (2002).

[10] V. I. Arnold, *Mathematical Methods of Classical Mechanics*, Springer-Verlag, New York, 3rd edition (1978).

[11] M. D. Kruskal, *Asymptotic Theory of Hamiltonian and other Systems with all Solutions Nearly Periodic*, J. Math. Phys. **3**, 806 (1962).

[12] D. Anderson, M. Lisak, P. Johannisson and M. Marklund, *Basic Plasma Physics – Theory and Application*, Reproservice, Chalmers Tekniska Högskola, Gothenburg (2006).

[13] J. R. Cary and A. J. Brizard, *Hamiltonian theory of guiding-center motion*, Rev. Mod. Phys. **81**, 693 (2009).

[14] R. G. Littlejohn, *Variational principles of guiding centre motion*, J. Plasma Phys. **29**, 111 (1983).

[15] T. G. Northrop, *Adiabatic charged-particle motion*, Rev. Geophys. **1** (3), 283 (1963).

[16] J. A. Wesson and A. Sykes, *Tokamak Beta Limit*, Nucl. Fusion **25**, 85 (1985).

[17] E. J. Strait, *Stability of high beta tokamak plasmas*, Phys. Plasmas **1** (5), 1415 (1994).

[18] R. L. Miller and R. W. Moore, *Shape Optimization of Tokamak Plasmas to Localized Magnetohydrodynamic Modes*, Phys. Rev. Lett. **43**, 765 (1979).

[19] J. D. Meiss and R. D. Hazeltine, *Canonical coordinates for guiding center particles*, Phys. Fluids B **2**, 2563 (1990).

[20] P. Helander and D. J. Sigmar, *Collisional Transport in Magnetized Plasmas*, Cambridge University Press, Cambridge, 1st edition (2002).

[21] Ya. I. Kolesnichenko, *The Role of Alpha Particles in Tokamak Reactors*, Nucl. Fusion **20** (6), 727 (1980).

[22] L. D. Landau, *On the Vibrations of the Electronic Plasma*, Sov. J. Phys. **10**, 25 (1946).

[23] T. O'Neil, *Collisionless Damping of Nonlinear Plasma Oscillations*, Phys. Fluids **8** (12), 2255 (1965).

[24] R. W. B. Best, *Energy and momentum densities of a Landau-damped wave packet*, J. Plasma Phys. **63** (4), 371 (2000).

[25] C. Mouhot and Cédric Villani, *On Landau Damping*, Acta Math. **207**, 29 (2011).

[26] M. Lisak, *On the Linear and Quasi-Linear Theory of Thermonuclear Instabilities in a Tokamak Reactor*, Phys. Scripta **29** (1), 87 (1984).

[27] A. Fasoli, B. N. Breizman, D. Borba, R. F. Heeter, M. S. Pekker and S. E. Sharapov, *Nonlinear Splitting of Fast Particle Driven Waves in a Plasma: Observation and Theory*, Phys. Rev. Lett. **81** (25), 5564 (1998).

[28] B. V. Chirikov, *A Universal Instability of Many-Dimensional Oscillator Systems*, Phys. Rep. **52** (5), 263 (1979).

[29] H. L. Berk, B. N. Breizman and M. S. Pekker, *Nonlinear Dynamics of a Driven Mode near Marginal Stability*, Phys. Rev. Lett. **76** (8), 1256 (1996).

[30] H. L. Berk, B. N. Breizman and N. V. Petviashvili, *Spontaneous hole-clump pair creation in weakly unstable plasmas*, Phys. Lett. A **234**, 213 (1997).

[31] R. F. Heeter, A. F. Fasoli and S. E. Sharapov, *Chaotic Regime of Alfvén Eigenmode Wave-Particle Interaction*, Phys. Rev. Lett. **85** (15), 3177 (2000).

[32] S. D. Pinches, H. L. Berk, M. P. Gryaznevich, S. E. Sharapov and JET-EFDA Contributors, *Spectroscopic determination of the internal amplitude of frequency sweeping TAE*, Plasma Phys. Control. Fusion **46**, S47 (2004).

[33] E. Fredrickson, N. Gorelenkov, R. Bell, J. Menard, A. Roquemore, S. Kubota, N. Crocker and W. Peebles, *Fast ion loss in a 'sea-of-TAE'*, Nucl. Fusion **46**, S926 (2006).

[34] D. Maslovsky, B. Levitt and M. E. Mauel, *Observation of Nonlinear Frequency-Sweeping Suppression with RF Diffusion*, Phys. Rev. Lett. **90** (18), 185001 (2003).

[35] B. N. Breizman, H. L. Berk, M. S. Pekker, F. Porcelli, G. V. Stupakov and K. L. Wong, *Critical nonlinear phenomena for kinetic instabilities near threshold*, Phys. Plasmas **4** (5), 1559 (1997).

[36] M. K. Lilley, B. N. Breizman and S. E. Sharapov, *Destabilizing Effect of Dynamical Friction on Fast-Particle-Driven Waves in a Near-Threshold Nonlinear Regime*, Phys. Rev. Lett. **102**, 195003 (2009).

[37] H. L. Berk, B. N. Breizman and M. S. Pekker, *Nonlinear Theory of Kinetic Instabilities Near Threshold*, Plasma Phys. Rep. **23** (9), 778 (1997).

[38] M. K. Lilley, B. N. Breizman and S. E. Sharapov, *Effect of dynamical friction on nonlinear energetic particle modes*, Phys. Plasmas **17**, 092305 (2010).

[39] H. L. Berk, C. Boswell, D. Borba, A. Figueiredo, T. Johnson, M. Nave, S. Pinches, S. E. Sharapov and JET-EFDA Contributors, *Explanation of the JET $n = 0$ chirping mode*, Nucl. Fusion **46**, S888 (2006).

[40] P. M. Bellan, *Fundamentals of Plasma Physics*, Cambridge University Press, Cambridge, 1st edition (2006).

[41] N. F. Cramer, *The Phsyics of Alfvén Waves*, Wiley, Berlin, 1st edition (2001).

[42] K. L. Wong, R. J. Fonck, S. F. Paul, D. R. Roberts, E. D. Fredrickson, R. Nazikian, H. K. Park, M. Bell, N. L. Bretz, R. Budny, S. Cohen, G. W. Hammett, F. C. Jobes, D. M. Meade, S. S. Medley, D. Mueller, Y. Nagayama, D. K. Owens and E. J. Synakowski, *Excitation of Toroidal Alfvén Eigenmodes in TFTR*, Phys. Rev. Lett. **66** (14), 1874 (1991).

[43] W. W. Heidbrink, E. J. Strait, E. Doyle, G. Sager and R. T. Snider, *An Investigation of Beam Driven Alfvén Instabilities in the DIII-D Tokamak*, Nucl. Fusion **31** (9), 1635 (1991).

[44] K. L. Wong, J. R. Wilson, Z. Y. Chang, G. Y. Fu, E. Fredrickson, G. W. Hammett, C. Bush, C. K. Phillips, J. Snipes and G. Taylor, *Expansion of parameter space for toroidal Alfvén eigenmode experiments in TFTR*, Plasma Phys. Control. Fusion 36, 879 (1994).

[45] A. Fasoli, D. Borba, C. Gormezano, R. Heeter, A. Jaun, J. Jacquinot, W. Kerner, Q. King, J. B. Lister, D. Start and L. Villard, *Alfvén eigenmode experiments in tokamaks and stellarators*, Plasma Phys. Control. Fusion **39**, B287 (1997).

[46] K. L. Wong, G. L. Schmidt, S. H. Batha, R. Bell, Z. Chang, L Chen, D. S. Darrow, H. H. Duong, G. Y. Fu, G. W. Hammett, F. Levinton, R. Majeski, E. Mazzucato, R. Nazikian, D. K. Owens, M. Petrov, J. H. Rogers, G. Schilling and J. R. Wilson, *First Evidence of Collective Alpha Particle Effect on Toroidal Alfvén Eigenmodes in the TFTR D-T Experiment*, Phys. Rev. Lett. **76** (13), 2286 (1996).

[47] R. Nazikian, G. Y. Fu, S. H Batha, M. G. Bell, R. E. Bell, R. V. Budny, C. E. Bush, Z. Chang, Y. Chen, C. Z. Cheng, D. S. Darrow, P. C. Efthimion, E. D. Fredrickson, N. N. Gorelenkov, B. Leblanc, F. M. Levinton, R. Majeski, E. Mazzucato, S. S. Medley, H. K. Park,

M. P. Petrov, D. A. Spong, J. D. Strachan, E. J. Synakowski, G. Taylor, S. Von Goeler, R. B. White, K. L. Wong and S. J. Zweben, *Alpha-Particle-Driven Toroidal Alfvén Eigenmodes in the Tokamak Fusion Test Reactor*, Phys. Rev. Lett. **78** (15), 2976 (1997).

[48] J. P. Freidberg, *Ideal magnetohydrodynamic theory of magnetic fusion systems*, Rev. Mod. Phys. **54** (3), 801 (1982).

[49] J. Candy, B. N. Breizman, J. W. Van Dam and T. Ozeki, *Multiplicity of low-shear toroidal Alfvén eigenmodes*, Phys. Lett. A **215**, 299 (1996).

[50] M. S. Ruderman, M. Goossens and I. Zhelyazkov, *Comment on "Alfvén 'resonance' reconsidered: Exact equations for wave propagation across a cold inhomogeneous plasma"*, Phys. Plasmas **2** 9, 3547 (1995).

[51] B. N. Breizman, M. S. Pekker, S. E. Sharapov and JET EFDA contributors, *Plasma pressure effect on Alfvén cascade eigenmodes*, Phys. Plasmas **12**, 112506 (2005).

[52] H. L. Berk, J. W. Van Dam, Z. Guo and D. M. Lindberg, *Continuum damping of low-n toroidicity-induced shear Alfvén eigenmodes*, Phys. Fluids B **4** (7), 1806 (1992).

[53] M. N. Rosenbluth, H. L. Berk, J. W. Van Dam and D. M. Lindberg, *Mode structure and continuum damping of high-n toroidal Alfvén eigenmodes*, Phys. Fluids B **4** (7), 2189 (1992).

[54] L. Chen and A. Hasegawa, *Plasma heating by spatial resonance of Alfvén wave*, Phys. Fluids **17** (7), 1399 (1974).

[55] A. Hasegawa and L. Chen, *Kinetic processes in plasma heating by resonant mode conversion of Alfvén wave*, Phys. Fluids **19** (12), 1924 (1976).

[56] G. T. A. Huysmans, J. P. Goedbloed and W. O. K. Kerner, p. 371 in *Proc. of the CP90 Conference on Computational Physics, Amsterdam*, World Scientific, Singapore, 1991.

[57] C. Z. Cheng, L. Chen and M. S. Chance, *High-n Ideal and Resistive Shear Alfvén Waves in Tokamaks*, Ann. Phys. **161**, 21 (1985).

[58] B. N. Breizman, H. L. Berk, M. S. Pekker, S. D. Pinches and S. E. Sharapov, *Theory of Alfvén eigenmodes in shear reversed plasmas*, Phys. Plasmas **10** (9), 3649 (2003).

[59] B. N. Breizman and S. E. Sharapov, *Energetic particle drive for toroidicity-induced Alfvén eigenmodes and kinetic toroidicity-induced Alfvén eigenmodes in a low-shear tokamak*, Plasma Phys. Control. Fusion **37**, 1057 (1995).

[60] A. B. Mikhailovskii, G. T. A. Huysmans, W. O. K. Kerner and S. E. Sharapov, *Optimization of Computational MHD Normal-Mode Analysis for Tokamaks*, Plasma Phys. Rep. **23** (10), 844 (1997).

[61] S. E. Sharapov, B. Alper, H. L. Berk, D. N. Borba, B. N. Breizman, C. D. Challis, A. Fasoli, N. C. Hawkes, T. C. Hender, J. Mailloux, S. D. Pinches, D. Testa and contributors to the EFDA-JET work programme, *Alfvén wave cascades in a tokmak*, Phys. Plasmas **9** (5), 2027 (2002).

[62] M. N. Rosenbluth and P. H. Rutherford, *Excitation of Alfvén Waves by High-Energy Ions in a Tokamak*, Phys. Rev. Lett. **34** (23), 1428 (1975).

[63] J. W. Connor, W. M. Tang and J. B. Taylor, *Influence of gyroradius and dissipation on the Alfvén wave continuum*, Phys. Fluids **26** (1), 158 (1983).

[64] J. Candy and M. N. Rosenbluth, *Nonideal theory of toroidal Alfvén eigenmodes*, Phys. Plasmas **1** (2), 356 (1994).

[65] G. Y. Fu and J. W. Van Dam, *Excitation of the toroidicity-induced shear Alfvén eigenmode by fusion alpha particles in an ignited tokamak*, Phys. Fluids B **1** (10), 1949 (1989).

[66] V. S. Belikov and Ya. I. Kolesnichenko, *Quasilinear theory for a tokamak plasma in the presence of cyclotron resonance*, Plasma Phys. Control. Fusion 36, 1703 (1994).

[67] V. S. Marchenko, *The Interaction of a Finite Amplitude RF Field with Trapped Electrons in Tokamaks*, Nucl. Fusion **34**, 740 (1994).

[68] B. N. Breizman, *Nonlinear travelling waves in energetic particle phase space*, Nucl. Fusion **50**, 084014 (2010).

[69] K. L. Wong, N. Bretz, G. Y. Fu, J. Machuzak, J. R. Wilson, Z. Chang, L. Chen, D. K. Owens and G. Schilling, *Evidence of coupling between toroidal Alfvén eigenmodes and kinetic Alfvén waves*, Phys. Lett. A **224**, 99 (1996).

[70] A. Jaun, A. Fasoli, J. Vaclavik and L. Villard, *Global Alfvén eigenmode stability in thermonuclear tokamak plasmas*, Nucl. Fusion **39**, 2095 (1999).

[71] R. R. Mett and S. M. Mahajan, *Kinetic theory of toroidicity-induced Alfvén eigenmodes*, Phys. Fluids B **4** (9), 2885 (1992).

[72] H. L. Berk, R. R. Mett and D. M. Lindberg, *Arbitrary mode number boundary-layer theory for nonideal toroidal Alfvén modes*, Phys. Fluids B **5** (11), 3969 (1993).0

[73] W. W. Heidbrink, *Alpha particle physics in a tokamak burning plasma experiment*, Phys. Plasmas **9** (5), 2113 (2002).

[74] E. D. Fredrickson, N. Gorelenkov, C. Z. Cheng, R. Bell, D. Darrow, D. Johnson, S. Kaye, B. LeBlanc and J. Menard, *Observation of Compressional Alfvén Modes During Neutral-Beam Heating on the National Spherical Torus Experiment*, Phys. Rev. Lett. **87** (14), 145001-1 (2001).

[75] C. T. Hsu, C. Z. Cheng, P. Helander, D. J. Sigmar and R. White, *Particle Dynamics in Chirped-Frequency Fluctuations*, Phys. Rev. Lett. **72** (16), 2503 (1994).

[76] H. S. Zhang, Z. Lin and I. Holod, *Nonlinear Frequency Oscillation of Alfvén Eigenmodes in Fusion Plasmas*, Phys. Rev. Lett. **109**, 025001 (2012).

[77] A. Ödblom, B. N. Breizman, S. E. Sharapov, T. C. Hender and V. P. Pastukhov, *Nonlinear magnetohydrodynamical effects in precessional fishbone oscillations*, Phys. Plasmas **9** (1), 155 (2002).

[78] G. J. Kramer, S. E. Sharapov, R. Nazikian, N. N. Gorelenkov and R. V. Budny, *Observation of Odd Toroidal Alfvén Eigenmodes*, Phys. Rev. Lett. **92** (1), 015001 (2004).

[79] P. Sandquist, S. E. Sharapov, M. Lisak and T. Johnson, *Bidirectional tornado modes on the Joint European Torus*, Phys. Plasmas **14**, 122506 (2007).

Paper A

Paper B

Paper C

Paper D